March 30, 2021

Resonance in Marine Outfall Pipes Subject to Wave Excitation

MSc Thesis

Abstract

In this report, we address the problems of water hammer and transient phenomena in water-filled pipes. Indeed, water hammer and vibrations cause troubles and damages on hydraulics installations. Here, we report a numerical approach to understand and avoid the problems inherent to these two phenomena. A Method Of Characteristics (MOC) computational model was used to study the resonance frequencies within the pipe and their location. We investigated the parameters that influence vibration and transient phenomena in pipelines and more specifically in sea outfalls and we studied the pressure response in time and frequency domain. In a first step, we defined a typical pipe to be studied in our experiments. Then we adapted an open-source MATLAB MOC code that runs simulations to our typical pipeline with several outlet conditions. The code was compared and validated with Allievi software in a tank-pipe-valve-tank system to simulate water hammer and verifying the code that we adapted. Finally, we included a coastal wave spectrum in the code to simulate sea waves at the pipe's outlet. With this project, we showed the link between resonance frequencies for the three first mode of vibration in function of several input parameters and the location of the pressure peaks within the pipe and the levels of pressure at resonance. The peak frequencies inside the pipe can be as large as 95 times the excitation pressure.

Under the supervision of:

Prof. Mário Franca, Dr David Ferras, Dr Daniel Valero Huerta

Supervising professor at HES-SO:

Prof. Roberto Putzu

Student:

Alexandre Kolly

Contents

List of Figures

List of Tables

Nomenclature

Symbol	Unit	Definition
a	m/s	wave celerity
A	m^3	pipe cross section
Ap	m	pressure wave amplitude
Ap_0	m	initial pressure wave level
At	-	dimensionless valve wave amplitude
At_0	-	dimensionless valve aperture initial level
B	m^2/s	pipe constant
C^+	-	positive characteristics line
C^-	-	negative characteristics line
C_p	m^3/s	characteristic positive variable
C_m	m^3/s	characteristic negative variable
D	m	inner pipe diameter
e	m	absolute roughness
f	-	Darcy friction factor
g	m/s^2	earth acceleration
H	m	hydraulic head
H_s	m	significant wave height
J	m	friction term
L	m	length of pipe
m	-	valve closure modulation
n	-	number of wave
P	$kg/m/s^2$	gauge pressure
Q	m^3/s	volumetric flow rate
R	s/m^5	friction factor variable simplification
Re	-	Reynolds number
T	s	wave period
t_c	s	closure time of valve
t_d	s	closure start time of valve
V	m/s	fluid velocity
z	m	depth of water
θ	rad	angle of pipe slope
λ	m^2/s	MOC variable
τ	-	dimensionless aperture of valve
ϕ	rad	wave phase
ω	rad	wave pulsation

Indices A, B, P indicate the node in the computing MOC scheme with: P, the actual computing node, A, the upstream node to P and B, the downstream node to P (see Figure 4.1).

Acknowledgement

I warmly thank to my three professors in the Institute for Water Education Delft, Prof. Mário Franca, Dr Daniel Valero Huerta and Dr David Ferras, for their precious advice, their time and their great patience during this project. I also would like to thank my supervisor in Switzerland, Prof. Roberto Putzu, who encouraged me to learn and go abroad for this work.

A special thanks goes to my close relatives and family for their support and all my thanks to my wife who encourage me to follow her and, above all, who believes in me at every moment. The time you spent for me moves me forward.

Finally, I would like to thank all the friends who spent time with me, helping me to take my mind off things, with their bike rides, their skype-lunches or their phone calls.

Introduction

1 State of the Art

Water hammer is a phenomenon of pressure surge that appears when confined fluid have a sudden change in velocity, when a valve closes or a pump stops suddenly, for example. It results in a surge of pressure that can damage the installation. This wave of pressure travels along the pipe and can be reflected at each sides.

Water hammer has been a subject of interest for civilian and mechanical engineers since the beginning of the industrialization. Studying and understanding the hydraulics transient was critical to design and build fluid system [1]. A paper from 1878 [2] is the first known publication about water hammer. It contains a formula to approach the pressure surge for a long valve closing time. This approach was later on corrected by Joukowsky [3] and Allievi [4] by the beginning of the 20th Century. Joukowsky's fundamental equation is still used today to calculate the surge of pressure after an abrupt valve closure.

More recently and in parallel to the experimental methods, there was an increase of interest for computational fluid dynamics (CFD). In parallel a new computational method to compute water hammer was developed. The Method Of Characteristics (MOC) is an algorithm based on the transformation of the mass and momentum balance in wave equations. Lister produced the first known review with this method in 1960 [5].

Although water hammer was described many years ago, research is still ongoing to precise the MOC and the boundaries conditions. More particularly the distribution portability of breaking wave heights. The JONSWAP spectrum was used to model the free surface of the water in 1975 [6].

In parallel to the research about the water hammer, many papers relate problems about water management for ecological, geological or technical reasons. In the 80s, the aim was to avoid sediments intrusion into the diffuser, which can block the diffuser's ports, and avoid lifting of the pipeline due to airpockets and insufficient sandcover of the pipe. For example, in [7], the authors use a MOC code to study a seabed pipeline with several outfall. Boundary conditions are implemented like simple pressure wave or JONSWAP spectrum for wave.

Another example of what is observed in the pipes are the steady and transient phenomena. Steady flow is a state where the speed is not time-depend, whereas the unsteady flow is a state where the flow properties varies over time. Transient phenomena are studied to prevent surge of pressure, vibrations and pressure rise. They are observed in pipes for gas and water, in two-phase flows and on pumps and turbines. In *Technique de l'ingénieur*, we find a chapter dedicated to the sizing of the pipes and the security of the installation in relation to these phenomena [8].

In 1996, a review based on fluid-structure interaction in liquid-filled pipe system [9] highlights the fact that the most important source of vibration in pipes is water hammer. In conclusion of this paper, the most common method for computing transient is MOC and finite-element method (FEM) or a combination of both. 3D models are used for better accuracy of simulation.

Many software were created to simulate hydraulic transients in water systems. Such is the case,

for instance, of Dyagats or Allievi. The method of characteristics is popular to simulate transient simulation because it is computationally efficient and according to Izquierdo and Iglesias in 2002 [10], it illustrates perfectly the wave propagation.

The general aim of Seck's PhD thesis in 2017 [11] was to offer a new functional and decision-making approach for technicians and engineers in order to better model the water hammer for increased control of each step of a project. The first finite volume diagram is an algorithm that takes into account the dynamic friction during the phenomenon of water hammer propagation in a pipe, and the second algorithm takes into account the response of the pipe wall material via its viscoelasticity during the impact. Seck offers a solution for all the design phases of project.

The difference between water hammer software and algorithms was studied by Andreasen in 2018 [12]. This master thesis presented a comparison between many models (CFD, Method Of Characteristics, Discrete Vapor Cavity Model and Discrete Gas Cavity Model) with tree different frictions models (Quasi-Steady Friction Model, Vardy & Brown Friction Model and Brunone Friction Model). The CFD was realised with Fluent and the MOC code and alternatives (DVCM and DGCM) with MATLAB. It resulted from this study that the best model to compute a two-phase water hammer and to get an accurate estimation of the pressure and of the oscillation time is DGCM. In a second study the authors presented their code for modelling 1D water hammer [13]. The aim was to present the code and the MOC code implemented in it. The link for Subversion deposits of the MATLAB code is available in chapter 6, section 1.

Finally, the first study about development of steady-oscillatory flows in marine outfall was done by Ferras and Covas in 2019 [14]. The authors aimed at better understand the performances of marine outfall. In this aim, they simulated the behaviour of the fluid-structure interaction during steady-oscillatory flows considering the axial pipe vibration. A frequency and time-domain analysis is used to study the vibrations constrained by the different cases anchored outfall conditions. The authors investigated on one vibration mode and concluded that future investigations could be about two modes of vibration including the fluid and the solid. The relations between vibrations in the fluid and the pipe-wall should be studied: "the outcome of this sensitivity analysis suggests further investigation on those pipe harmonics corresponding to pipe-wall vibration modes."

2 Problem Statement

Since the beginning of the industrialisation, water hammer and other transient phenomena are critical factors of fluid systems [1]. Although water hammer is the most dangerous surge of pressure within a pipe, smaller transient phenomena may also cause substantial damages by inducing vibrations or cavitation in the installation. Vibrations within the pipe have different effects: they may damage the structure of the installation by cracking propagation of fatigue. They may also damage the pumps or the valves. Due to vibration, the pipeline may experience resonance, which causes peaks of pressure at some locations of the pipe, which is also a cause of damage. It is therefore important to study these vibrations to prevent resonance phenomena and to protect the installation downstream the pipe.

3 Research Questions and Objectives

During this research, we aimed to better understand the transient and vibrating phenomena in sea outfalls pipes. In particular, the propagation of waveform were studied to understand the influence of external parameters on a typical pipeline (length, diameters, temperature, wave

conditions, etc).

1. How pressure distribute inside a marine outfall when excited by a coastal wave?
2. How can we modify the outfall design to reduce mechanical stresses derived from a water hammer?

To answer these questions, the following points were addressed:

1. Definition of a typical pipe installation that represents the mean of seabed pipeline, by determining typical parameters of that pipe.
2. Development of a Method Of Characteristics (MOC) code in 1D in a typical pipe.
3. Implementation of the boundary conditions on the code and on the simulations (valves, waves at the free surface on the water, pressure head, ...)
4. Analysis of the outcomes pressure and flow rate of simulation.

4 Approach

There are two classical approaches to study transient phenomena: the practical method with experimental experimental modelling and measurements in real installation, and the numerical method, which can be validated by experiments. The advantage of a numerical method is to predict flow phenomena without having to build a complex, real installation and in a minimum of time. For this report, we chose to use a numerical approach given that flexibility.

The most know numerical method is the Computational Fluid Dynamics (CFD). It is a powerful numerical analysis method by finite volume or finite element method, which is used to study the motions of a fluid and their effects, by numerical solving of the fluid governing equations. CFD is very flexible and can be used in complex geometry to study steady and transient fluid mechanics and it is more and more used for engineering design and simulations as the software and hardware performances evolve. However to study abrupt transient phenomena, the Method Of Characteristics (MOC) is simpler to set up than using CFD. Besides, it is more adapted regarding the study of water hammer and wave propagation in pipes.

Finally, there is a third numerical approach used to study a solid pipe impregnated in a fluid: the fluid-solid coupling. Fluid-solid interactions (FSI) appear as soon as a structure subjected to vibration is immersed in a fluid. The vibration is transmitted by the fluid and induces a force on the mechanical structure. The coupling of the viscous fluid to the structure induces a dumping to the installation [15]. In terms of analysis, it is highly complicated to couple fluid-solid interactions, as the two phenomena are different (and therefore the code to analyse them). However taking in consideration the interaction between a solid structure and the fluid in which it is immersed is necessary in the fields of multiphysic or to study interaction between several bodies.

To choose the best method adapted to our question, we evaluated these different methods (see chapter 3, section 2).

5 Challenges and Risks

The study of transient phenomena in a pipe is a complex topic that includes many domains such as: hydraulics, interaction fluids and solid and structural domains. Numerical modelling of the internal behaviour of a complete pipe is a complex work, which requires thorough understanding

of the phenomena. Omnipresence of mathematics and physics in that project were a challenge during the whole process, as well as acquiring coding proficiency in MATLAB.

Another challenge was the compression of the method of characteristics. This method is the most used method to simulate transient phenomena and especially water hammer in software. The mathematics of the method of characteristics had to be studied in order to understand the implementation method in the software, which allowed me to be efficient while using a software using this mathematical method. As this was a new research area for me, it was be a challenging part of the project.

Methodology

1 Definition of a Typical Pipe

The first step of the research was to define a typical pipeline that has common parameters. Indeed, to choose an average case of study, the range of all parameters in the pipeline have to be evaluated. Then a choice was made in function of the recurrence or the average of them.

The range and common parameters were found principally in two books about marine outfalls and seawater facilities [16] and [17].

The next table is a summary of all parameters in a submarine pipeline. The values for defining a typical pipeline for the research were based on Table 3.1.

Parameter	Range	Typ. value	Source	Chap.	Page
Geometry					
Diameter (internal) (m)	0.3 - 2.4	1.079	[16]	9.3	281
Thickness (m)	0.006 - 0.079	0.0514	[16]	9.3	281
Length (m)	100 - 16'000	900	[16]/[17]	Appx A	449
Stand. length (m)	6	6	[16]	7.3.0	236
Weight / meter (kg/m)	368	207	[16]	9.3	281
Depth range (m)	0 - 200		[16]	9.8	319
Normal range depth (m)	20 - 40 / 5 -15	10	[16]/[17]	9.8/ 18.4	319/ 408
Material and anchored					
Material (-)	polyethylene (PE) or (HDPE), polypropylene (PP), polyvinyl chloride (PVC), GRP (fiberglass), steel, ductile iron, cast iron	polyethylene (HDPE)	[16]	7.1	231
Young modulus (MPa)	600 -1500	970	[18]		
Roughness (mm)	0.05 - 0.1	0.1	[16]	9.7.6	290
Anchored (-)	Ballast weight, mechanical anchors, articulated concrete block mats (ACBM)		[16]	9.4	283
Water					
Temperature (°C)	-2 to 40	15	[19]		
Ocean density (kg/m^3)	1000 - 1060	1036	[19]		
Brine dis. density (kg/m^3)		1088	[20]		
Salinity (g/kg)	0 - 42	35	[19] [21]/[17]	17.2	371
Velocity in pipe(m/s)	0.5 - 2 / < 1	1	[16]/[17]	9.1/ 18.6.2.1	280/ 417
Current velocity	0.05 - 0.35	0.2	[17]	20.4.2	487
Pressure					
Pressure lost (m)	10 - 25.0	0.86	[16]/ Allievi[1]	7.2.2	235
Pressure loss (m/m)		0.00034	Allievi[1]		
ISO nom. pressure (bar)	3.2 -12.5	4	[16]	9.2	279
Pressure wave speed (m/s)	168 - 270	215	Allievi[1]		

Table 3.1: Typical value of a typical sea pipeline for the research

*[16] = Marine Wastewater Outfalls and Treatment Systems (2010)
*[17] = Intakes And Outfalls For Seawater Reverse-Osmosis Desalination Facilities (2015)

The typical values of the length and diameter of sea pipe were calculated with a distribution density of a list from 145 project found in the annexes of [17]. This list is available in Ap-

[1]See chapter 5, section 2.

pendix section 1.

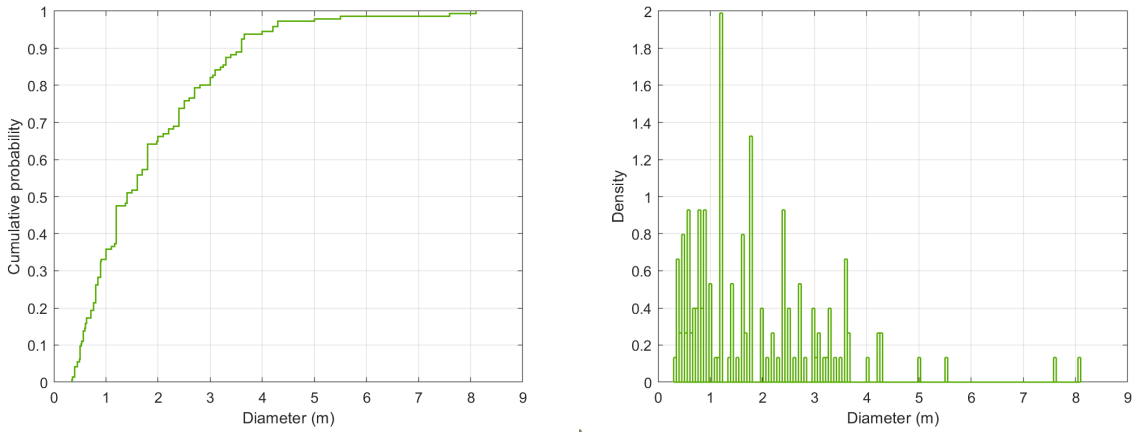

Figure 3.1: Cumulative portability and density of probability for diameter

The distribution of density probability of the diameter (Figure 3.1) shows that the most used internal diameter for a pipe is 1.2 m of diameter.

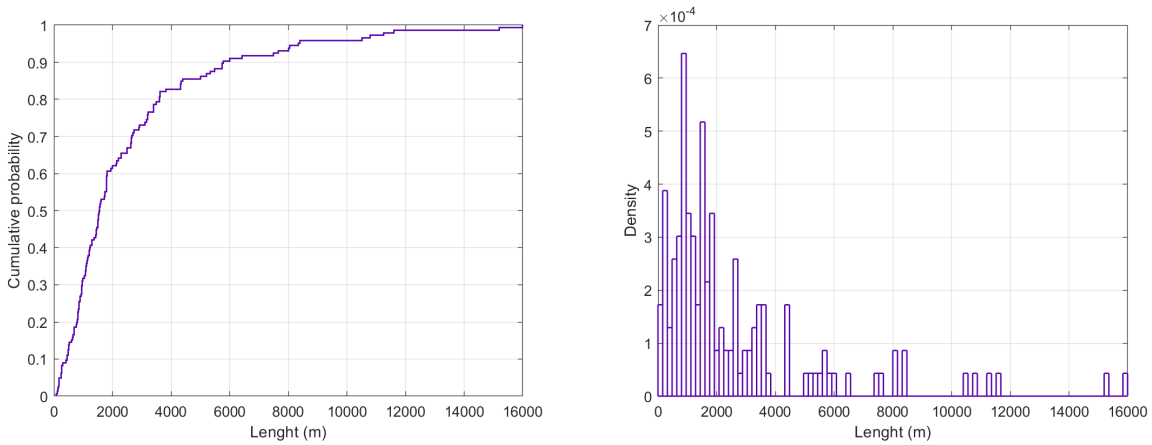

Figure 3.2: Cumulative portability and density of probability for length

The distribution of density probability of the length (Figure 3.2) shows that the most used length of a pipe measures between 800 m and 960 m. 900m was retained as the typical length for this project.

The typical installation is a seabed pipe with a constant diameter, which goes from the coast until 900 meters in the sea, with a constant slope towards the sea ground to arrive 10 meters depth at the end. The downstream of the pipe is open. Below is a scheme of the installation (Figure 3.3):

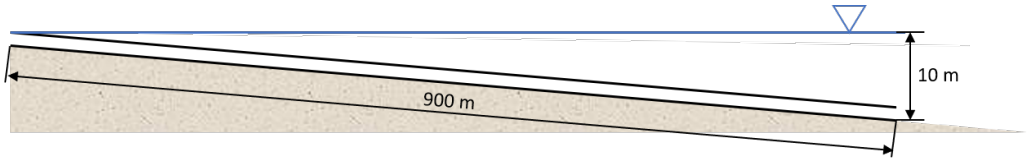

Figure 3.3: Diagram of the typical pipe

The installation diagram needed to be simplified to be simulated by the software. Indeed, the boundary conditions had to be known by the software. To implement upstream and downstream pressure, two tanks were added at both extremities of the pipe. A valve was placed at the end of the pipe before the tank in order to study water hammer. To use Allievi and MATLAB (Figure 3.4), we used the following simplified set up:

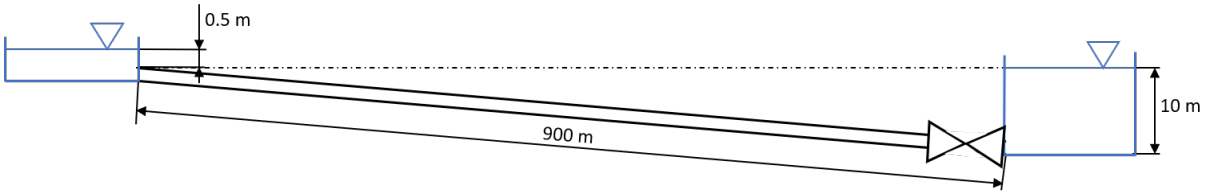

Figure 3.4: Diagram of the typical pipe simplified for software implementation

This Tank-Pipe-Valve-Tank diagram is a simplification of the typical pipe diagram for implementation in Allievi and MATLAB simulations. The upstream tank has a 0.5 meter initial water level and the downstream one is placed 10 meters lower down and has an initial level placed at the initial upstream level to simulate the level of the sea[2] Both tanks have constant water level to simulate infinite reservoir. The valve was placed to test water hammer behaviour in the same conditions in Allievi and MATLAB software.

There are two principal standards for sizing pipeline: ISO and ASTM [16]. The next table is a summary of the size and pressure resistance of the typical pipe according to these standards:

Standard	**Standardless**	**ISO PE100**	**ASTM**
Internal diameter (m)		1.079	1.092
Thickness (m)		0.051	0.052
Diameter to thickness ratio (-)		21	21
Roughness (mm)	0.1		
Length (m)	900		
Weight (kg/m)		207	213
Young modulus (MPa)	0.97		
Pressure nominal (bar)		10	6.7
Maximum pressure (bar)		80	69
Resistance time (years)		50	50

Table 3.2: Summary of typical pipe according to the standards

As both standards have similar nominal pressures and because it is the most commonly used, ISO standard was chosen.

[2]In some experiments, the slope is null. In that case, we referred to it as "typical pipe without slope".

2 Software and Adaptation

Literature present a MOC or similar code to describe 1D water hammer and transient phenomenon in pipes. The purpose of the next step of the present research was to compile some existing codes in MATLAB or Python to obtain a 1D code that describes the fluid-structure interaction of a sea pipe.

The conditions of pressure in both sides of the pipe were implemented in the code. In some simulations, a valve was implemented downstream to test the behaviour of propagation of a pressure wave (water hammer) in the pipe. In other cases, a spectrum of sea waves at the free surface of water was added downstream the pipe in order to study the distribution of the pressure in the pipe.

The table below is a summary of advantages and disadvantages of software or method of programming:

Method	**Scheme**	**Advantage**	**Disadvantage**
MATLAB MOC + adaptation	MOC + FSI	appropriate all code	coupling FSI myself with existing MOC
MATLAB + FEATool (Multiphysics toolbox)	CFD + FSI	Flexibility	No control of code, computation time
MATLAB FSI	MOC + FSI	Performing solution for my application and real MOC code	Don't found direct the code (only mathematic formula)
ANSYS (or other CFD soft)	coupled scheme + one-way coupling/ two-way coupled (FSI)	Knowledge in the domain, many scheme, visualization and treatment	No MOC
Wanda (Delft software)	MOC	Simple to use and built for water network	No FIS

Table 3.3: Summary of the retained solutions for numerical simulations

Based on the analysis above, the two approaches chosen for the project were:

1. Allievi software, which will be used to have a reference on which to rely on.
2. Rune Kjerrumgaard Jensen, Jesper Kær Larsen and Kasper Lindgren Lassen MATLAB MOC code (2018), which will be used because it is open source and very flexible .

Allievi is a professional software used to simulate the behaviour in the steady state and transient phase of water entire complex networks. It is reliable and has already proven itself in several projects. Allievi has a limited number of conditions and theses are not modifiable. Therefore Allievi does not allow us to implement our own parameters, such as modify the anchor of pipe or initialise a complex pressure variation in one side of pipe. In this project, Allievi was used as a reference to verify the simulations of the other software.

The MATLAB MOC code can used for the same aim as Allievi. However, as it is an open source software, the code can be modified to implement others boundary conditions or fluid-structure interactions, for example. For this reason, we chose to use in this project and adapt the MATLAB MOC code for our needs. We validated our modified MATLAB MOC code by comparing with Allievi set up with the same configuration.

To summary, we initially used both programs and when the limitations of Allievi were reached, we used only MATLAB.

Method Of Characteristics Review

This review is based on the articles [12] and [10] and [22]. The Method Of Characteristics (MOC) is a mathematical method used to transform a partial differential equation into an ordinary differential equation. This method is especially effective and useful in wave propagation simulation because of its simplicity and low computing power demand. "Its simplicity is almost too good to believe and, when used properly, the accuracy of its predictions in practical applications is a great comfort." (Arris Tijsseling, [23])

1 Transient Model Equations

The transient wave is represented with the continuity (4.1) and momentum (4.2) equations.

$$\frac{\partial P}{\partial t} + V\frac{\partial P}{\partial x} + \rho a^2 \frac{\partial V}{\partial x} = 0 \tag{4.1}$$

$$\frac{\partial V}{\partial t} + V\frac{\partial V}{\partial x} + \frac{1}{\rho}\frac{\partial P}{\partial x} + g\sin\theta + \frac{fV|V|}{2D} = 0 \tag{4.2}$$

In the equations (4.1) and (4.2), P is the pressure, V is the velocity of the fluid and f is the Darcy friction factor, which depends of the Reynolds number and the roughness of the pipe. These equations describe the water hammer wave propagation in 1D system.

These equations can also be transformed to describe the system in terms of hydraulic head and volume flow rate. With the changing variable (4.3), (4.4), (4.5) and the definition of the partials derivation of pressure (4.6) and (4.7).

$$P = \rho g\,(H - z) \tag{4.3}$$

$$V = \frac{Q}{A} \tag{4.4}$$

$$f = 2DA^2R \tag{4.5}$$

In the equation (4.3), $\frac{P}{\rho g}$ is the pressure head, z is the elevation and H is the hydraulic head. In the equation (4.4), Q is the volume flow rate, V is the velocity and A the internal section of the pipe. The following equations are the partial derivative of the pressure (4.3).

$$\frac{\partial P}{\partial t} = \rho g\left(\frac{\partial H}{\partial t} - \frac{\partial z}{\partial t}\right) \tag{4.6}$$

$$\frac{\partial P}{\partial x} = \rho g\left(\frac{\partial H}{\partial x} - \frac{\partial z}{\partial x}\right) = \rho g\left(\frac{\partial H}{\partial x} - \sin\theta\right) \tag{4.7}$$

With the definition of the partial derivative (4.7) and the variable translation (4.4) and (4.5), the equations (4.1) and (4.2) are transformed in equations (4.8) and (4.9).

$$\rho g\left(\frac{\partial H}{\partial t} - \frac{\partial z}{\partial t}\right) + \frac{Q}{A}\rho g\left(\frac{\partial H}{\partial x} - \sin\theta\right) + \frac{\rho a^2}{A}\frac{\partial Q}{\partial x} = 0 \tag{4.8}$$

$$\frac{1}{A}\frac{\partial Q}{\partial t} + \frac{Q}{A^2}\frac{\partial Q}{\partial x} + \frac{1}{\rho}\rho g\left(\frac{\partial H}{\partial x} - \sin\theta\right) + g\sin\theta + \frac{R}{A}Q|Q| = 0 \tag{4.9}$$

In many cases $V << a$ and the therms with the convective acceleration $\frac{\partial H}{\partial x}$ can be neglected. The term $\frac{\partial z}{\partial t}$ is equal to zero because the pipe doesn't move. After simplification of the equations (4.8) and division by ρg, leads to the equation (4.10). After simplification of the equation (4.9) and multiply by A, it give us (4.11).

$$\frac{\partial H}{\partial t} + \frac{a^2}{gA}\frac{\partial Q}{\partial x} - \frac{Q}{A}\sin\theta = 0 \tag{4.10}$$

$$\frac{\partial Q}{\partial t} + gA\frac{\partial H}{\partial x} + RQ|Q| = 0 \tag{4.11}$$

For quasi horizontal pipes the term $\frac{Q}{A}\sin\theta$ can be dropped to the equation 4.10.

2 Method Of Characteristics

The Method Of Characteristics is a method for transforming the Partial Differential Equations (PDE) (4.10) and (4.11) into Ordinary Differential Equations (ODE). In order to solve the pressure H and the volume flow rate Q, the mass balance and momentum are summed and a λ is added to the second equation (4.12). The ODE is reorganised to highlight the terms containing pressure and flow (4.13)

$$\left(\frac{\partial Q}{\partial t} + gA\frac{\partial H}{\partial x} + RAQ|Q|\right) + \lambda\left(\frac{\partial H}{\partial t} + \frac{a^2}{gA}\frac{\partial Q}{\partial x} - \frac{Q}{A}\sin\theta\right) \tag{4.12}$$

$$\underbrace{\left(\frac{\partial Q}{\partial t} + \frac{\lambda a^2}{gA}\frac{\partial Q}{\partial x}\right)}_{\mathrm{d}Q/\mathrm{d}t} + \lambda\underbrace{\left(\frac{\partial H}{\partial t} + gA\frac{\partial H}{\partial x}\right)}_{\mathrm{d}H/\mathrm{d}t} - \lambda\frac{Q}{A}\sin\theta + RQ|Q| = 0 \tag{4.13}$$

The expanding expression of the total derivative for Q and H leads to the following equations (4.14) and (4.15).

$$\frac{\mathrm{d}Q}{dt} = \frac{\partial Q}{\partial t} + \frac{\partial Q}{\partial x}\frac{\mathrm{d}x}{\mathrm{d}t} \tag{4.14}$$

$$\frac{\mathrm{d}H}{\mathrm{d}t} = \frac{\partial H}{\partial t} + \frac{\partial H}{\partial x}\frac{\mathrm{d}x}{\mathrm{d}t} \tag{4.15}$$

Assuming the total derivative $\mathrm{d}Q$ and $\mathrm{d}H$ in equation (4.13) give the equation (4.16).

$$\frac{\mathrm{d}Q}{\mathrm{d}t} + \lambda\frac{\mathrm{d}H}{\mathrm{d}t} - \lambda\frac{Q}{A}\sin\theta + RQ|Q| = 0 \tag{4.16}$$

The definition of the total derivative (4.14) and (4.15) are used to find the value of λ in equation (4.13).

$$\frac{\mathrm{d}x}{\mathrm{d}t} = \frac{\lambda a^2}{gA} = gA \tag{4.17}$$

Equation (4.17) imposes two conditions for the resolution of the mass and moment balance. The positive/negative characteristics line and the time/space dependence in calculation slope. Equation (4.18) and (4.19).

$$\lambda = \pm\frac{gA}{a} \tag{4.18}$$

$$\frac{\mathrm{d}x}{\mathrm{d}t} = \pm a \tag{4.19}$$

Equation (4.16) is written in function of λ found in the equation (4.18) for which the highlighted terms become total derivatives.

$$\frac{\mathrm{d}Q}{\mathrm{d}t} \pm \frac{gA}{a}\frac{\mathrm{d}H}{\mathrm{d}t} \mp \frac{gQ}{a}\sin\theta + RQ|Q| = 0 \tag{4.20}$$

The positive/negative characteristics line (4.18) imposes a resolution of mass and momentum balance at the present nodes with one of the closest points. Equation (4.19) links the time steps with the distance between two nodes by means of the propagation speed of the wave. Thus we can write the positive and negative characteristics of the equation (4.20) in two equations (4.21) and (4.22).

$$\text{For } C^+ \begin{cases} \dfrac{\mathrm{d}Q}{\mathrm{d}t} + \dfrac{gA}{a}\dfrac{\mathrm{d}H}{\mathrm{d}t} - \dfrac{gQ}{a}\sin\theta + RQ|Q| = 0 \\ \text{with: } \dfrac{\mathrm{d}x}{\mathrm{d}t} = +a \end{cases} \tag{4.21}$$

$$\text{For } C^- \begin{cases} \dfrac{\mathrm{d}Q}{\mathrm{d}t} - \dfrac{gA}{a}\dfrac{\mathrm{d}H}{\mathrm{d}t} + \dfrac{gQ}{a}\sin\theta + RQ|Q| = 0 \\ \text{with: } \dfrac{\mathrm{d}x}{\mathrm{d}t} = -a \end{cases} \tag{4.22}$$

The characteristics lines C^+ and $C^-$are represented in the next diagram.

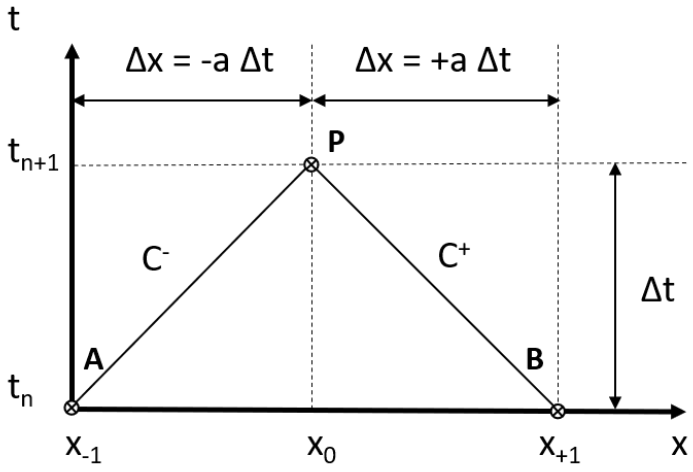

Figure 4.1: Diagram of positive and negative line in space/time plan (adapted from [13])

Figure 4.1 represents the normal scheme of resolution for internal nodes. The point P is the current calculation point. The current pressure at point P for the next time step is found by integrating the equation (4.20) from the point A.

$$\int_A^P \mathrm{d}Q + \frac{gA}{a}\int_A^P \mathrm{d}H - \frac{g\sin\theta}{a}\int_A^P Q\mathrm{d}t + R\int_A^P Q|Q|\mathrm{d}t = 0 \tag{4.23}$$

The linear integration of the equation (4.23) gives the difference between finite elements:

$$Q_P - Q_A + \frac{gA}{a}(H_P - H_A) - \frac{g\sin\theta}{a}Q_A\Delta t + RQ_A|Q_A|\Delta t \tag{4.24}$$

The next step is to define a variable that simplifies the equation. The variable $B = \frac{gA}{a}$ is introduced and the characteristic positive variable C_p is defined as:

$$C_p = BH_A + Q_A + \frac{B\sin\theta}{A}Q_A\Delta t - \underbrace{RQ_A|Q_A|\Delta t}_{J} \tag{4.25}$$

and

$$H_P = \frac{C_p - Q_P}{B} \tag{4.26}$$

The previous steps (equation (4.23) to (4.26)) are reproduced with the negative line. Equation (4.25) is transformed into equation (4.27) and equation (4.26) is transformed in equation (4.28).

$$C_m = BH_B - Q_B + \frac{B\sin\theta}{A}Q_B\Delta t - \underbrace{RQ_B|Q_B|\Delta t}_{J} \tag{4.27}$$

and

$$H_P = \frac{C_m + Q_P}{B} \tag{4.28}$$

The term $(RQ_B|Q_B|\Delta t)$ within C_p and C_m equations is called J. This term is the friction term in meter. The implementation of the friction term J in the MATLAB code is described in chapter 6, section 3.

These systems of equation with the two positive characteristics equation (4.25) and (4.26) and the two negative characteristics equations (4.27) and (4.28) are used to resolve the pressure and volume flow rate at each point of the system. The equations are defined for inner nodes, and each boundary conditions.

3 Inner Nodes Solution

The pressure H_P and the volume flow rate Q_P are obtained with the previous system of equation. The pressure is obtained with the previous node A and the next node B.

$$H_P = \frac{C_p + C_m}{2B} \tag{4.29}$$

The volume flow rate is obtained with the pressure at point P and the negative characteristics:

$$Q_P = BH_P - C_m \tag{4.30}$$

4 Upstream Boundary Conditions

A constant pressure level condition is used to define the condition at the first node (upstream condition) of the pipe.

$$H_P = H_{res} = \text{cst} \tag{4.31}$$

The volumetric flow rate is calculated with the equation (4.30).

5 Downstream Boundary Conditions

The calculation of downstream pressure and volume flow rate depends on the outfall type. There are diverse types of outflow, including: valve, open orifice, multiple orifices, injectors, etc.

The implementation of some of them are explained in the chapter 6, section 4, in which the MATLAB code is described.

Allievi

1 Software and Configuration

Allievi is a free software created by the Universitat Politecnica de Valencia (UPV, Spain). It uses a MOC scheme to compute steady state condition and transient flow in water network. Allievi allows the estimation of the pressures, the flow rate and other parameters for each pipe and node of the system. The addition of each compound of the network is realised with a graphical interface that allows easy parameter input.

The software uses the difference of pressure, which means that the initial volume flow rate is calculated with the imposed pressures at each side of the pipe by water level of the reservoirs. At steady state, the water level at each side of pipe imposes a certain volume flow rate. Therefore the user can't choose especially the velocity of the fluid inside the pipe and measure the difference of pressure at the bottom of the pipe.

2 Typical Pipe Implementation

Figure 5.1 represents the Reservoir-Pipe-Valve-Reservoir installation with in Allievi.

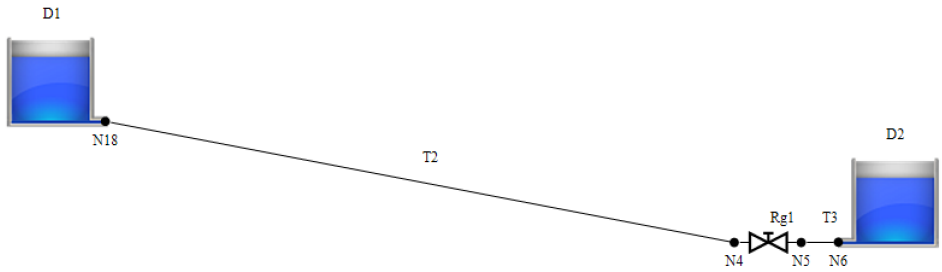

Figure 5.1: Scheme of the typical pipeline in Allievi

The next tables (5.1, 5.2, 5.3) are the summary of the geometrics parameters form generate by Allievi.

Pipes - Basic data										Losses
Name	**Ni**	**Zi (m)**	**Nf**	**Zf (m)**	**Dint (mm)**	**L (m)**	**e (mm)**	**a (m/s)**	**Rough (mm)**	**k**
T2	N18	0	N4	-10	1079	900	60.5	215	0.1	0
T3	N5	-10	N6	-10	1079	4	60.5	215	0	0

Table 5.1: Summary of the pipes in typical pipe simulation with Allievi

In Table 5.1, Ni is the upstream node, Zi is the upstream altitude, Nf is the downstream node, Zf is the downstream altitude, Dint is the internal diameter.

Tanks - Basic data					
Name	**Ni**	**Nf**	**Zs (m)**	**Type**	**Z0 (m)**
D2	N6	—	-10	GD	0
D1	—	N18	0	GD	0.5

Table 5.2: Summary of the tanks in typical pipe simulation with Allievi

In Table 5.2, the type of tank is set in *Great Dimension* to have constant pressure level.

Regulation valve - Basic data							Maneuvrer
Name	**Ni**	**Nf**	**Z (m)**	**ND (mm)**	**k Branch**	**Type**	**Type**
Rg1	N4	N5	-10	1079	0	Gate	Tabulated

Table 5.3: Summary of the valve in typical pipe simulation with Allievi

Once the hydraulic diagram is done and the parameters are correctly entered into the system, all that remains is to enter the simulation parameters (time step and simulation timed).

The steady state simulation can be started and the pressure losses and constant volume flow rate is calculated. Then, the transient calculation can be started with the steady state parameters found in the previous step.

MATLAB Code

1 Software and Configuration

The MATLAB code used for this project was based on the free open source 1D water hammer presented in these papers: [12] [13] and available in SVN depot platform: water hammer code - Subversion deposits: https://savannah.nongnu.org/svn/?group=whammer.

The diagram of the code is displayed below in Figure 6.1.

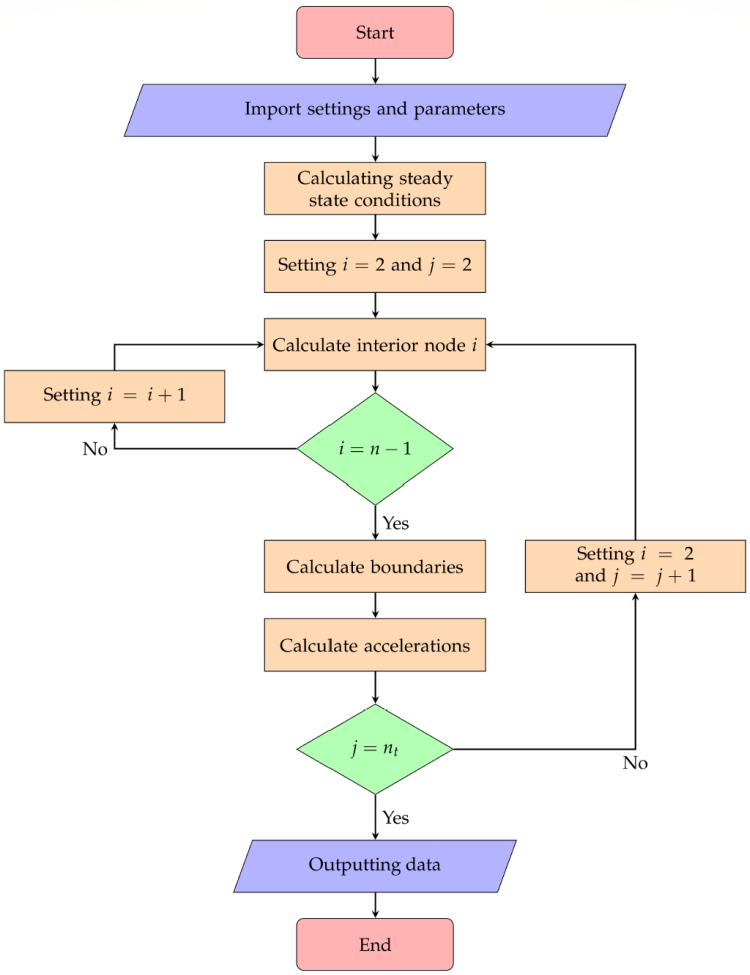

Figure 6.1: Diagram of MOC code implementation ©2018 *Implementation and Validation of a Free Open Source 1D Water Hammer Code* [13]

In Figure 6.1, i describes the space, and more precisely, the node at which is the simulation and j describes the time, and more precisely, the time step at which is the simulation. The main code calls the function in the following order: Master (which calls the solver and the input) →

Steady condition resolving → Boundary condition resolving → Solver for all nodes → Output data.

The code is running a main code (Master), which calls functions and subfunctions. Master is running and calls the input first and the solver code. An input code that corresponds on the hydraulic sea pipeline is created.

2 Typical Pipe Implementation

To implement the configuration of the typical pipe, some files had to be changed or adapted for the simulation of the typical pipe in the same condition as in Allievi.

Name	Value	Unity	Remarks
a	215	m/s	wave celerity
A	0.91	m^2	internal section
D	1.08	m	internal diameter
Downstream_boundary	Valve_Instantaneous _Closure	-	explanation in section 4
dt	0.05	s	time step
dx	10.71	m	distance between nodes
e	0.06	m	thickness of pipe
E	970'000'000	N/m^2	Young modulus
f_pre	0	-	initial friction ratio
Friction_Type	Prescribed_Steady _State_Friction	-	explanation in section 3
H_r	0.5	m	reservoir level
K	2'200'000'000	N/m^2	bulk modulus of water
L	900	m	length of pipe
Q_0	37.88	m^3/s	initial volume flow rate
rho	1036	kg/m^3	density of water
roughness	0.0001	m	inner pipe roughness
Solver	1D_SinglePhase	-	solver type describe in [13]
t_max	133.95	s	simulation time
theta	-0.637	deg	angle of pipe
u_0	41.43	m/s	initial velocity
Upstream_boundary	Reservoir	-	
viscosity	0.001	kg/m/s	dynamic viscosity
WaveSpeed_Type	WaveSpeed_Known	-	no calculation of wave speed

Table 6.1: Summary of the input in MATLAB for typical pipe simulation without frictions

3 Friction in Pipe

MATLAB needs an input file that contains input parameters in order to run the simulation parameters enumerate in Table 6.1. In this file the way of computing the friction is chosen from seven possibilities:

```
1 % Choose friction type:
```

```
% 1)     Prescribed_Steady_State_Friction     (insert value in
    f_pre)
% 2)     Steady_State_Friction
% 3)     Quasi_Steady_Friction
% 4)     Unsteady_Friction_Brunone
% 6)     Unsteady_Friction_Zielke
% 7)     Unsteady_Friction_VardyBrown
% 8)     Unsteady_Friction_Zarzycki
Friction_Type = 'Steady_State_Friction';
```

Listing 6.1: *Input* file, choose of friction type

The friction term J equal to $RQ_B|Q_B|\Delta t$ in Equation 4.25 and Equation 4.27 is the sum of the steady friction, quasi-steady friction and unsteady friction.

$$J = J_s + J_q + J_u \tag{6.1}$$

Listing 6.1 indicates how MATLAB compute the friction term J. In the case of *Steady State Friction*, J is:

$$J = J_s = \frac{f\mathrm{d}x}{2gDA^2}|Q_0|Q_0 \tag{6.2}$$

In Equation 6.2, Q_0 is the volume flow at steady state condition and f is equal to the Darcy friction factor describe in Equation 6.3.

$$\frac{1}{\sqrt{f}} = -2\log_{10}\left(\frac{e}{3.7D} + \frac{2.51}{Re\sqrt{f}}\right) \tag{6.3}$$

The friction factor f depends on the absolute roughness of the pipe e, the internal diameter of pipe D and the number of Reynold Re which describe the regime of the flow.

In the simulation that compared MATLAB to Allievi software, the prescribed steady state friction type was used in order to have the same Darcy friction factor in both software. The steady state friction type was used in the next simulations because it offers a good friction type with similar conditions in function of the steady state conditions. The aim was to have frictions losses close to the reality and the same friction losses in function of the software.

4 Implementation of Downstream Conditions

In this chapter, the boundary conditions of pressure and volume flow rate used for the outfall of the pipe are described. Of note, the mathematics used to describe the MOC operations in the chapter 4 are not the same.

4.1 Fully open valve

Equation (6.4) is already implemented in the code.

$$\tau = 1 - \left(\frac{t}{t_c}\right)^m \tag{6.4}$$

In equation (6.4), τ is the dimensionless aperture of the vale, t is the time of the simulation, t_c is the closing time of the valve m is the modulation coefficient, which implements a non linear closure time. In order to have a fully open valve, a switch case that constrain $m = \text{inf}$ and $t_c = \text{inf}$ was added to the code.

4.2 Delay Valve

The delay valve is a valve that has a delay before it starts to close. It can be useful to establish a complete steady condition before starting to close the valve. t_d is the closure start time. The source code is available in appendix section 2,Listing A.4.

$$\tau = 1 - \left(\frac{t - t_d}{t_c}\right)^m \tag{6.5}$$

4.3 Sinusoidal Valve

The sinusoidal valve equation (6.6) imposes a sinusoidal valve closure signal after a delay. This valve allows to study pressure and flow behaviour along the pipeline with periodic pressure and flow changes at the valve. The source code is available in appendix section 2,Listing A.5.

$$\tau = At_0 + At \sin\left(\frac{2\pi}{T}t + \phi\right) \tag{6.6}$$

In equation (6.6), Ap_0 is the initial dimensionless aperture of the valve, Ap is the dimensionless sinusoidal amplitude of the valve, T is the period of valve oscillation and ϕ is the constant phase.

4.4 Sinusoidal Pressure Wave

The implementation of the upstream boundary condition for a pressure wave was based on the report [7] that implemented a linear wave and JONSWAP spectrum in seabed outfall. The following equations (6.7) and (6.9) were used to calculate the pressure head and the volume flow rate at the end of the pipeline with a linear wave in boundary condition.

$$H_P = Ap_0 + Ap \sin\left(\omega t + \frac{\omega}{a}x\right) = Ap_0 + Ap \sin\left(\frac{2\pi}{T}t + \frac{2\pi}{T}\frac{x}{a}\right) \tag{6.7}$$

$$H_P = Ap_0 + Ap \sin\left(\omega t + \phi\right) = Ap_0 + Ap \sin\left(\frac{2\pi}{T}t\right) \tag{6.8}$$

In equation (6.7), Ap_0 is the initial level of pressure in meter, Ap is the amplitude pressure of the wave in meter, ω is the angular frequency, t is the time of simulation in second, T is the wave period in second, a is the celerity of the wave in meter per second, x is the location in the axis of the pipe in meter.

$$Q_P = \frac{C_p - H_P}{B} \tag{6.9}$$

Equation (6.9) gives the volume flow rate at the end of the pipe in function of H_P and the positive line characteristics C_p. B is a pipe constant equal to $\frac{a}{gA}$. The source code is available in appendix section 2,Listing A.6.

4.5 Pressure Wave Spectrum

In the next step of the simulation, a complete pressure wave spectrum of frequencies was imposed in the outlet. The aim was to replicate the condition of pressure of a real coastal wave at the end of the pipe. The first step was to create a pressure-time vector that simulates a real coastal wave spectrum. This spectrum was constructed with measures at Ebro Delta, described [24]. The wave signal based on these measurements was generated by the MATLAB function [25].

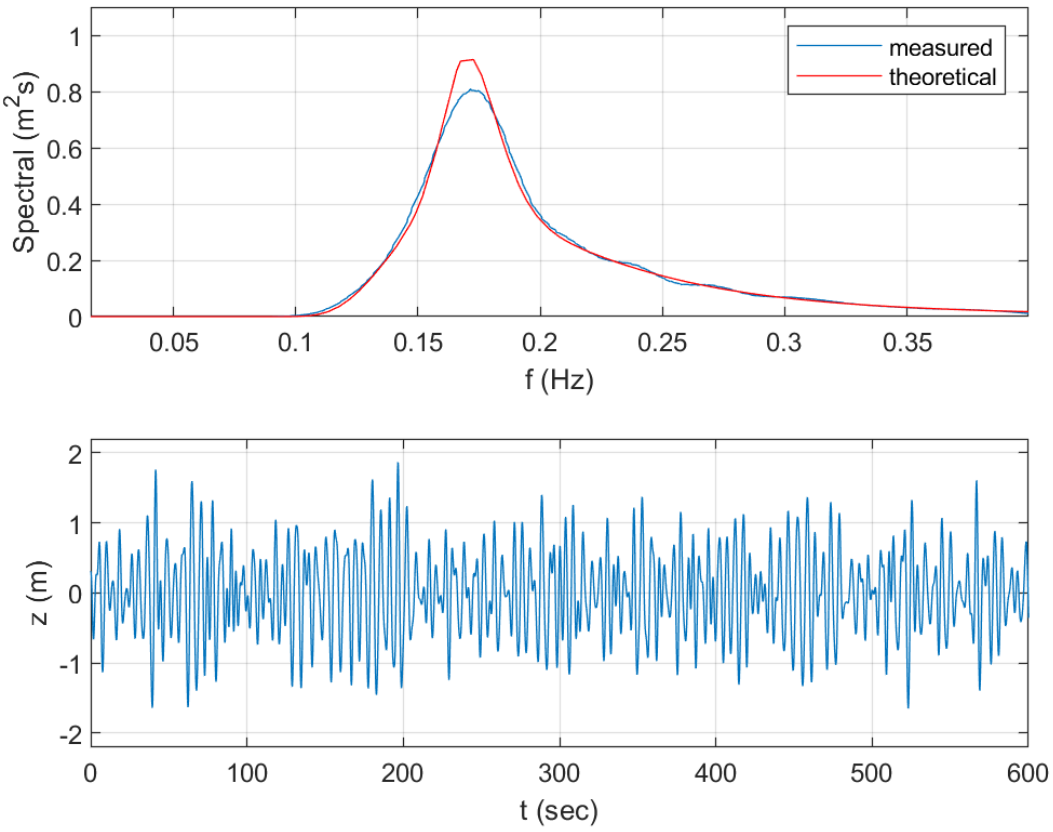

Figure 6.2: Example of waves created with the MATLAB function *cobagelombang3* from [25]

Figure 6.2 shows the theoretical JONSWAP spectrum target in red and the simulation of the coastal wave spectrum that reproduces the target.

The source code of the outfall pressure wave spectrum implementation is available in appendix section 2, Listing A.7. After its creation, the waveform is saved in order to use the same waveform for all simulations. This saves calculation time and ensures that all simulations are made in the same conditions.

Comparisons of Software

1 Introduction

The aim of this part was to compare the MATLAB code to Allievi in order to understand similarities and differences in output measurement. Both software have different ways to implement input parameters. For example, Allievi needs the pressure at each boundary conditions (reservoir pressures at each side of pipe) and MATLAB needs a velocity and a pressure at the intake and compute the others boundary conditions. These differences had to be studied in order to understand the limit of each software.

This chapter is divided in three experiments. One full open system was implemented in order to study the stability of the system. The full open system implements the steady state conditions of the next experiments. By this way, we were able to determine the stability of the software and test the basic inputs parameters to ensure that both software are calibrated. The second experiment was an instantaneous closure valve to test the behaviour of the water hammer within the pipe. In the last experiment, we introduced a sinusoidal valve signal at the end of the pipe in order to compare the propagation of a wave of pressure and volume flow rate in the pipe. The behaviour of both software were compared with similar inputs and valve conditions. Condition of similarities were established and input parameters were chosen in order to have similar conditions.

Some downstream conditions had to be implemented in the MATLAB code in order to have similar conditions with Allievi outfall. These different vanes and pressure outfall implementations are explained in chapter 6, section 4.

2 Fully Open Valve System

The first experiment consisted in comparing the behaviour of each software without valve closure. The aim was to determine if the pressure and the volume flow were stable over time. The full open system is a system at steady state condition. If the conditions were changing during time, the input conditions would need to be studied in order establish steady state condition before simulation.

The experiment was realised with similar conditions of pressure and volume flow rate for both software for the typical pipe (see chapter 3, section 1).

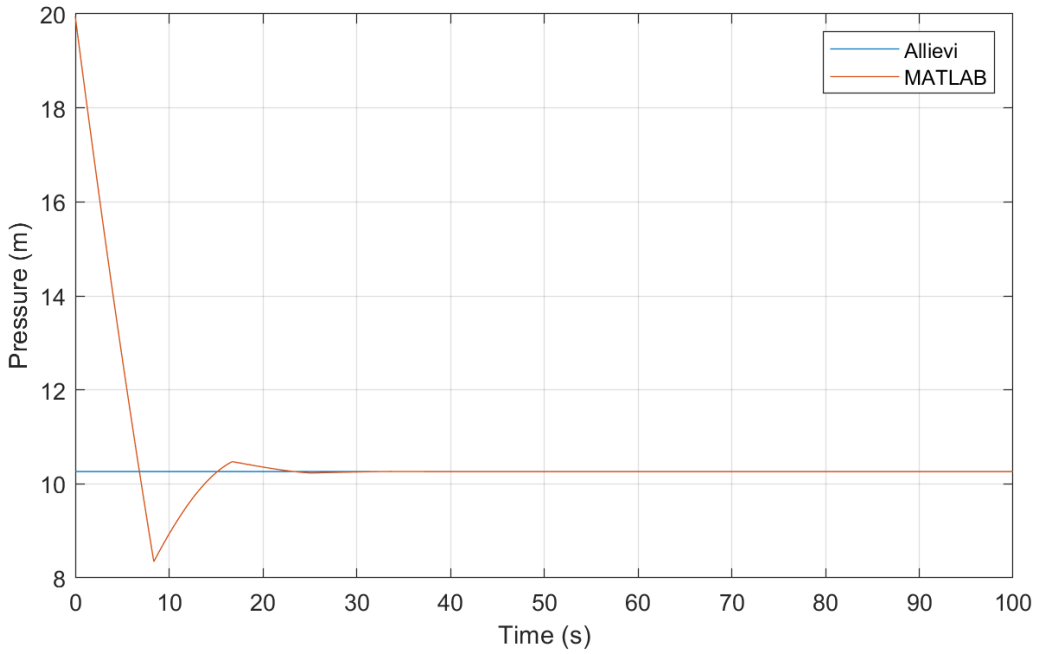

Figure 7.1: Pressure outfall in function of time for Allievi and MATLAB with open valve

Figure 7.1, shows that the pressure is stable after thirty seconds and at the exact same value in both software. The warm up time (time before complete stabilisation) is inexistent with Allievi while it lasts about twenty-five seconds with MATLAB. Indeed, Allievi computes the steady state after many iterations and is closer to the transient condition than MATLAB, which only sets the pressure losses at the first time step.

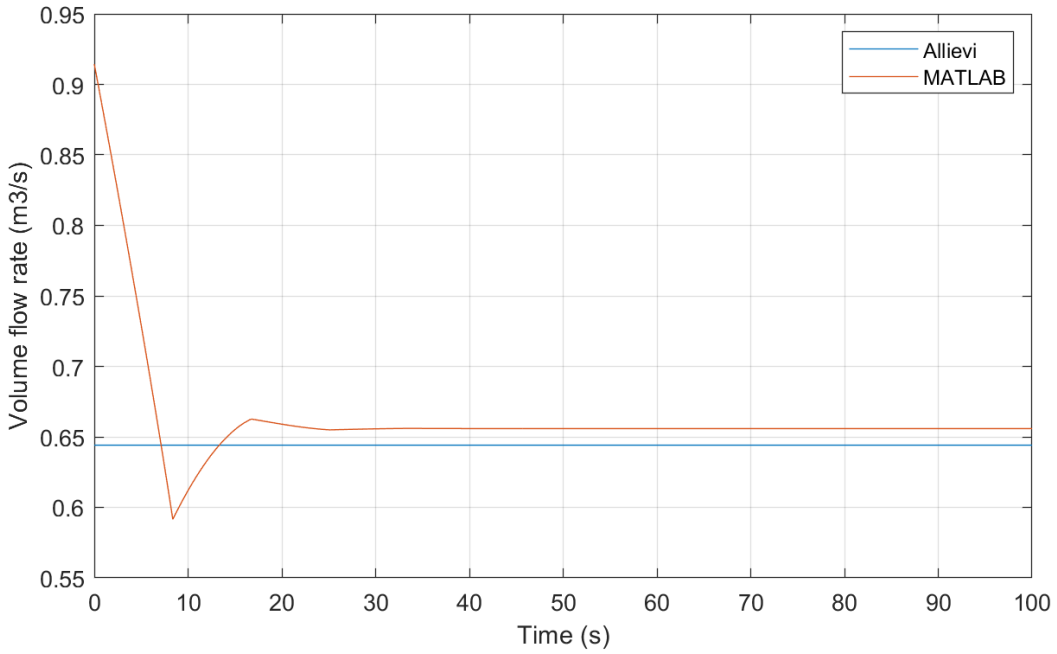

Figure 7.2: Outfall volume flow rate in function of time for Allievi and MATLAB with open valve

The volume flow rate was stable during the simulation with Allievi while a warm up time of about twenty-five second was observed in MATLAB simulation. This abrupt fall of pressure with MATLAB was due to the fact that the initial velocity (or volume flow rate) was set by the user select initial conditions and set for all nodes at steady state condition.

	Allievi	**MATLAB**
Pressure stabilised (m)	10.263	10.260
Comparison with Allievi (%)	-	-0.03
Volume flow stabilised (m^3/s)	0.644	0.656
Comparison with Allievi (%)	-	1.83

Table 7.1: Comparison of pressure and volume flow rate for open valve system

The Table 7.1 shows the difference of pressure and volume flow rate after stabilisation between both software. There was a difference of 0.03% in pressure head when comparing MATLAB to Allievi. The volumetric flow rate had a difference of 1.83% when comparing MATLAB to Allievi. This difference is explained by the implementation of setting of pressure and volume flow rate for between the two software. Indeed, the target velocity was set with MATLAB and the difference of pressure was set with Allievi.

The volume flow rate and pressure were similar (respectively 1.8% and -0.03% of difference between software) and stable in both software. The open system gave similar value for both software and could be used for starting simulations with steady state condition for more complex simulations. The next step was to study the valve closure.

3 Instantaneous Valve Closure

The instantaneous valve closure experiment was divided in two parts. The first one included an experiment without friction and in the second one, friction losses in pipe were introduced. The aim of this part was to compare the software with the water hammer analytical solutions, especially the level of pressure and the damping of the pressure wave when friction is added.

The following equation determines the surge of pressure resulting of a variation of fluid velocity in pipeline system.

$$\Delta P = \rho a \Delta V \tag{7.1}$$

In equation (7.1), ΔP is the pressure surge, ρ is the density of fluid, a is the celerity of wave and ΔV is the difference of velocity of the fluid. This formula is the well-known Joukowsky equation and the pressure can be transformed in pressure head:

$$\Delta H = \frac{a \Delta V}{g} \tag{7.2}$$

In equation (7.2), ΔH is the pressure head and g is earth gravity. This formulation was used in the next experiment to compare the experimental surge level with theories.

3.1 System without Friction

In this part, an instantaneous closure valve was set, with the friction factor set to zero.

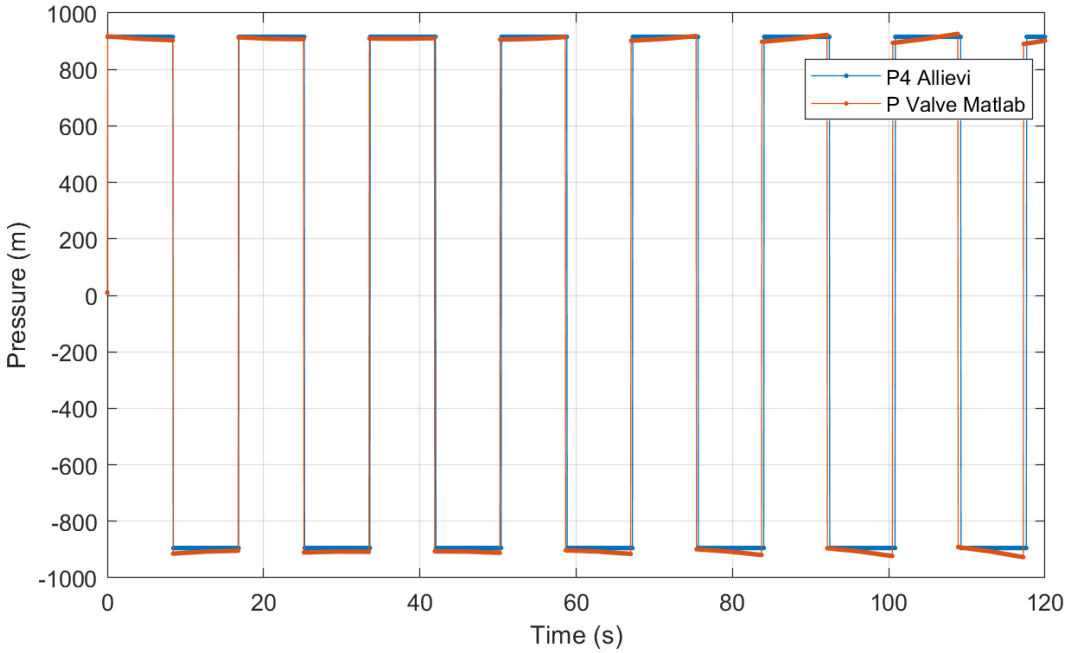

Figure 7.3: Pressure at the valve in function of time for Allievi and MATLAB without friction, for instantaneous closure

The maximum pressure was recorded for each simulation and compared to the theoretical equation (7.2) in the Table 7.2.

	Theory	**MATLAB**	**Allievi**
Pressure max (m)	908.00	929.64	929.64
Comparison with theory (%)	0	2.38	0.83

Table 7.2: Comparison of pressure surge between theory, MATLAB and Allievi without friction, for instantaneous closure

The first pressure surge was 2.4% and 0.8% bigger respectively for MATLAB and Allievi than the theory. These differences with the theory were acceptable to valid the software with the theory.

Allievi's plot shows horizontal maxima (i.e. constant in time) while MATLAB shows decreasing maxima until forty seconds and increasing maxima after forty seconds. In order to study this phenomena, we plotted a graph until one thousand and five hundred seconds:

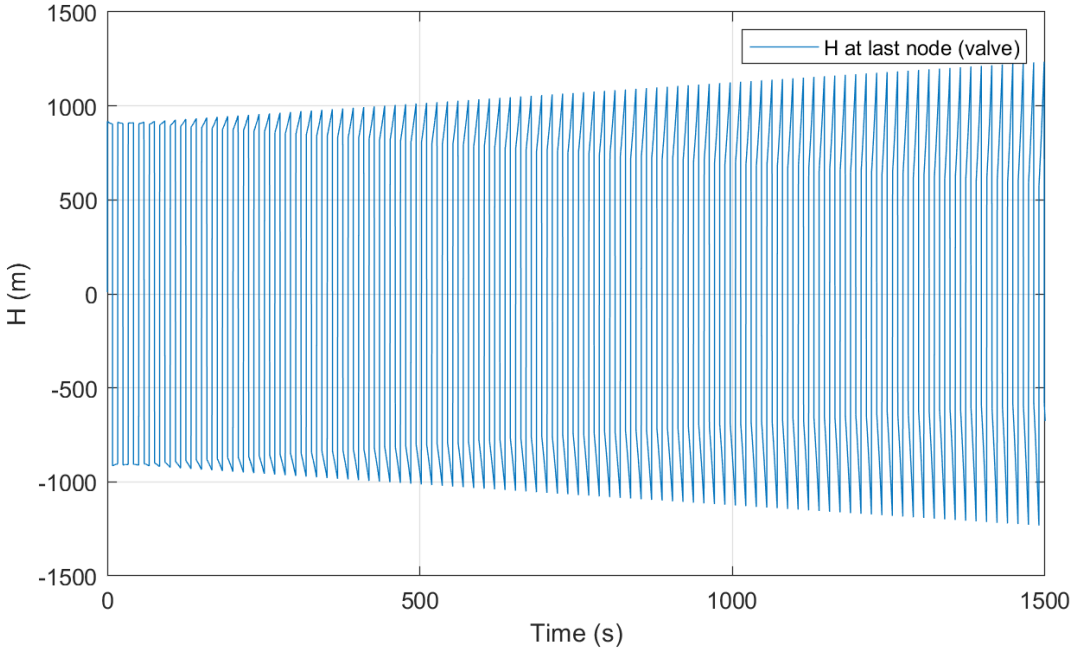

Figure 7.4: Pressure at the valve in function of time for MATLAB without friction, for instantaneous closure

In Figure 7.4 we observed that the pressure head was increasing during time. The squared signal at starting time became progressively a sawtooth waveform. The energy was conserved despite the fact that the maximum pressure increased at each iteration. Because of the law of conservation of energy, a time-dependent increase in pressure is only possible in situations with energy input.

In this section, we observed that the level of pressure for the first peaks was similar to the theory for both software. The problem was the evolution of the MATLAB pressure over the

time. Indeed, in MATLAB the pressure was increasing over time while energy was maintained. However, in real installations, the energy is never conserved because of friction in the system. For this reason, in the next section friction in the system were introduced in order to damp the pressure peaks and compare behaviour of software in situations closer to reality.

3.2 System with Friction

In this part the friction was added to the system with instantaneous closure valve. The aim was to compare the behaviour between Allievi and MATLAB. In Allievi, we added the absolute roughness of pipe in order to activated the friction in the simulation. The software computed the friction factor in the pipe in function of the roughness, diameter and Reynolds number with the so called Colebrook Equation 6.3.

In MATLAB, eight friction types were implemented (see chapter 6, section 3).

The case "Steady State Friction" was set to have a similar Colebrook equation in order to compute the Colebrook equation with a friction factor determinate before ruining the simulation. Indeed, the first step was to run the simulation with Allievi and the friction factor was saved and implemented as an input parameter in MATLAB. This method ensured that both software had the same friction losses conditions.

Figure 7.5 shows a comparison of the pressure head between Allievi and MATLAB:

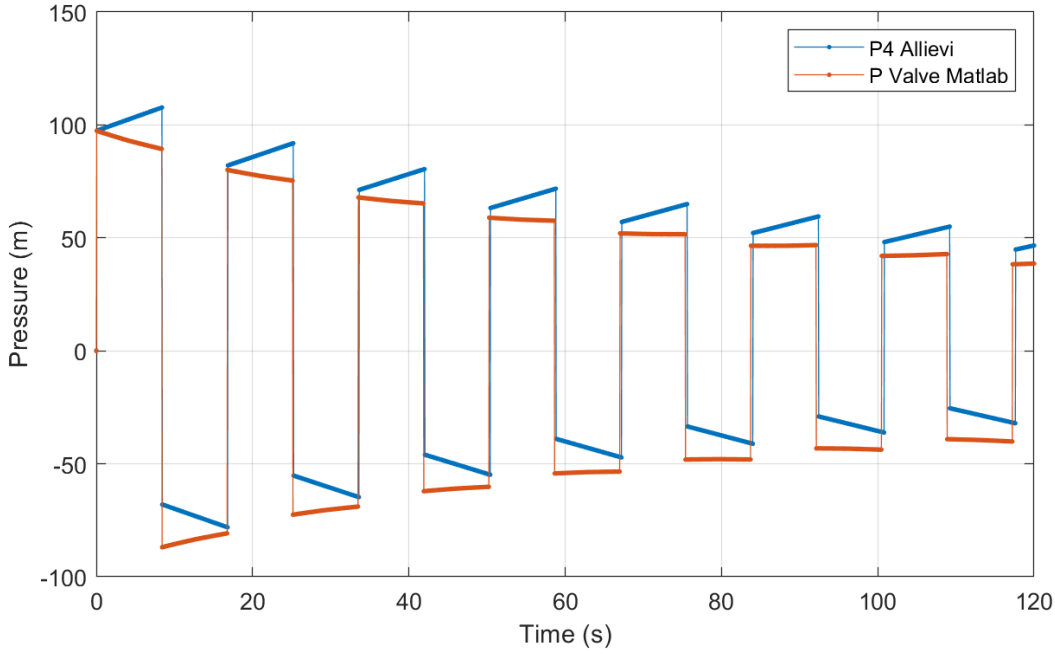

Figure 7.5: Pressure at the valve in function of time for Allievi and MATLAB with friction for instantaneous closure

As shown in Figure 7.5, the period of the waves for Allievi was 1.69% bigger than in MATLAB. This difference was probably due to the difference of the time step between the two software. Indeed, Allievi had 0.4% bigger time steps than MATLAB. In the next Table 7.3, the size of the first pressure surge for both software were compared.

	Theory	MATLAB	Allievi
Pressure max (m)	97.53	97.43	107.71
Difference from theory (%)	0	-0.10	10.44

Table 7.3: Comparison of pressure surge between theory, MATLAB and Allievi with friction for instantaneous closure

Table 7.3 shows a comparison of the size of the first pressure surge to the theoretical Joukowsky equation (7.2). MATLAB had -0.10% of pressure less than the theory and Allievi 10.44% more pressure.

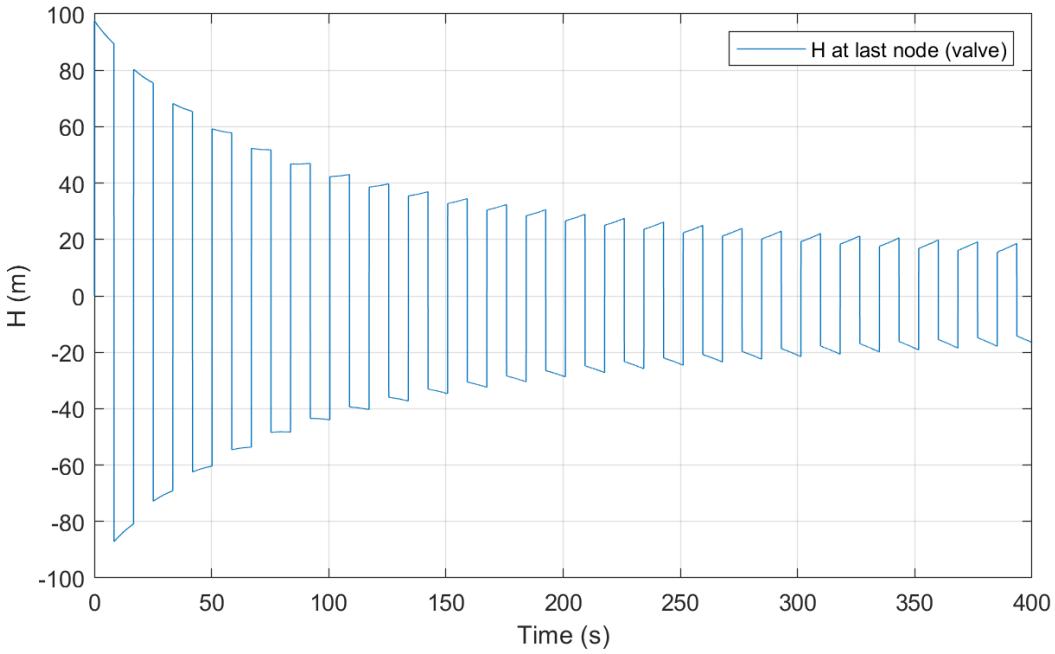

Figure 7.6: Pressure at the valve in function of time for MATLAB with friction for instantaneous closure

In Figure 7.6 the slopes of maxima and minima of the signal changed over time. In this case the slope was considered positive when it tended towards to the positive or negative infinity and it was considered negative when it tended towards zero. Here we observed that the slope was negative for the first 75 second and positive until the end of the simulation. The positive slope is called line packing effect. The line packing appeared in pipes with friction because the water hammer wave looses velocity due to friction. Indeed the displacement of the wave is subject to friction. The friction slows down and the pressure increases again. The negative slope appeared because the regime was not fully established at the beginning of the simulation. Indeed the steady state conditions of velocity were not stable and the velocity in the pipe decreased during the first seconds of the simulation. The water hammer wave was relaxed as it moved forward because the speed slowed down in the pipe in front of it.

In this section, the damping factor was not studied because the shape of the peaks were not the same and it was difficult to take a value in the peaks which was the same for both software (mean of the peak, left side or right side). This section showed that the maximum level of pressure were

similar and validated the behaviour of water hammer experiment for the software. It proved that a warming up time (time of simulation with no wave command) had to be added to the simulation to stabilise the pressure and velocity condition before starting the simulation in the next experiments too.

4 Sinusoidal Valve Signal

The aim of this experiment was to compare the behaviour of the system with a sinusoidal valve closure. The sinusoidal was added to the system because it was the system implemented in Allievi that came closest to a pressure wave. It was important to know whether the sinusoidal valve could replace a pressure wave in order to simulate coastal valve in a system to simulate a pipeline in real conditions. The sinusoidal valve was implemented in MATLAB according to the equation (6.6) and the initial aperture and amplitude were the following:

$$\tau = 0.8 + 0.2 \sin\left(\frac{2\pi}{2}t + \frac{\pi}{4}\right) \tag{7.3}$$

The equation 7.3 respects the condition of the experiment with an initial aperture equal to 80% of the total aperture and an amplitude equal to ±20% of the total aperture.A fifty seconds warm up time is implemented in MATLAB in order to stabilise the velocity and pressure along the pipe before starting the sinusoidal valve closure.

The following graphs show the pressures and flow rates at the valve.

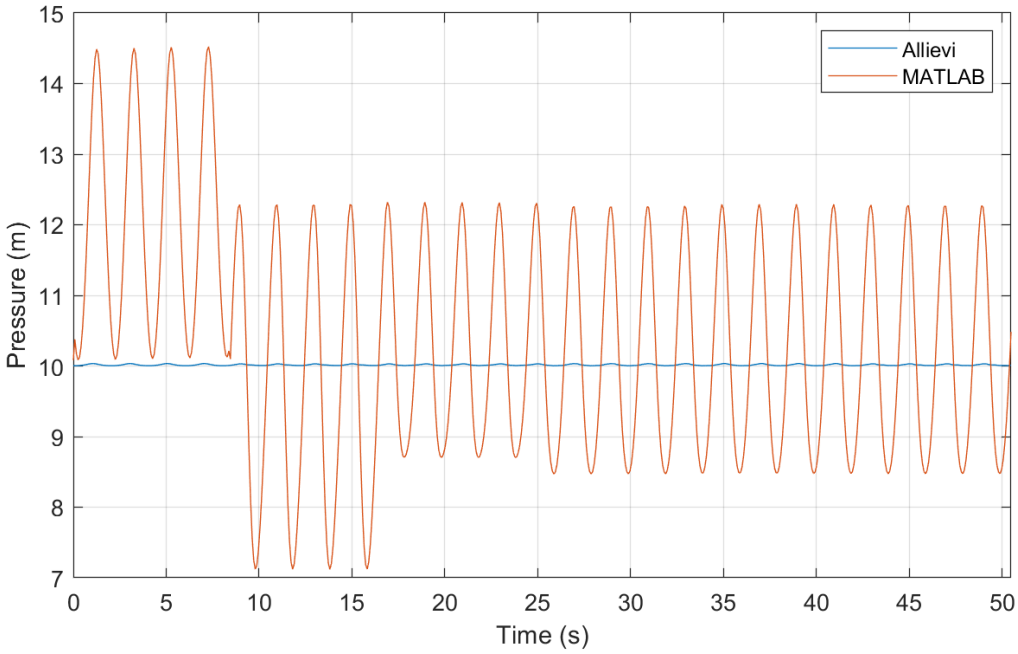

Figure 7.7: Pressure at the valve in function of time for Allievi and MATLAB with sinusoidal valve closure

The pressure plot (Figure 7.7) shows the difference of pressure between both software. The MATLAB amplitude after stabilisation is of the order of 3.8 m and Allievi has an amplitude wave of 0.0334 m. MATLAB difference compared to Allievi is equal to -99.12%.

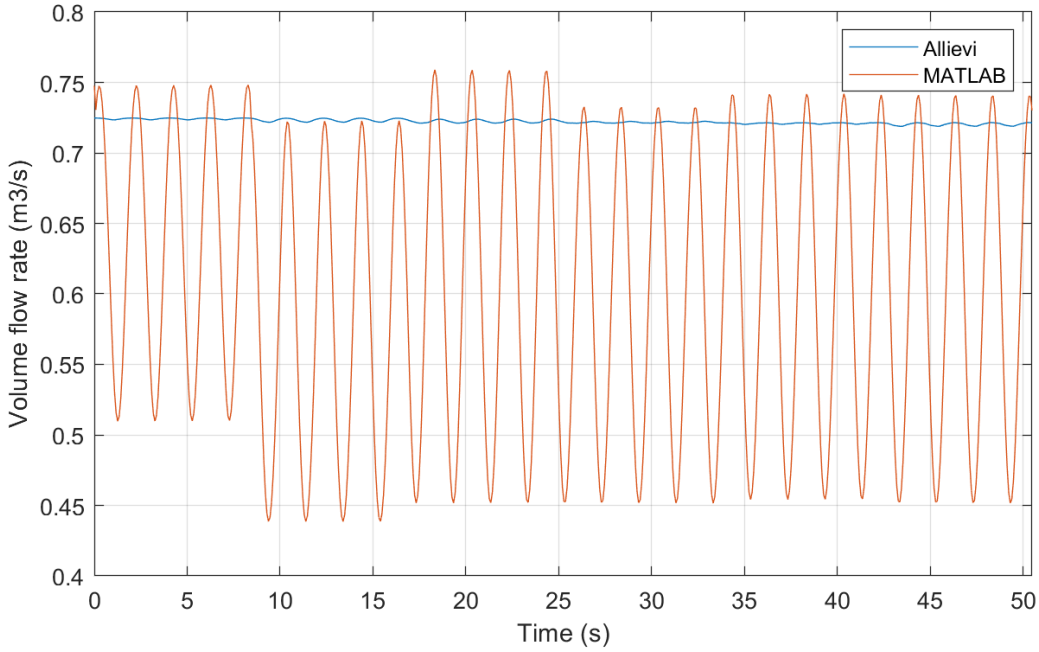

Figure 7.8: Volume flow rate at the valve in function of time for Allievi and MATLAB with sinusoidal valve closure

The flow rate plot (Figure 7.8) shows the difference of volume flow rate between both software. The MATLAB flow rate amplitude was of the order of 0.3 m^3/s after stabilisation and Allievi had a volume flow rate amplitude wave of 0.008 m^3/s. MATLAB difference compared to Allievi was equal to -99.33%.

In this experiment, the pressure and flow rate calculated by the two software had a difference that exceeded 99%. This difference was too significant to admit an equivalence between the two software. The difference could come from the implementation of the boundary condition. Indeed Allievi impose the reservoir pressure at both sides of the pipe, which induces a flow rate by difference of pressure even if the valve restricts the orifice at the downstream. MATLAB implements other boundary conditions, indeed, the flow rate is created with a condition of pressure and an initial velocity at the upstream. The conditions of flow rate and pressure at the downstream of the pipe are calculated. The difference of flow rate is explain by this difference of implementation of the boundary conditions in both software. With these boundary conditions, MATLAB computes the volume flow rate in function of the dimensionless closure of the valve. The volume flow rate was more similar to what was expected: 0.75 m^3/s when the valve was open and 0.45 m^3/s at low level, which corresponded to the 60% of closing aperture of the minimum limit of sinus.

In this section, the limit of the comparison between software was reached. Indeed, the difference between the implementation of boundary condition gave too many differences in output pressure and volume flow rate. MATLAB has implementation of boundary condition that correspond of the theory of flow in this experiment and the folum flow rate allong the pipe make sense while Allievi had non-compliant results. The boundary conditions of MATLAB were more recommended to simulate the typical pipe because all the parameters were known in the intake and the pressure and flow rate in computed in the outfall. This way of implementation gives more freedom in outflow boundary implementation. The sinusoidal valve couldn't be used to simulate

a coastal wave. In the next chapter only MATLAB was used with other condition to be as close as possible to the typical pipe conditions.

5 Discussion

In this chapter, we studied the volume flow rate and pressure in the output of similar pipeline in two software. This chapter was divided in thee parts: a full open valve system, an instantaneous valve closure and a sinusoidal closure valve signal. The similarity for the two first experiment were the level of pressure and the frequency peaks of the water hammer phenomenon. Similarity between these two output parameters proved that both software had similar mathematical implementation. Indeed, the level of pressure and the wave propagation time depends on the MOC code implementation (see chapter 4).

Even if the level of pressure peaks were the same in both software, differences were present in the implementation of the pressure losses. Indeed, the line packing effect was present in water hammer peaks in Allievi and the same effect was observed after a few travel time in MATLAB simulations. The line packing effect was a consequence of friction losses in pipe and the implementation of code in Allievi could not be studied (no open source system). However the behaviour of the water hammer wavefronts were more in line with reality in Allievi (see test bench experiments in report: [1], [26], [27]).

In the last experiment the limit of both software was reached in reason of the implementation of the boundary condition. Indeed, MATLAB implements a volume flow rate and pressure in the input and the pressure and volume flow rate at output are computed while Allievi needs pressure in the input and output and compute the volume flow in pipe rate from this difference of pressure. The pressure in Allievi software was more constant and the volume flow rate in the system was constant too. In our case, MATLAB method was more recommended because we wanted to impose conditions at the beginning and study what happens at the outfall.

Overall, this chapter showed that a sinusoidal valve couldn't be used to simulate a coastal wave because the implementation of a coastal wave in the output doesn't affect the section of the outfall but the pressure in the outfall. It was the reason why the next step of the project was to replace the valve at the outfall by an input pressure that simulates a pressure wave at the end of the pipe. This experiment could be run only with MATLAB because Allievi have no similar boundary conditions.

Sinusoidal Excitation

1 Introduction

The aim of this chapter was to study the inner pipe phenomena with a simple periodic wave at the outfall, especially the level of pressure, location of this pressure peaks and periodicity of pressure and flow rate phenomenon.

This chapter was divided in three parts. The first part included an analysis with a simple sinusoidal pressure wave without friction. It also included a sensitivity analysis of the pressure inside the tube according to diverse parameters related to the geometry of the tube or to the pressure injected. The second part included the same condition and analysis and included friction the system. The third part included a wave spectrum and a sensitivity analysis. The aim was to understand which parameters have a significant impact on the pressure and volume flow rate inside the pipe.

The configuration of the installation in this chapter was the typical pipe (see chapter 3, section 1), with no slope. Analysis with and without friction were realised. The steady state friction was used as explained in chapter 6, section 3.

2 Sinusoidal Excitation without Friction

In this part, a simple pressure wave was setup as boundary condition in the nozzle (see chapter 6 subsection 4.4). The friction was deactivated during the simulations. A typical wave with an amplitude of 0.27 m and period of 3 second was chosen to simulate a simple coastal wave [28]. The pressure head along the pipe for the 9 travel periods are available in appendix (3).

Unidirectional wind speed (km/h)	19
Average height of wave (m)	0.27
Average wavelength (m)	8.5
Average wave period (s)	3.0
Average wave speed (km/h)	10.2

Table 8.1: Summary of typical sea wave with 19 km/h of wind speed according to Wikipedia [28]

Table 8.1 is a summary of the wind wave used in the pressure sinus wave simulations.

2.1 First Sensitivity Analysis

This experiment started with a sensitivity analysis. The aim was to highlight the parameters that had the greatest impact on the pressure increases in the pipe. For that purpose, four independent input parameters were identified and individually varied. The measured responses were the max of pressure and volume flow rate in the pipe. The input parameters varied as follows:

Value	nominal	min	max	variation
Length of pipe (m)	900	675	1125	±25%
Wave celerity in pipe (m/s)	215	161	269	±25%
Pressure wave amplitude (m)	0.27	0.20	0.34	±25%
Pressure wave period (s)	3.00	2.25	3.75	±25%

Table 8.2: Input parameters and variation for sensitivity analysis

Other parameters such as the internal pipe diameter, the pipe roughness Poisson's ratio of the pipe material, the pipe Young modulus and the density of the pipe water could have been included in the experiment. However all these parameters were comprised within the wave celerity (a). This is why it was chosen to vary only the pressure wave celerity.

After each experiment, a plot of the mean, the max and min values of the pressure and the flow rate along the pipe was generated. Figure 8.4 is the plot of these 5 responses for a typical pipe, without slope.

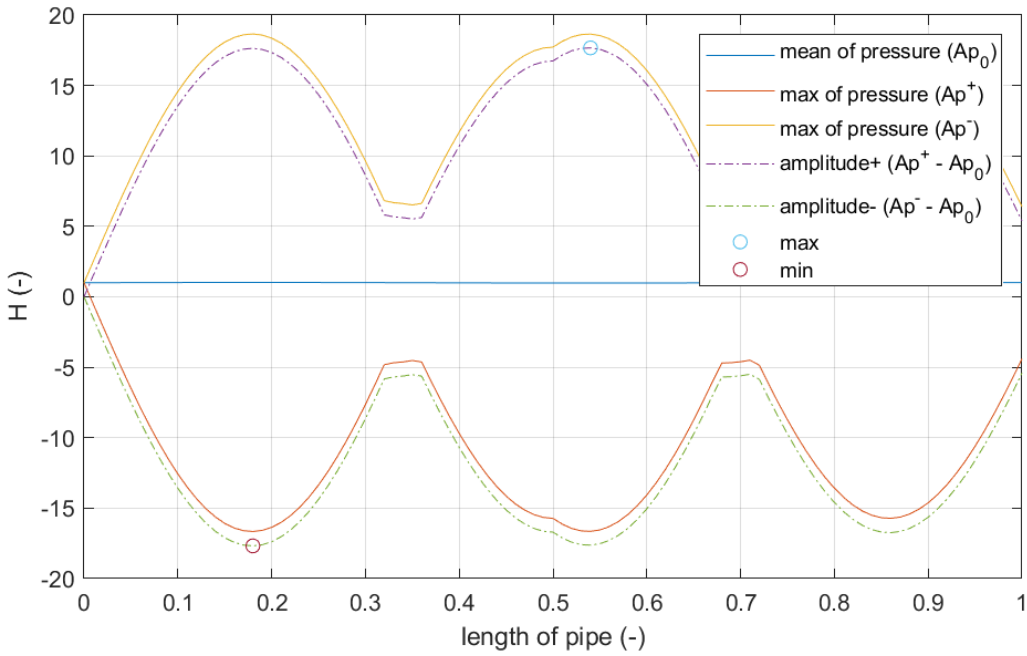

Figure 8.1: Mean, max and min of pressure for the typical pipe experiment without friction

The graph summarises an analysis over 20 oscillations. The mean of pressure line (Ap_0) represents the pressure at steady state conditions. For each position in the pipe, the max and min values over the 20 oscillations were calculated. Then the min (red) and max (yellow) pressure lines (Ap^- and Ap^+) represent the envelope of pressure along the pipe. The amplitude+ and amplitude− lines represent the subtraction of the maximum and minimal pressure to the mean line.

Table 8.3 presents the results of the maximal amplitude and period of the pressure wave. The amplitude normalised is the scaling of the pressure by the pressure of the reservoir.

Simulation	H ampl. max (m)	H ampl. max norm. (-)	H period (s)
Typical pipe	0.88	17.67	3.00
Pipe length max	0.54	10.80	3.00
Pipe length min	1.87	37.49	3.00
Wave celerity max	0.81	16.25	3.00
Wave celerity min	0.70	14.04	3.00
Wave amplitude max	1.10	22.09	3.00
Wave amplitude min	0.66	13.25	3.00
Wave period max	0.81	16.19	3.75
Wave period min	0.70	14.04	2.25

Table 8.3: Absolute pressure results for ±25% sensitive analysis

Table 8.4 presents the results of the maximal amplitude and period of the volume flow rate wave. The amplitude normalised is the scaling of the flow rate by flow rate at steady state conditions.

Simulation	Q ampl. max (m)	Q ampl. max norm. (-)	Q period (s)
Typical pipe	3.81E-02	4.03E-02	3.00
Pipe length max	2.35E-02	2.79E-02	3.00
Pipe length min	7.98E-02	7.28E-02	3.00
Wave celerity max	2.84E-02	3.00E-02	3.00
Wave celerity min	4.03E-02	4.26E-02	3.00
Wave amplitude max	4.76E-02	5.03E-02	3.00
Wave amplitude min	2.86E-02	3.02E-02	3.00
Wave period max	3.53E-02	3.73E-02	4.19
Wave period min	3.02E-02	3.19E-02	2.25

Table 8.4: Absolute volume flow rate results for ±25% sensitive analysis

In order to analyse the two previous tables, a comparison of the maximum amplitude and period to the typical pipe experiment was realised. The results are presented in Table 8.5.

Simulation	H max norm.	H period	Q max norm.	Q period
Typical pipe	0%	0%	0%	0%
Pipe length max	-39%	0%	-31%	0%
Pipe length min	112%	0%	81%	0%
Wave celerity max	-8%	0%	-26%	0%
Wave celerity min	-21%	0%	6%	0%
Wave amplitude max	25%	0%	25%	0%
Wave amplitude min	-25%	0%	-25%	0%
Wave period max	-8%	25%	-7%	40%
Wave period min	-21%	-25%	-21%	-25%

Table 8.5: Response value compare to typical pipe

Table 8.5 shows the impact of each input parameter on the maximum pressure, the maximum

flow rate, the period of pressure and the period of volume flow rate. The input parameter that most impacted the pressure and flow rate was the length of the pipe. Indeed, a 25% reduction of the length increased the pressure by more than 110% and the flow rate by more than 80%. While a 25% increase of the pipe length reduced the system's response level by more than 30%.

To understand the evolution of the response regarding the different input parameters, the next section was a study of the stability of the system response relatively to the different input parameters in a larger range of data. The response phenomena in a large range are described on section 3 page 39.

2.2 Convergence of Simulation

The aim of this second part was to test the stability of the system's response in function of the number of oscillation (i.e. the number of time steps) of the simulation. The aim was to determine whether the pressure and volume flow rate response depended on the time of simulation. As a result of the simulation, the graph of the maximum pressure and volume flow rate in function of the number of oscillations was generated:

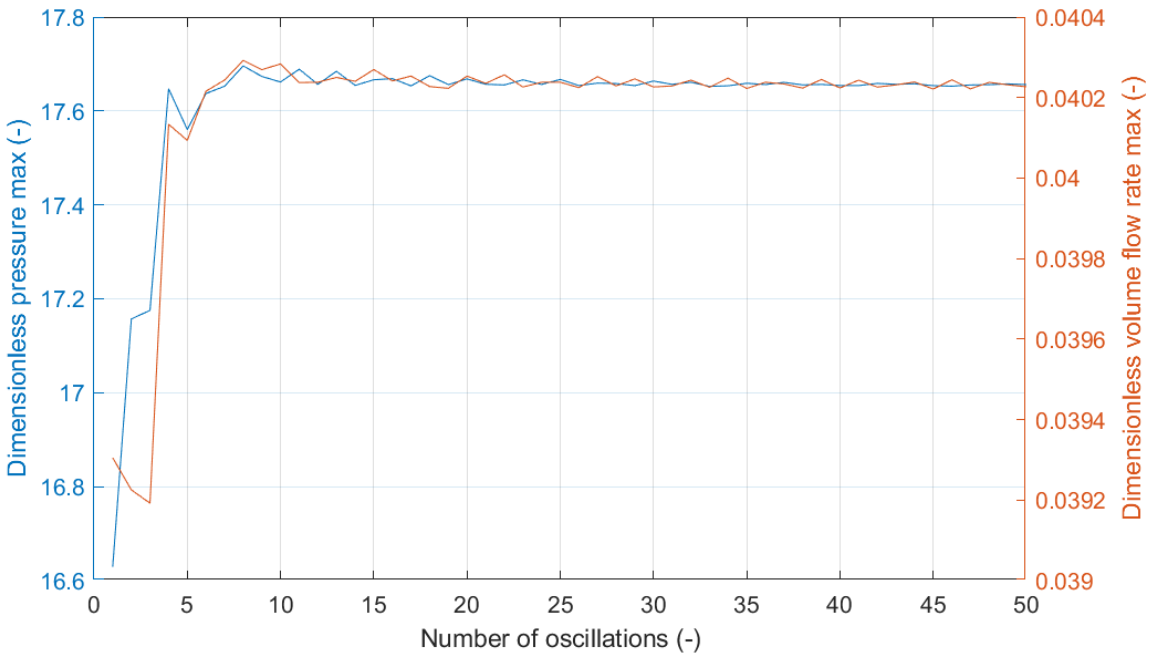

Figure 8.2: Maximum of dimensionless pressure and volume flow rate in function of the oscillations number of the typical pipe without friction simulation

Figure 8.2 shows the response's stability in function of the number of oscillations of the simulation. This figure shows that the maximal pressure and the volume flow rate were stable after 10 oscillations. Therefore, to reach the point of stability during the next experiments, the number of oscillations was fixed to 20.

The phenomenon of resonance appeared when the number of wave reaches a multiple or a multiple plus a half of a natural number along the pipe (see subsection 3.3, page 43). One point of resonance was studied (typical pipe without friction and $a = 150$ m/s) with the simulation without frictions.

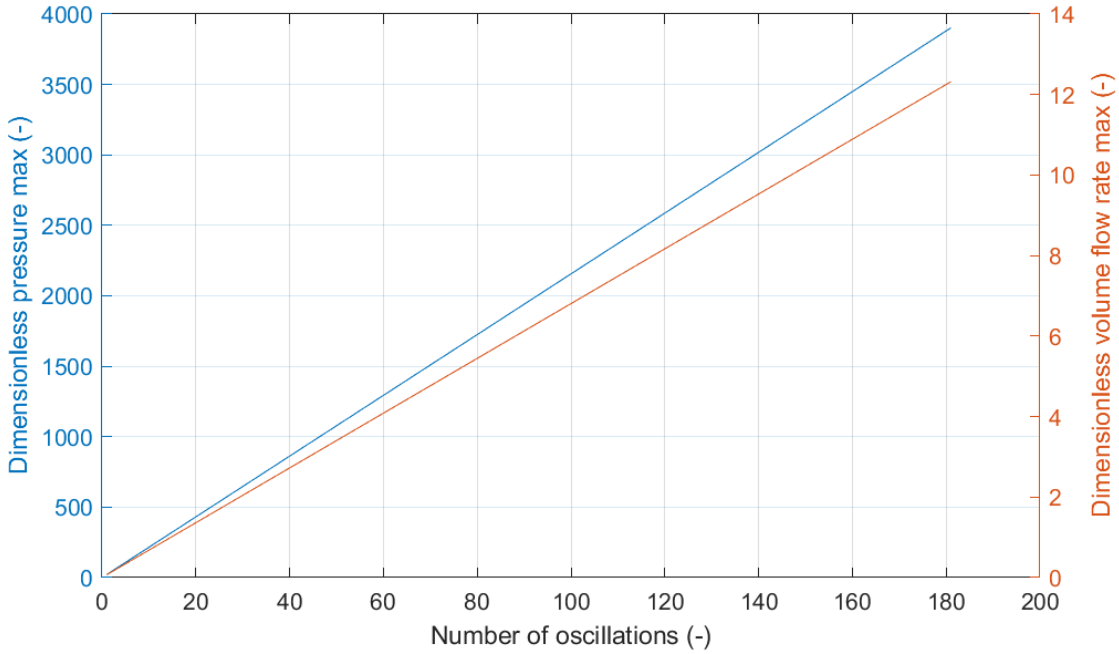

Figure 8.3: Maximum of dimensionless pressure and volume flow rate in function of the oscillations number of a simulation without friction with $a = 150$ m/s

Figure 8.3 shows the constant increasing pressure and volume flow rate at resonance point. The responses increased at an infinite level during the time of the simulation. For this reason, simulations without friction were useful to study the resonance frequencies of the pipe but the pressure and volume flow levels were not exploitable. The next section shows the same simulation but with the addition of friction. The resonance points, pressure and flow rate comparison were treated in the next section.

Few conclusions can be drawn from this experiment. First of all periods of the pressure wave and volume flow wave were similar between simulations and corresponded exactly with the pressure period injected. The maximum of pressure would have to be studied with a bigger range of input parameter to be understood. Indeed, it was not possible to interpret such a wide variety of output pressure measurement with only 3 simulations (a range of three simulation for each variate input parameters). In subsection 2.2, we showed that at certain simulation point the resonance phenomenon appeared and the the volume flow rate and pressure grew until the infinite. In the next section these points of resonance with friction were studied to determine the maximum pressure level of this point. It should also be noted that the location of pressure peaks was not listed here. To understand the evolution of the pressure response reported to the different input parameters, the next section studied the different input parameters in a larger range of data.For example a loop can be added to the MATLAB simulation in order to run the simulation with the aim of studying the impact of wave celerity (or other parameters) on the pressure response.

3 Sinusoidal Excitation with Friction

In this part, a simple pressure wave was injected in the outfall (see chapter 6, subsection 4.4) and the friction equations were activated during the simulations. A typical wave with an amplitude of 0.27 m and a period of 3 second was chosen to simulate a simple coastal wave [28]. The

summary of the wave is available in Table 8.1.

3.1 First Sensitivity Analysis

This experiment started with a sensitivity analysis. The aim was to highlight the parameters that had the greatest impact on the pressure increase in the pipe. For that purpose, four independent input parameters were identified and individually varied. The measured response was the max of pressure and volume flow rate in the pipe. The input parameters varied as follows:

Value	nominal	min	max	variation
Length of pipe (m)	900	675	1125	±25%
Wave celerity in pipe (m/s)	215	161	269	±25%
Pressure wave amplitude (m)	0.27	0.20	0.34	±25%
Pressure wave period (s)	3.00	2.25	3.75	±25%

Table 8.6: Input parameters and variation for sensitivity analysis

Other parameters such as the internal pipe diameter, the pipe roughness Poisson's ratio of the pipe material, the pipe Young modulus and the density of the pipe water could have been included in the experiment. However all these parameters were comprised within the wave celerity (a). This is why it was chosen to vary only the pressure wave celerity.

After each experiment, a plot of the mean, the max and min values of the pressure and the flow rate along the pipe was generated. Figure 8.4 is the plot of these 5 responses for a typical pipe, without slope.

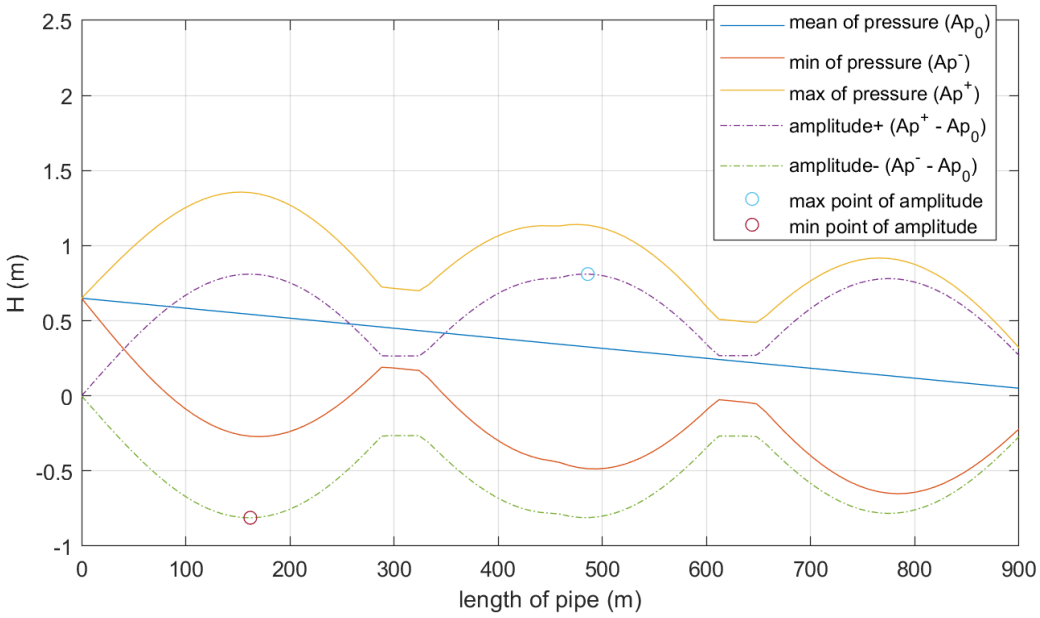

Figure 8.4: Mean, max and min of pressure for the typical pipe experiment

The graph summarises an analysis over 20 oscillations. The mean of pressure line (Ap_0) represents the pressure at steady state conditions. For each position in the pipe, the max and min values

over the 20 oscillations were calculated. Then the min (red) and max (yellow) pressure lines (Ap^- and Ap^+) represent the envelope of pressure along the pipe. The amplitude+ and amplitude− lines represent the subtraction of the maximum and minimal pressure to the mean line.

Table 8.7 presents the results of the maximal amplitude and period of the pressure wave. The amplitude normalised is the scaling of the pressure by the pressure of the reservoir.

Simulation	**H ampl. max (m)**	**H ampl. max norm. (-)**	**H period (s)**
Typical pipe	0.81	1.25	3.00
Pipe length max	0.52	0.65	3.00
Pipe length min	1.66	2.57	3.00
Celerity wave max	0.78	1.19	3.00
Celerity wave min	0.66	1.01	3.00
Amplitude wave max	1.01	1.56	3.00
Amplitude wave min	0.61	0.94	3.00
Period wave max	0.76	1.17	3.75
Period wave min	0.66	1.01	2.25

Table 8.7: Absolute pressure results for ±25% sensitive analysis

Table 8.8 presents the results of the maximal amplitude and period of the volume flow rate wave. The amplitude normalised is the scaling of the flow rate by flow rate at steady state conditions.

Simulation	**Q ampl. max (m)**	**Q ampl. max norm. (-)**	**Q period (s)**
Typical pipe	3.45E-02	3.64E-02	3.00
Pipe length max	2.20E-02	2.33E-02	3.00
Pipe length min	6.99E-02	6.37E-02	3.00
Celerity wave max	2.65E-02	2.80E-02	3.00
Celerity wave min	3.73E-02	3.94E-02	3.00
Amplitude wave max	4.31E-02	4.55E-02	3.00
Amplitude wave min	2.59E-02	2.74E-02	3.00
Period wave max	3.26E-02	3.44E-02	3.75
Period wave min	2.79E-02	2.94E-02	2.25

Table 8.8: Absolute volume flow rate results for ±25% sensitive analysis

In order to analyse the two previous tables, a comparison of the maximum amplitude and period to the typical pipe experiment was realised. The results are presented in Table 8.9.

Simulation	H ampl. max	H period	Q ampl. max	Q period
Typical pipe	0%	0%	0%	0%
Pipe length max	-36%	0%	-36%	0%
Pipe length min	106%	0%	103%	0%
Celerity wave max	-4%	0%	-23%	0%
Celerity wave min	-19%	0%	8%	0%
Amplitude wave max	25%	0%	25%	0%
Amplitude wave min	-25%	0%	-25%	0%
Period wave max	-6%	25%	-6%	25%
Period wave min	-19%	-25%	-19%	-25%

Table 8.9: Response value compare to typical pipe

Table 8.9 shows the impact of each input parameter to the maximum pressure and flow rate and the impact on the period of pressure and volume flow rate. The input parameter that impacted the most the pressure and flow rate was the length of the pipe. Indeed, a 25% reduction of the length increased the pressure and flow rate more than 100%. While a 25% increase of the pipe length reduced the system's response level by almost 36%.

The first conclusion of this section is that the period of the wave of pressure and the wave of volume flow rate were similar between simulations and corresponded exactly with the pressure period injected. Like in the previous section, the maximum of pressure should have been studied with a bigger range of input parameters to be understand. This is why the evolution of the response reported to the different input parameters, the stability of the system response and the different input parameters in a larger range of data were studied in the next section. It should also be noted that the location of pressure peaks was not listed here.

3.2 Convergence of the Simulation

The aim of this third part was to test the stability of the system's response in function of the number of oscillation (i.e. the number of time steps) of the simulation. One oscillation time was equal to four travel time of a wave. With a typical pipe (L = 900 m, a = 215 m/s) one oscillation in MATLAB represents 16.7 seconds of simulation. The aim was to determine if the pressure and volume flow rate response depended on the time of the simulation. As a result of the simulation, the graph of the maximum pressure and volume flow rate in function of the number of oscillations was generated:

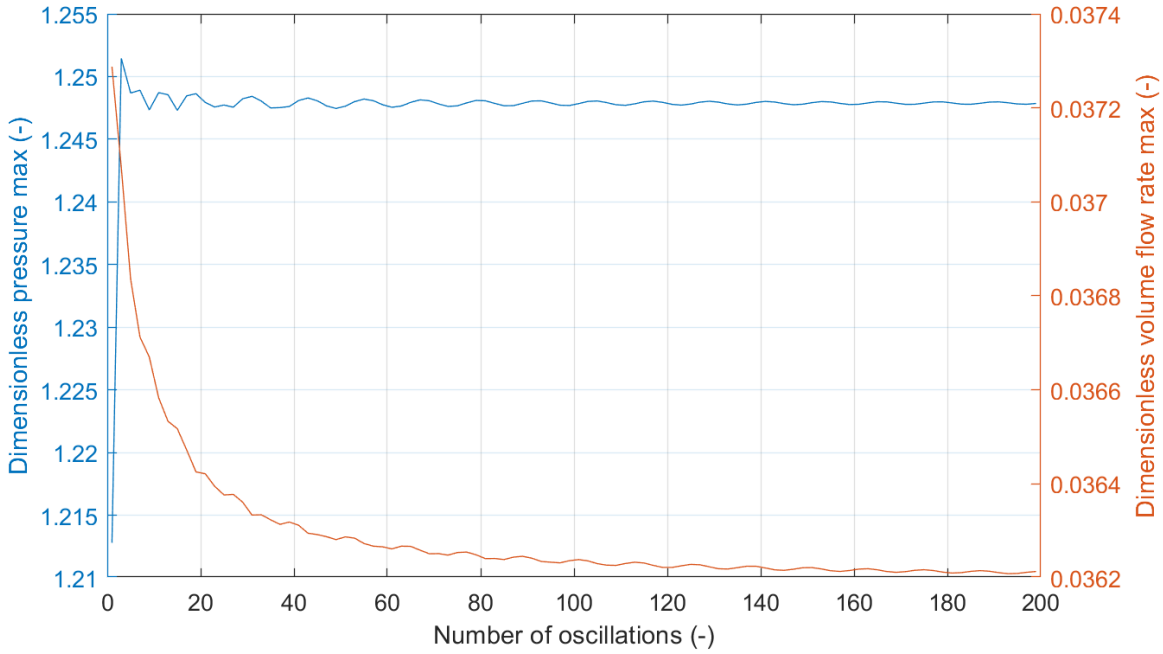

Figure 8.5: Maximum of dimensionless pressure and volume flow rate in function of the oscillations number of the simulation

Figure 8.5 shows the response's stability in function of the number of oscillations of the simulation. This figure shows that the maximal pressure was converged after 10 oscillations while the maximum volume flow rate decreased of 2.98% after 200 oscillations. Because the volume flow rate tended to stabilise as the oscillations occurred, and because the volume flow rate decreased by less than 3% over 200 oscillations, the number of oscillations was fixed to 20 for the next experiments. It saved computing time in order to ran simulation with a large number of oscillation.

3.3 Length of Pipe Analysis

The aim of this part was to analyse the impact of the pipe's length on the system's response. Simulations with the typical pipe condition were run for a length of the pipe starting from 10 meters to 2000 meters, increasing by 1 meter with each simulation.

Figure 8.6 shows the maximum of pressure and volume flow rate in function of the pipe's length.

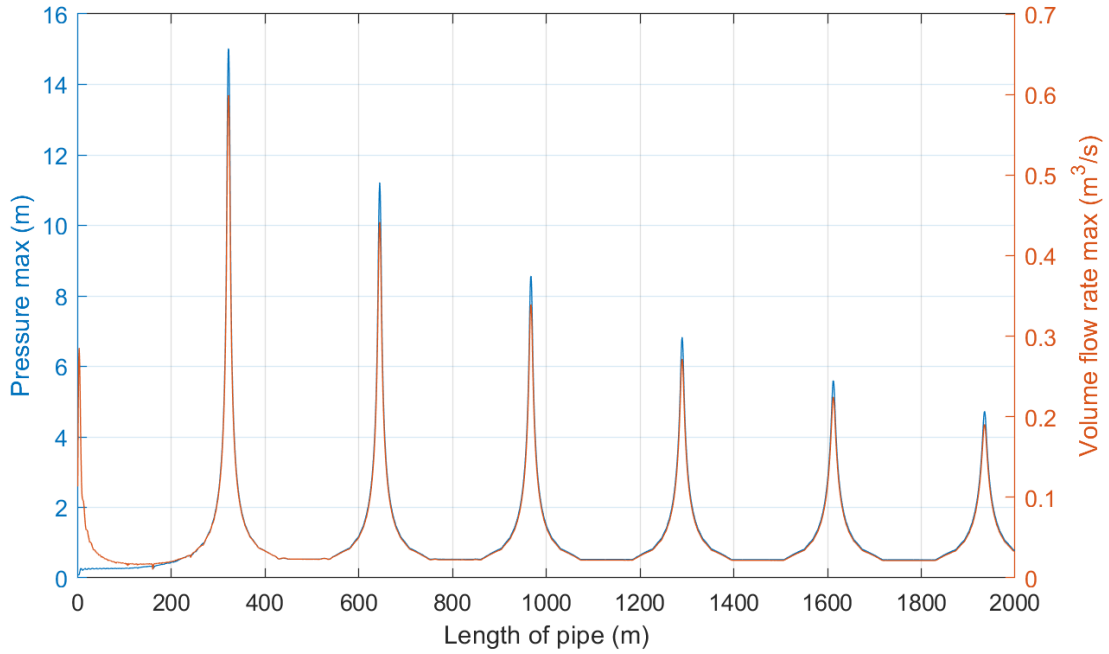

Figure 8.6: Maximum of pressure and volume flow rate in function of the pipe length

Pressure and volume flow rate for all peaks are reported in the table below:

L (m)	323	645	967	1290	1613	1935
H (m)	15.0	11.2	8.6	6.8	5.6	4.7
Q (m3/s)	0.599	0.442	0.339	0.272	0.224	0.191

Table 8.10: peaks of pressure and volume flow rate in function of the length of pipe

In order to analyse Figure 8.6, the pressure was adjusted with the reservoir pressure and the flow rate was adjusted with the initial flow rate in the dimensionless Figure 8.7.

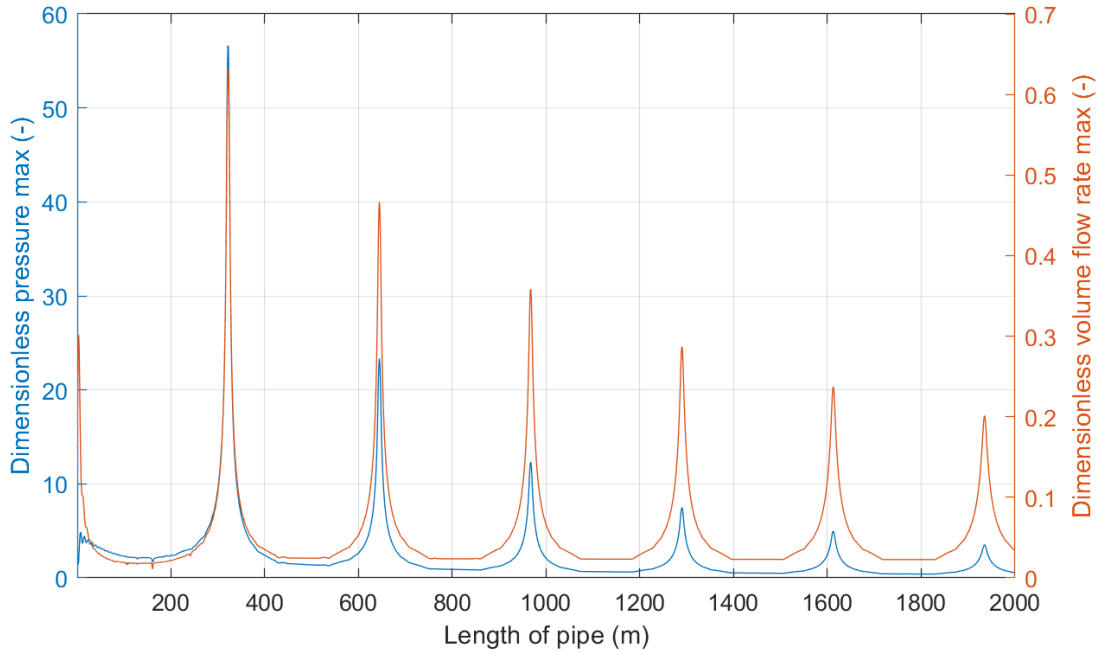

Figure 8.7: Maximum of dimensionless pressure and volume flow rate in function of the pipe length

Figure 8.7 shows the of pressure and volume flow rate where length of pipe corresponds to a multiple of pressure wave. The pressure peaks decreased with the length of pipe. The first peaks reached 56.6 times the pressure of the reservoir and is 3 times bigger than the second one. In order to calculate the length of the pipe that had the resonance peaks, the length of wave was defined with the equation Equation 8.1.

$$\lambda = aT \tag{8.1}$$

In Equation 8.1, λ is the number of wave, a is the wave celerity and T is the wave period. This equation was included in Equation 8.2 to find the length of pipe that created peaks of pressure and volume flow rate.

$$L = n\lambda \tag{8.2}$$

In Equation 8.2, n is the number of waves in the pipe. In our case, it describes the number of sinuses in the pipeline. The equation shows the length of the pipe, where resonant frequency appeared in function of n. The fundamental frequency was found with n equal to 0.5. The following natural frequencies of pipe were found every of 0.5 waves because there was a whole sinusoidal number or a whole number of wave plus half one in the pipe to reach the natural frequency of resonance. The table below shows the dimensionless peaks of pressure and volume flow rate and the number of wave n.

n (-)	0.5	1	1.5	2	2.5	3
L (m)	323	645	967	1290	1613	1935
H (-)	56.6	23.4	12.3	7.5	5.0	3.5
Q (-)	0.63	0.47	0.36	0.29	0.24	0.20

Table 8.11: Dimensionless peaks of pressure and volume flow rate in function of the length of pipe

Table 8.10 shows the different resonance modes according to the pipe's length. The fundamental frequency was reached with n equal to 0.5 and the maximal pressure is 56 times bigger than the pressure of the reservoir.

This analysis linked the peaks of resonance to the length of pipe when n was a multiple of 0.5 in the formula: $L = \frac{n}{aT}$ The peaks of pressure and volume flow rate were present and they decreased with the increasing of the number n. The next step was to analyse the input parameter a to determine if the formulation above was correct with the variation of a instead of L.

3.4 Wave Celerity Analysis

The aim of this part was to analyse the impact of the wave celerity on resonance frequencies. In order to understand the impact of the wave celerity as a whole. In this experiment, we analysed the response of the system for a velocity range from a non-rigid pipe to a perfectly rigid pipe.

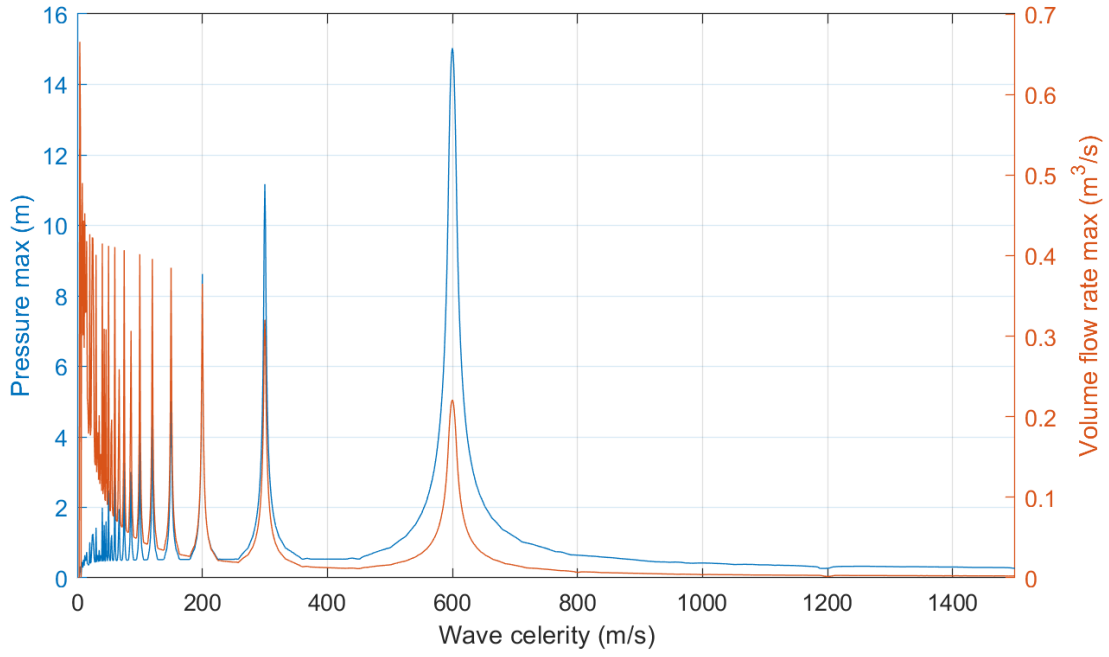

Figure 8.8: Maximum of pressure and volume flow rate in function of the wave celerity

The maximum pressure was reached with a celerity of 600 m/s, which corresponds to a material with a Young modulus equal to 9.5 GPa. This value does not correspond to any materials used in submarine pipelines. The maximal pressure was equal to 15.05 m. In order to analyse Figure 8.8,

the pressure was adjusted with the reservoir pressure and the flow rate was adjusted with the initial flow rate in the dimensionless Figure 8.9.

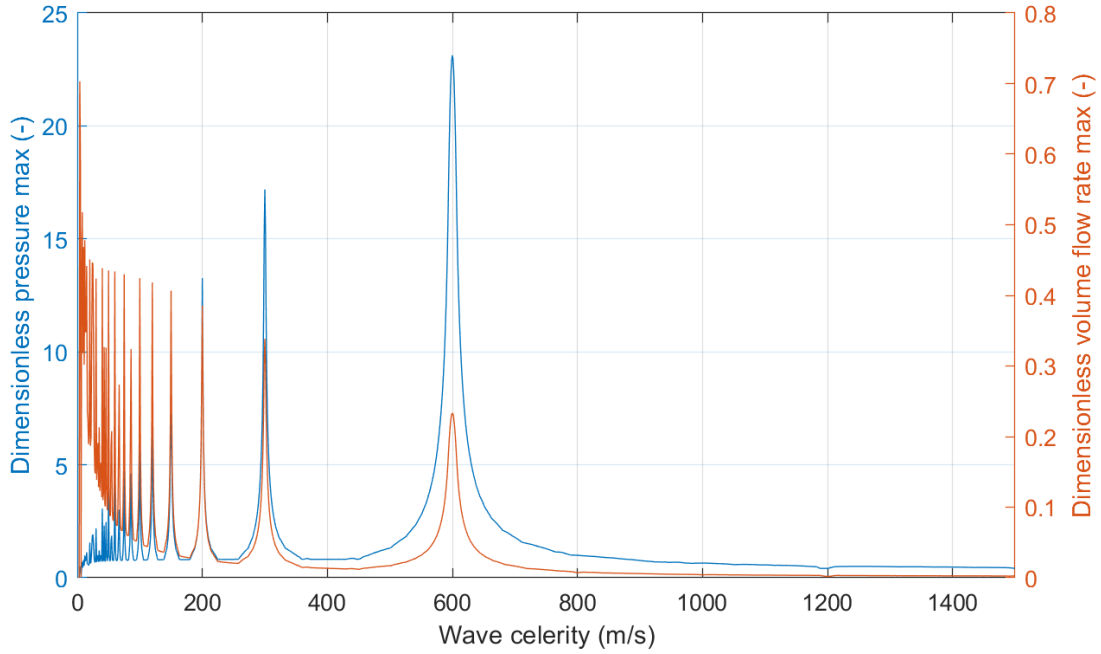

Figure 8.9: Maximum of dimensionless pressure and volume flow rate in function of the wave celerity

The peaks of pressure and volume flow corresponded on the x-axis. According to the theory of the length of wave and number of wave (see: Equation 8.2) the equation of the number of wave for in function of the wave celerity was found:

$$n = \frac{L}{aT} = \frac{900(m)}{a \cdot 3(s)} \tag{8.3}$$

A table of the wave celerity for the first peaks in function of the number of wave was built:

n (-)	0.5	1	1.5	2	2.5	3	3.5	4	4.5	5	5.5	6	6.5	7	7.5
a (m/s)	600	300	200	150	120	100	85.7	75	66.7	60	54.5	50	46.2	42.9	40

Table 8.12: Wave celerity correcting to the 15 first peaks in function of n

The value of the wave celerity in Table 8.12 corresponded perfectly with the value of a in Figure 8.9. The peaks of pressure and flow rate in the left of the graph had less relative precision than the others because of the precision of the simulations steps. Indeed, the simulations were made with a every m/s.

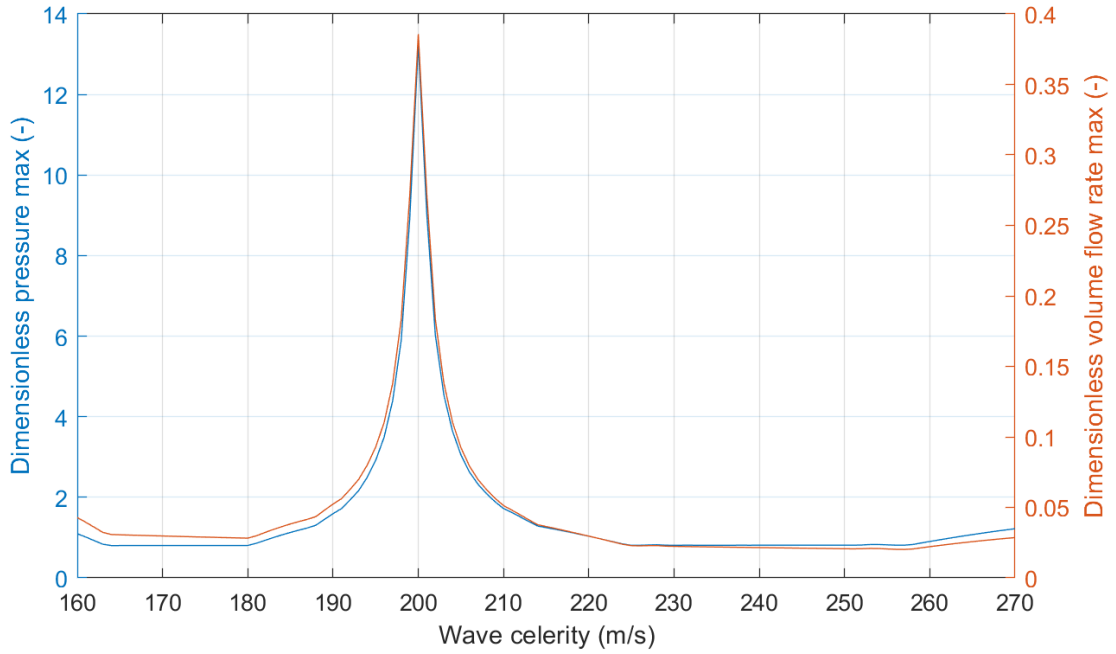

Figure 8.10: Zoom in typical pipe condition for maximum of dimensionless pressure and volume flow rate in function of the wave celerity

Figure 8.10 is a zoom in the wave celerity used in the simulation. Indeed, the wave celerity a in the typical pipe condition was 215 m/s. This graph shows the proximity between normal conditions and the peak of resonance. When the Young modulus of the material was 12% smaller or when the internal diameter was 16% bigger than in the typical condition, a was equal to 200 m/s. The maximum pressure reached in the pipeline would then be 10.8 times greater than in the typical conditions, increasing from 1.25 to 13.5 times the tank pressure.

This analysis allowed us to link the peaks of resonance to the wave celerity when $n = \frac{n}{aT}$ was a multiple of 0.5. The peaks of pressure and volume flow rate were present and they decreased with the increasing of the number n. The analysis showed that the typical pipe wave celerity was close to a resonance peak. We obserbed that the wave celerity change caused by the rigidity of the material introduced resonance in the pipe and grew the wave to 11 times the pressure injected with these conditions.

4 Discussion

In this section, we showed that the response pressure and flow rate were stable in function of the simulation time (or number of travel time oscillations). Indeed, the response of the system was stable after 20 travel time oscillations. This time of simulation represented 83 seconds of simulation for the typical pipe. This proved that the phenomena in the pipeline set up quickly and that short simulations were appropriate with a simple sinusoidal output pressure.

The sensitive analysis of the pipe's length revealed the critical pipe lengths where resonance phenomena occur. As a matter of fact, resonance phenomenon appeared for all integer multiples or integer multiple plus a half one (each 0.5 multiple) of the wave number inner the tube. In our case, the resonance phenomenon appeared when the length of the pipe was a multiple of 323 meters with the most critical length equal to 323 meters. At this length, the pressure in the

tube was increased of 56.6 times in comparison to the reservoir pressure. Therefore we decided to choose a pipe around 800 meters length in order to avoid the resonance phenomenon.

If the pipeline's length plays a role, the speed of the wave also influences the pressures within the system. Indeed, the wave celerity influences the pressure within the pipe by a coefficient proportional to the length of the pipe times the frequency of the injected sinusoidal. In the typical pipe the wave celerity was equal to 215 meters per second. This value was close to the 200 meters per second, which increased the maximum pressure of 13.5 times compared to the reservoir pressure. The report shows that in similar condition with a 12% less rigid material of pipe or with an inner diameter 16% bigger, the wave celerity could be modified to this critical value.

The experiment of this chapter was realised with a definite pressure sinusoidal wave at the end of the pipe. However, in a real case, these conditions would never be reached. For getting closer to reality, the implementation of a real wave is presented in the next part of the report, where the response of the pressure in the tube with an non periodic signal was analysed. The sizing of the pipe and real conditions of pressure were discussed in the next chapter.

In this chapter, the location of peaks were not studied. A spectrum of pressure signal composed with many sinus was implemented on the next chapter, where it was studied with a Fourier analysis. With this technique, we could locate the frequency (or period) of the sinus and the peaks. This method brought a better understanding of the phenomena and was introduced in the next simulations.

Sea Wave Excitation

1 Introduction

The aim of this part was to analyse the vibrations and resonances phenomenon in situation close to the reality. For this aim, the spectrum of a coastal wave, as described in the chapter 6, subsection 4.5 was setup in the nozzle as boundary condition in the outfall of the pipe. The excitation waves were created to be as close as possible a real situation, here the waves from Ebro Delta. An example of the 9 first travel times of the waves in the pipe can be found in appendix (4)

In the first part of this new experiment, we analysed and characterised the coastal waves. The second part was a sensitivity analysis with the variation of diverse input parameters. The analysis of resonance phenomenon was realised in time–frequency domain with a Fourier transform analysis in order to compare the frequency of resonance in pipe and the injected waves frequency in outfall. The aim was to find the link between frequency and amplitude of resonance in function of the input parameters. The third part was an analysis of the most critical parameters found in the previous section.

1.1 Vibration Modes

This section includes an analysis of the pressure within the pipe at different modes of resonance. The resonance is a term to describe a phenomenon of increasing the pressure (or other amplitude phenomenon) that appears with a periodic signal at a certain frequency. The first mode of vibration is called fundamental mode, natural mode or first normal mode of resonance and the other modes are called by their number. Each normal mode appears at a certain frequency, multiple of the fundamental (or natural) frequency. The number of the mode describes the number of half waves in the system. In other words, the vibration mode is named by the number of belly in the system. The resonance mode has to be studied because it describes where the pipe the peaks of pressures appear at certain frequencies. These maxima of pressure can theoretically grows up until to the infinite if there is no friction to damp the resonance phenomenon. It is the reason of studying these particular frequencies and pressures in the pipe. The following section includes the analysis of the fundamental mode (1^{st} mode), as well as the 2^{nd} and 3^{rd} mode. Others modes are present in pipe but the frequents are note study because the damping phenomenon are too big and the signal can be confused with noise.

1.2 Coastal Wave Proprieties

In order to analyse the inner pipe phenomenon the injected coastal wave had to be analysed to determine exactly what is injected. Figure 9.1 is a representation of the probability and density of the elevation wave.

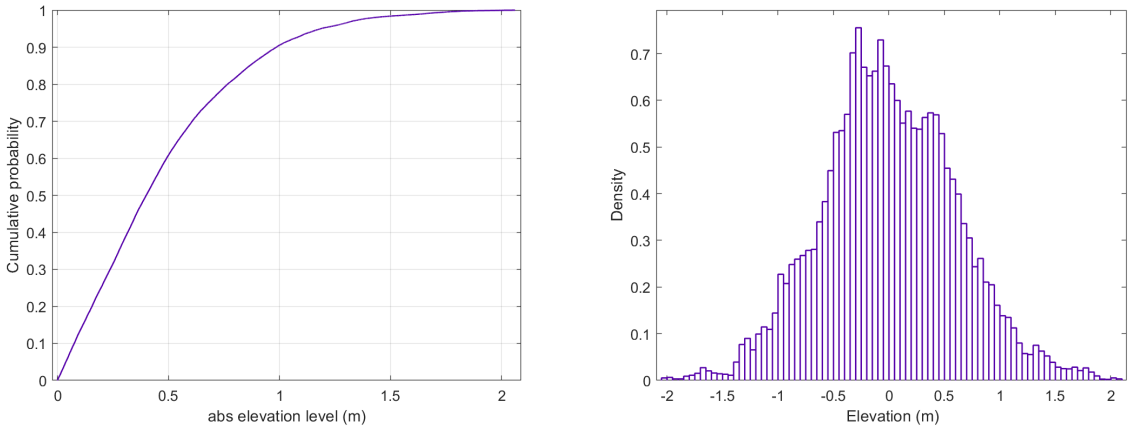

Figure 9.1: Cumulative portability for absolute wave elevation and density for wave elevation

Figure 9.1 shows the probability to have a certain wave elevation. Here for example, 90% of the waves were under 1 meter of absolute elevation.

Name	Value	Range
μ (-)	0.00138	[-0.00466, 0.00741]
σ (-)	0.60241	[0.5982, 0.60671]
H_s (m)	2.4193	

Table 9.1: Statistical moments μ, σ and H_s for a normal distribution of the coastal waves

Table 9.1 shows the mean of the distribution μ and the standard deviation σ of the distribution. The significant wave height H_s is defined as 4 times σ and indicates the mean wave height of the highest third of the waves. In the following analysis, dimensionless pressures were made by dividing the pressures by H_s.

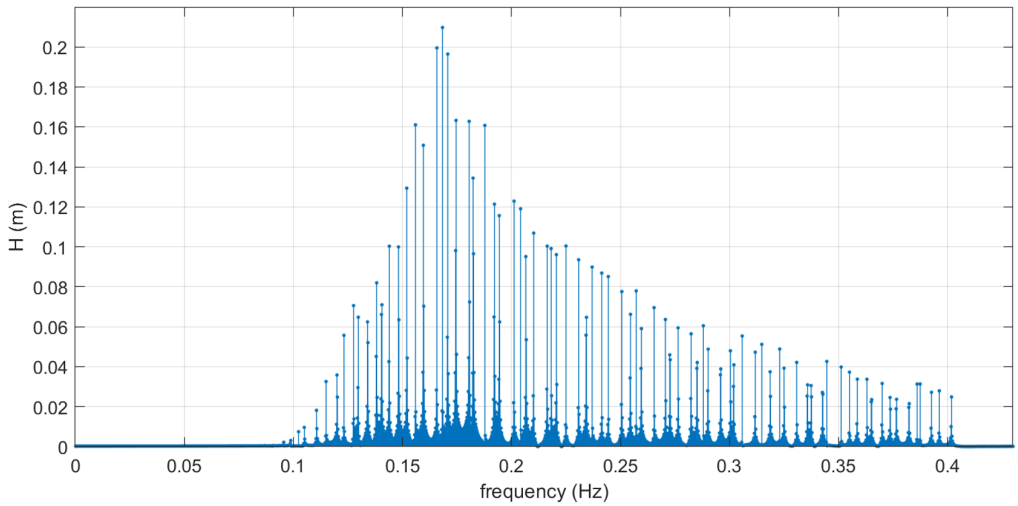

Figure 9.2: Magnitude of frequency response for the coastal wave signal

Figure 9.2 shows the pressure in meter in function of the frequency of the waves for 5000 seconds.

Figure 9.2 represents the raw analysis when the coastal wave was implemented. The outfall of the pipeline was under water and the elevation of the wave transmitted pressure from the free surface of water to the outlet of pipe. In order to implement the depth of the water, coastal waves had to be divided by the cosh of the depth.

$$H_{outfall} = \frac{H_{waves}}{\cosh(z)} \tag{9.1}$$

The factor $\cosh(z)$ is the waves attenuation factor in function of depth. Table 9.2 is a summary of the attenuation factor of the wave in function of the depth of the water.

Depth of water (m)	0	1	2	3	5	8	10	15
Attenuation factor (-)	1	1.5	3.8	10	74	1'490	11'013	1'634'509

Table 9.2: Waves attenuation factor in function of depth

For the next experiments, the pipeline was placed horizontally at 2 meters depth. These characteristics were chosen arbitrarily. The amplitudes of the waves were divided by 3.8 at the outfall compared to the free surface of the water amplitude level (see Table 9.2). The line plot was generated in order to build a continuous spectre.

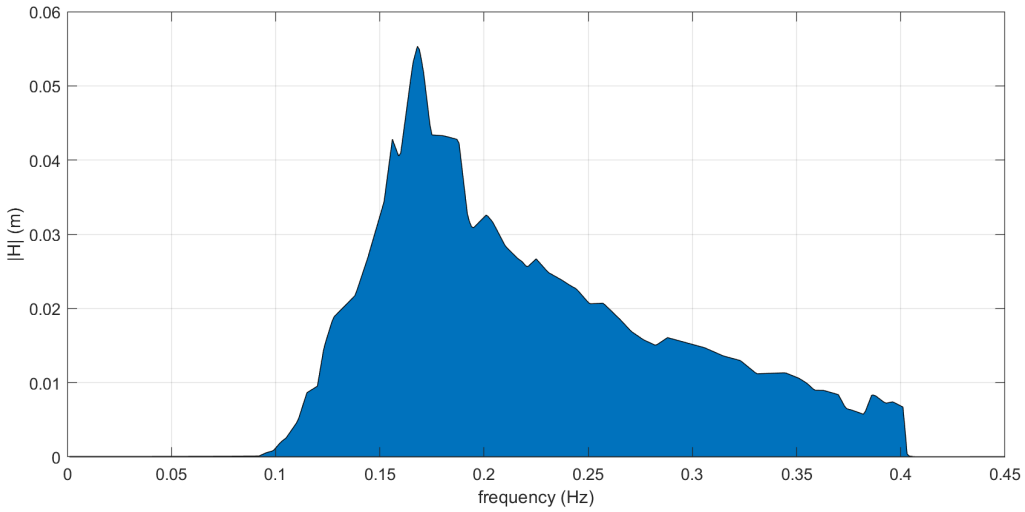

Figure 9.3: Magnitude area of frequency response for the injected output wave at 2 meters depth

Figure 9.3 shows the interpolate spectrum of the input wave injected at the pipeline's output, at a depth of 2 meters. H_s was equal to 0.6366 meter. The wave corresponding to this spectrum was injected at the output for the next simulations. The continuous spectrum was useful to compare frequency values with the injected spectrum values because the Fourier transform of both signal didn't give the same frequency sample.

1.3 Inner Pipe Fourier Analysis

To study the frequency and level of pressure in the pipe, a Fourier Transform was used on the matrix containing simulation results for the pressure and volume flow rate. The Fourier Transform made it possible to identify pressure levels as a function of frequencies in the pipe at each node.

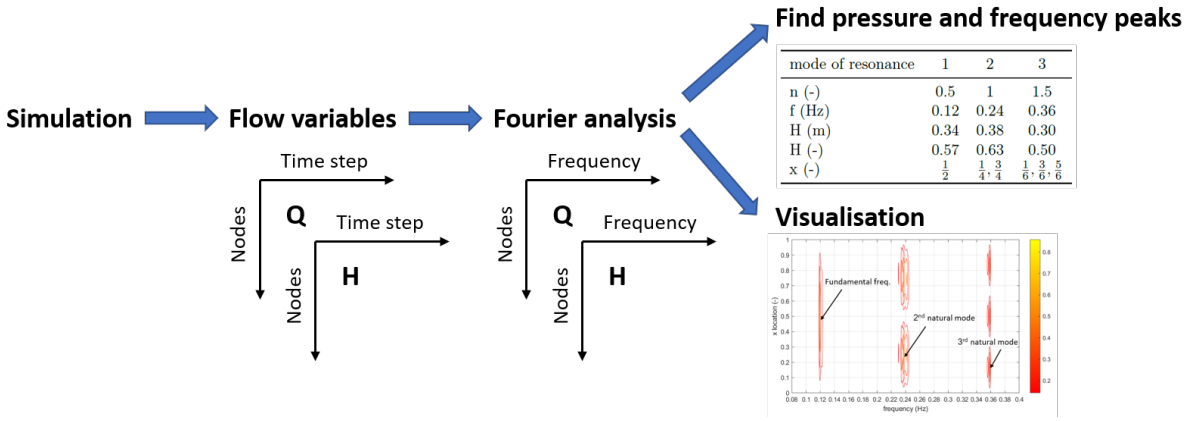

mode of resonance	1	2	3
n (-)	0.5	1	1.5
f (Hz)	0.12	0.24	0.36
H (m)	0.34	0.38	0.30
H (-)	0.57	0.63	0.50
x (-)	$\frac{1}{2}$	$\frac{1}{4}, \frac{3}{4}$	$\frac{1}{6}, \frac{3}{6}, \frac{5}{6}$

Figure 9.4: Fourier analyse diagram for pressure wave simulation

Figure 9.4 shows the sequence of analysis from the end of simulation until the display of results. A method was developed to automate the analysis of peaks and extract the corresponding frequencies, pipe locations and pressure levels.

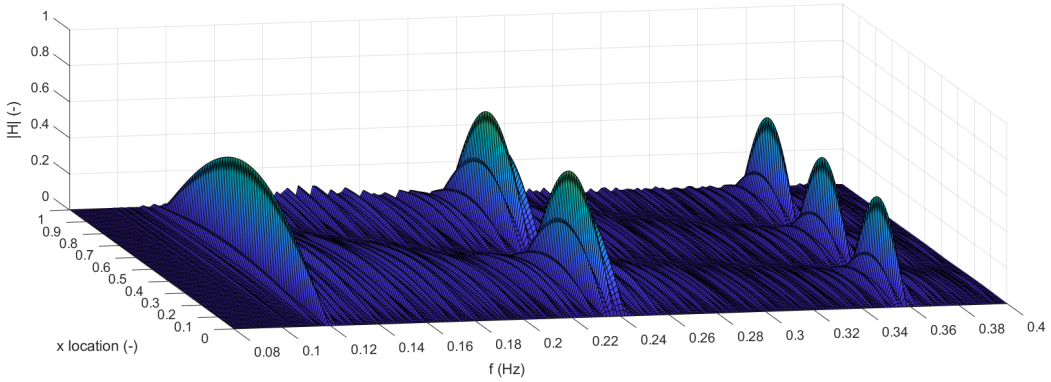

Figure 9.5: 3D visualisation of the dimensionless pressure in function of the frequency and location in pipe for typical pipe

Figure 9.5 is a 3D mesh of the Fourier transformation of the level of pressure at each location on the pipe. The number of bellies in the mesh correspond to twice the number of wave n. Indeed, one belly was added every 0.12 Hz. This frequency corresponds to the fundamental frequency of the typical pipe. The 3D mesh is transform in contour plot in order to track the location of pressure peaks.

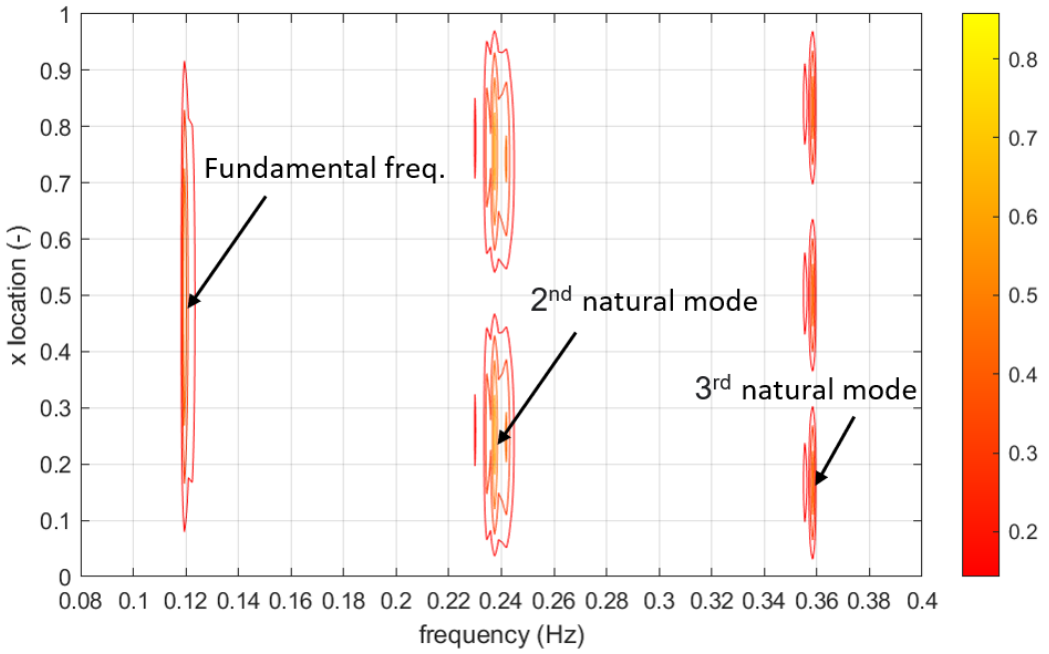

Figure 9.6: Contour of the dimensionless pressure in function of the frequency and location in pipe for typical pipe

Figure 9.6 shows the interval of frequency between the pressure peaks and the addition of a belly each normal mode. The x location axis correspond to the coordinates in pipe x divided by the length of the pipe. This graph is the 2D top view of the previous 3D graph. The resonance modes were located at precise intervals of frequency and one belly was adding at each mode. The following table shows the level of pressure and frequency and location of the peaks in function of the number of wave.

mode of resonance	1	2	3
n (-)	0.5	1	1.5
f (Hz)	0.12	0.24	0.36
H (m)	0.34	0.38	0.30
H (-)	0.57	0.63	0.50
x (-)	$\frac{1}{2}$	$\frac{1}{4}, \frac{3}{4}$	$\frac{1}{6}, \frac{3}{6}, \frac{5}{6}$

Table 9.3: Frequency, pressures and location of the peaks in function of the number of wave for typical pipe

This analysis showed that the frequencies and peak locations of resonance modes did correspond to what was expected according to the theory in chapter 9. The fundamental frequency had one half sinus and corresponded with the formulation:

$$F = \frac{1}{2}\frac{a}{L} \tag{9.2}$$

Each mode of frequency added a peaks of pressure and the modes were spaced by 0.12 Hz. The locations of the maximum pressures (locations of the resonance peaks) were all fractions

with the natural odd numbers in the denominator and a number equal to 2 times the number corresponding to the resonance mode.

$$x(-) = \frac{\sum_{c=1}^{c=4n} 2c+1}{4n} = \frac{\text{all odd numbers from 1 to } 4n}{2 \text{ times mode number}}, \text{with } c \in \mathbb{N} \tag{9.3}$$

This equation can be write for found the location in pipe in meter:

$$x(m) = \frac{\sum_{c=1}^{c=4n} 2c+1}{4n} L \tag{9.4}$$

This part included finding the resonance frequencies for each specific mode of vibration and the location of the pressure peaks. The next part was an analysis of the evolution of frequency and level of pressure in function of the length of the pipe.

2 Convergence Analysis

The aim of this part was to test the stability of the system's response in function of the number of oscillation (i.e. the number of time steps) and of the number of pipe's divisions (number of nodes) in the simulation. In MATLAB, one oscillation time was equal to four travel time of a wave. For example with a typical pipe (L = 900 m, a = 215 m/s) one oscillation in MATLAB represented 16.7 seconds of simulation. The aim was to determine if the pressure and frequency of the natural modes depended on the time of the simulation. As a result of the simulation, the graph of the maximum dimensionless pressure in function of the number of oscillations was generated with different number of nodes.

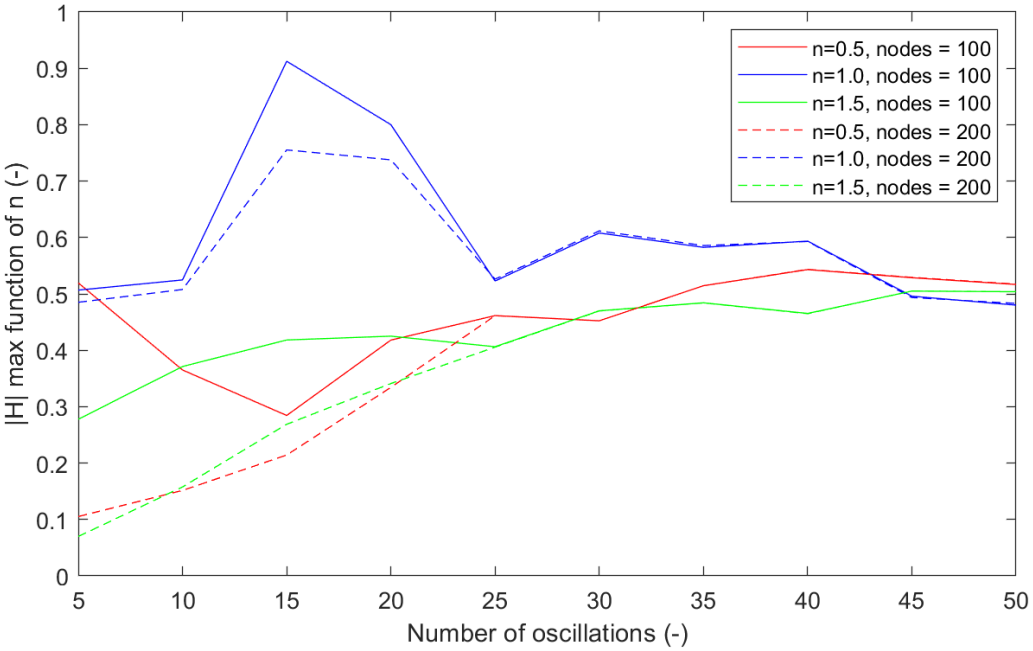

Figure 9.7: Maximum dimensionless pressure in function the number of oscillations and number of nodes for the three first normal modes

Figure 9.7 shows the stability of the level of the peaks of pressure for the first 3 normal modes

with 100 nodes and 200 nodes. At 25 oscillations, the variation of the number of knots was not different between conditions. The following simulation extended the tested oscillation range.

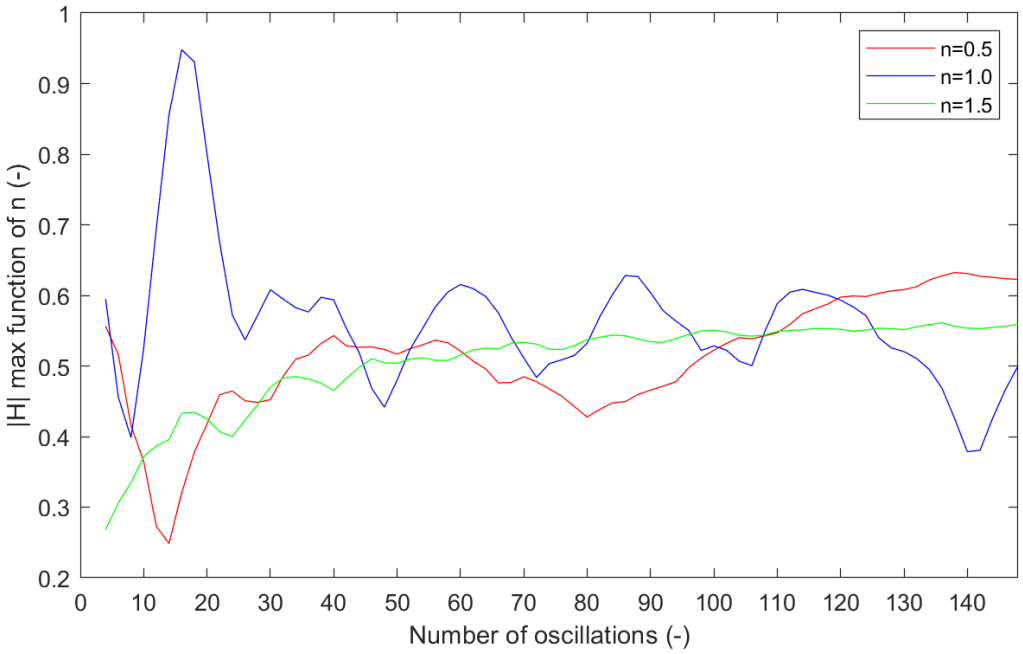

Figure 9.8: Maximum pressure in function the number of oscillations for the three first normal modes

n (-)	$\|\mathbf{H}\|_{min}$ (-)	$\|\mathbf{H}\|_{max}$ (-)	$\|\mathbf{H}\|_{mean}$ (-)	$\|\mathbf{H}\|_{35}$ oscil. (-)	% diff. $\|\mathbf{H}\|_{mean}$ & $\|\mathbf{H}\|_{35}$
0.5	0.249	0.632	0.513	0.515	0.5%
1.0	0.379	0.948	0.562	0.577	2.5%
1.5	0.268	0.562	0.506	0.482	-4.9%

Table 9.4: Comparison of the pressure in function of the number of oscillations

Figure 9.8 shows the response's stability in function of the number of oscillations of the simulation. This figure shows that after 35 oscillations, the value of pressure was close to the mean. Therefore, to reach the point of stability during the next experiments, the number of oscillations was fixed to 35. For a the typical pipe simulation with a length of 900 meters, a wave celerity equal to 215 meter pro second, 35 oscillations represented a simulation of 586 seconds.

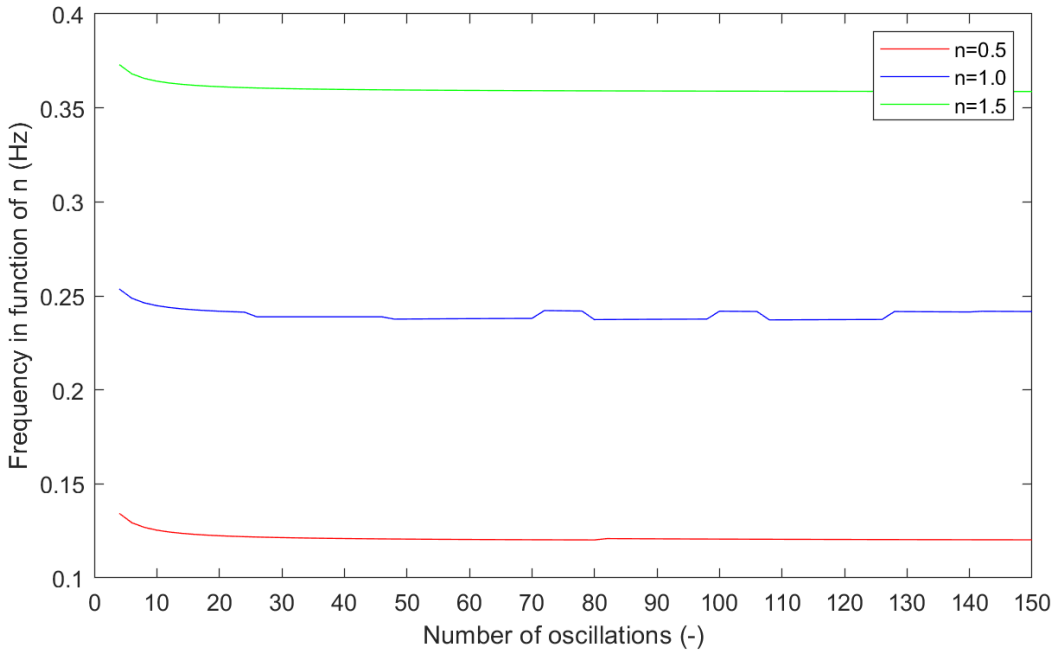

Figure 9.9: Frequency in function the number of oscillations and number of nodes for the three first normal modes

Figure 9.9, shows the frequency of the three first normal modes in function of the number of oscillations. The convergence was reached between 10 to 15 oscillations and the number of oscillations fixed for the rest of the simulations (35 oscillations) ensured the stability of the calculated frequencies.

The limit of 35 oscillations (586 seconds in typical pipe configuration) was chosen to save computing time in order to run a large number of simulations. This choice allowed to analyse the intake parameters in a large range because the purpose of this report was to find an analysis method for finding the critical parameters that cause resonance phenomena. It is important to highlight that the measures of pressure peaks could be affected by this choice.

3 Sea Depth Analysis

The aim of this part was to analyse the impact of the sea depth on the system's response. Simulations with the typical pipe condition were run for sea depth starting from 0 meter until 10 meters. We expected that depth of water will influence the amplitude (Ap) of the wave. Indeed, Equation 9.1 shows the influence of the depth of water on the pressure in outfall compared to the pressure in the free surface of the water. Simulation were run for typical pipe with a range from 0 meter to 10 meters of depth (simulation each 1 meter).

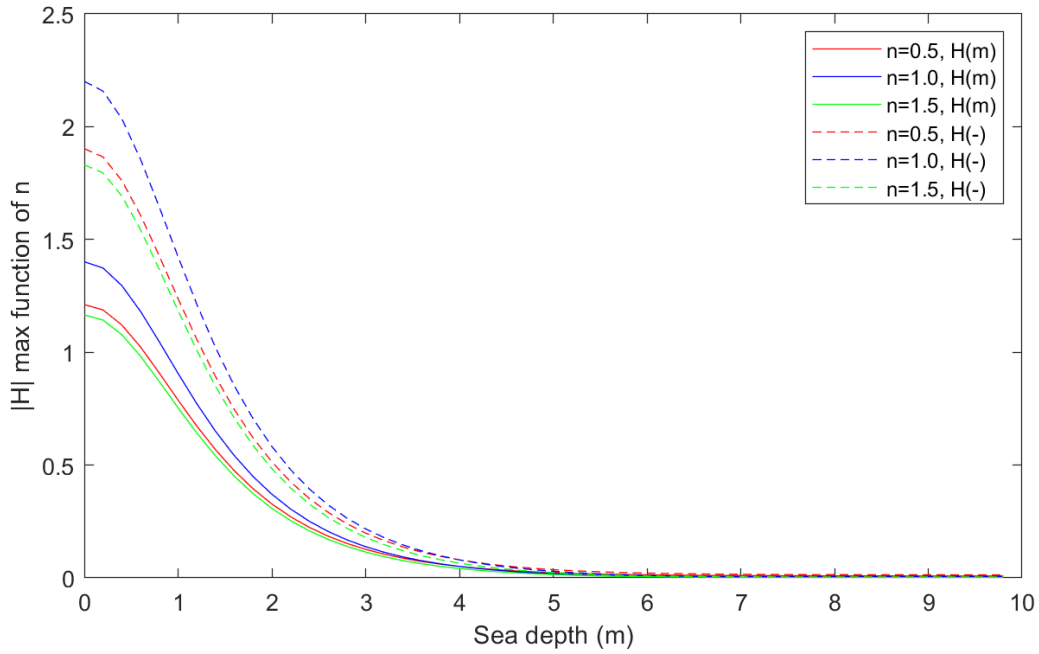

Figure 9.10: Maximum pressure in function of the depth of the sea for the three first normal modes

Pressure plotted against sea depth as shown in Figure 9.10 describes exactly the curve of the first value of pressure divided by hyperbolic cosinus of the depth of sea. The pressure at each resonance frequency could easily be found for all depth of water with the formulation Equation 9.1.

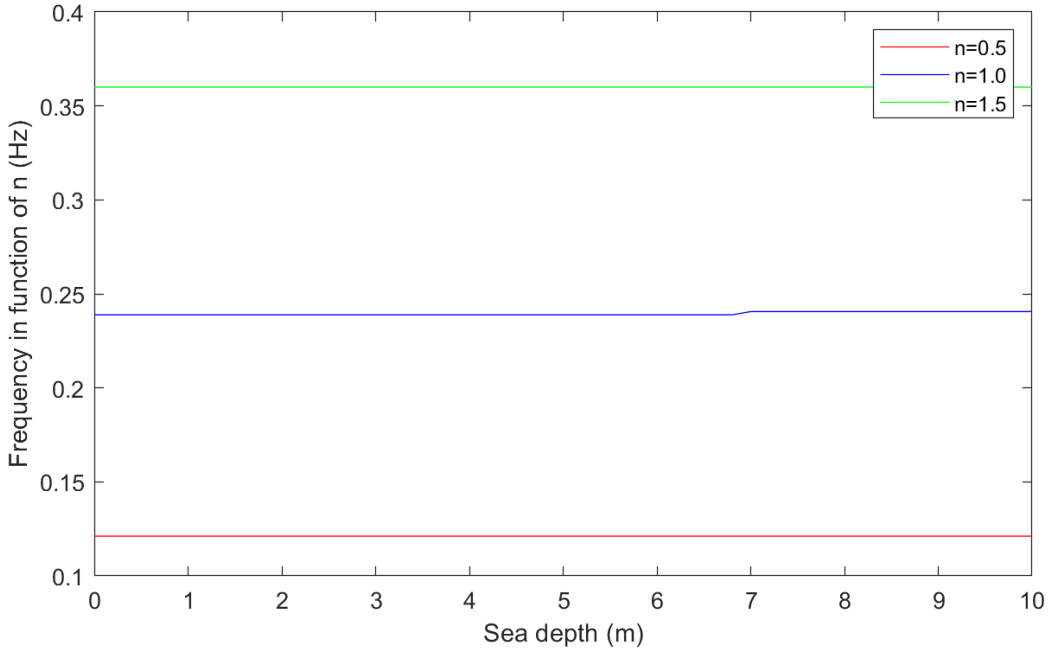

Figure 9.11: Frequency in function of sea depth for the three first normal modes

Figure 9.11 shows the frequency of the three first modes of resonance in function of sea depth. The frequencies were stable with the depth of water and only the amplitude was damped.

This part of the analysis showed that the depth of sea had only an influence on the damping of the maximal pressure in pipeline. Indeed, the pressure wave injected at a certain depth was the pressure wave at the free surface of the water divided by the hyperbolic cosinus of the depth. For example, at 2 meters depth the original wave was divided by 3.8 and at 10 meters depth it was divided by 11'013. The advantage of a deep pipeline is therefore to avoid the pressure wave in the outfall because of the damping of the phenomenon of wave on the surface.

4 Length of Pipe Analysis

The aim of this part was to analyse the impact of the pipe's length on the system's response. Simulations with the typical pipe conditions were run for a length of the pipe starting from 100 meters to 3800 meters.

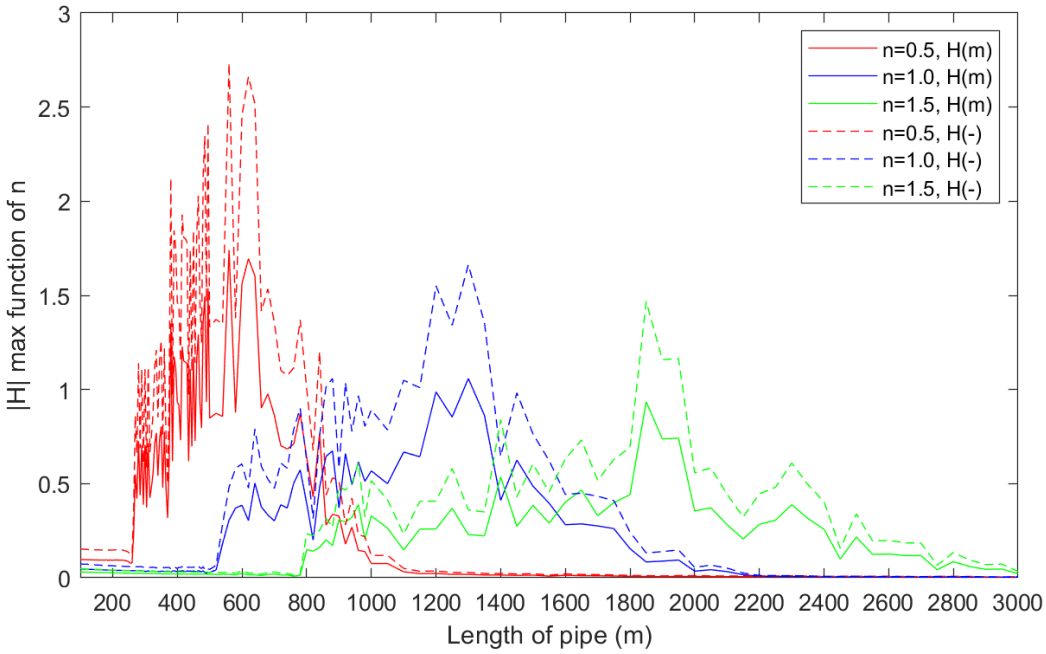

Figure 9.12: Maximum pressure in function of the length of pipe for the three first normal modes

Figure 9.12 shows the pressure response of the three first normal mode numbers in function of the pipe's length. Initially, at shortest pipe's lengths, the three normal mode curves had a pressure close to zero. Then with increasing pipe's length, pressures increased, with curves of pressure appearing at different lengths for the 3 modes. Besides, for all three modes, the curves had the same shape with an offset in y-axis and x-axis. Finally, for all of the three modes, the curve decreased to a flat close to zero pressure at higher pipe's lengths.

In order to analyse the previous data, each length of the pipe was linked to its own frequencies of resonance by the following equation:

$$F = \frac{a}{L} \tag{9.5}$$

Equation 9.5 was then applied to the x-axis of Figure 9.12 to transform the length of pipe in corresponding frequency of resonance. The code source that was used to analyse the spectrum is available in Listing A.8, page 85.

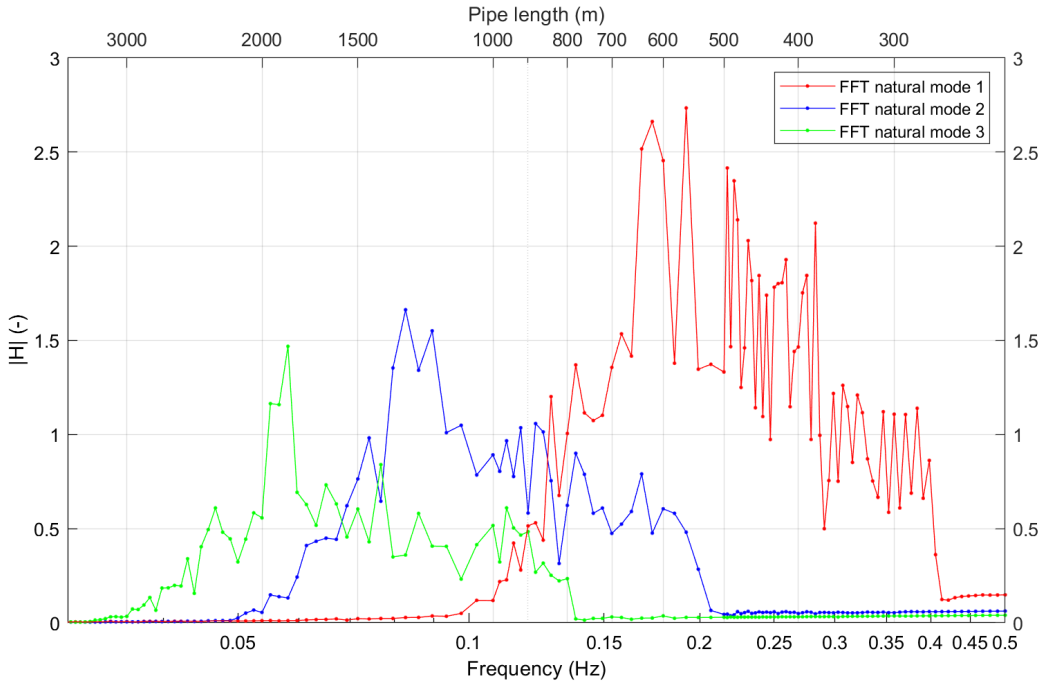

Figure 9.13: Maximum pressure in function of the length of pipe and corresponding frequency for the three first normal modes

mode of resonance	L (m)	H (m)	H (-)	F (Hz)
1	560	1.741	2.735	0.192
2	1300	1.058	1.662	0.083
3	1850	0.945	1.484	0.058

Table 9.5: Summery of the maximum pressure, length of pipe and frequency for each mode of Figure 9.13

Figure 9.13 has a double x-axis scale: a frequency scale at the bottom and a scale of length at the top. The plot orientation is reversed because of the formulation of the frequency equivalent length (i.e. highest values of pipe's length are on the left part and lowest values are on the right part of the graph). Indeed, Equation 9.5 implies that if the frequency increases, the length of pipe becomes shorter. In order to "fit" different normal mode, the following equation was used to adjust the curves according to the fundamental frequency.

$$F = \frac{n\,a}{L} \tag{9.6}$$

In Equation 9.6, n is the number of waves (0.5, 1, 1,5) attached respectively to the fundamental mode, 2^{nd} normal mode and 3^{rd} normal mode. The use of n in the formula brought the abscissa of the graphs back to the fundamental frequency scale.

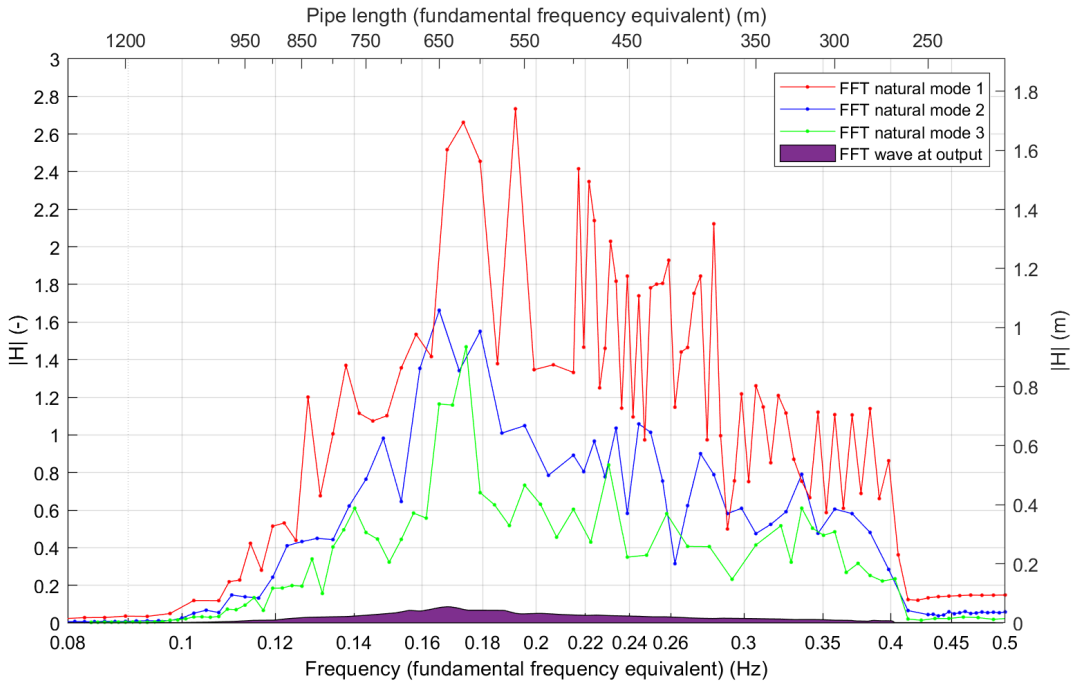

Figure 9.14: Maximum pressure in function of the equivalent length of pipe and corresponding equivalent frequency for the three first normal modes and comparison with the injected wave spectrum.

Figure 9.14 represents the peaks of pressure for the three first normal modes in function of the equivalent pipe's length in relation to the frequency of the fundamental mode of vibration. The aim of this graph was to place the equivalent frequency and equivalent length of pipe on the same scale in order to compare it with the spectrum of injected waves. To simplify the term "pipe's length equivalent to the pipe's length of the fundamental frequency" and "frequency equivalent to the fundamental frequency" in the following paragraph were simplified in "pipe's length" and "frequency". The pressure peaks could be compared to the injected wave spectrum with the right y-axis in meter or in dimensionless pressure (pressure divided by the H_s) with the left axis.

In the previous graphs, to obtain dimensionless measurements, the pressure of the three normal modes were divided by the significant wave of the injected waves H_s. In order to compare the normal modes with the injected waves for each frequency, the spectrum of pressure was divided by the input spectrum level at same frequency.

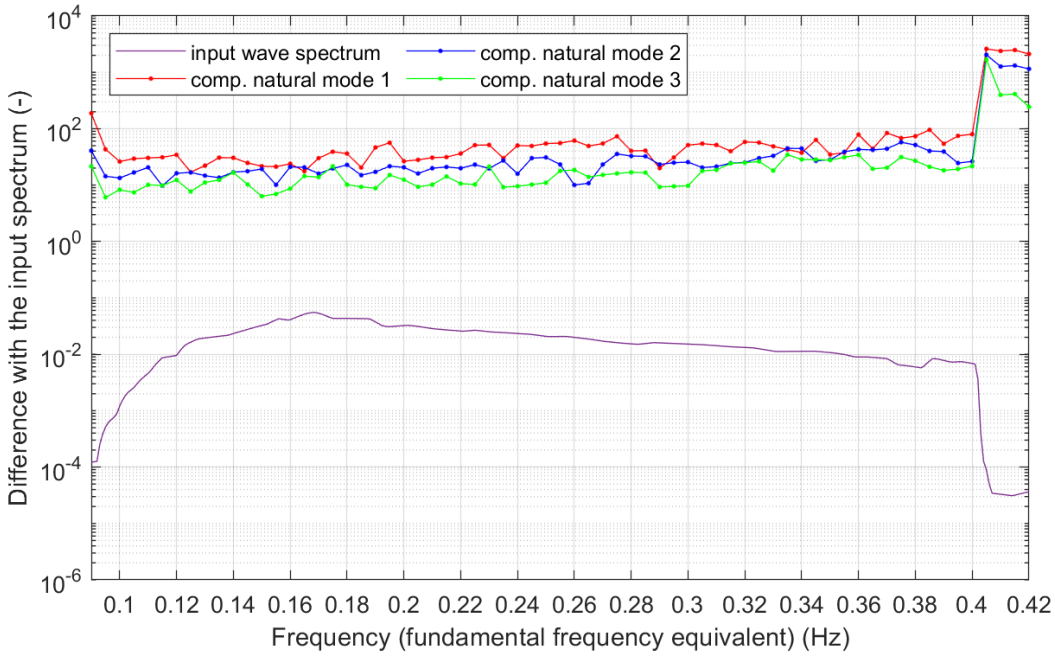

Figure 9.15: Spectrum comparison between the three first normal modes and the injected waves

Figure 9.15 shows a comparison of the difference between the original input wave spectrum and the three first normal modes. The next graph is a zoom between 0.1 Hz and after 0.4 Hz. Indeed, the large differences before 0.1 Hz and after 0.4 Hz was due to the input spectrum, which had values close to zero.

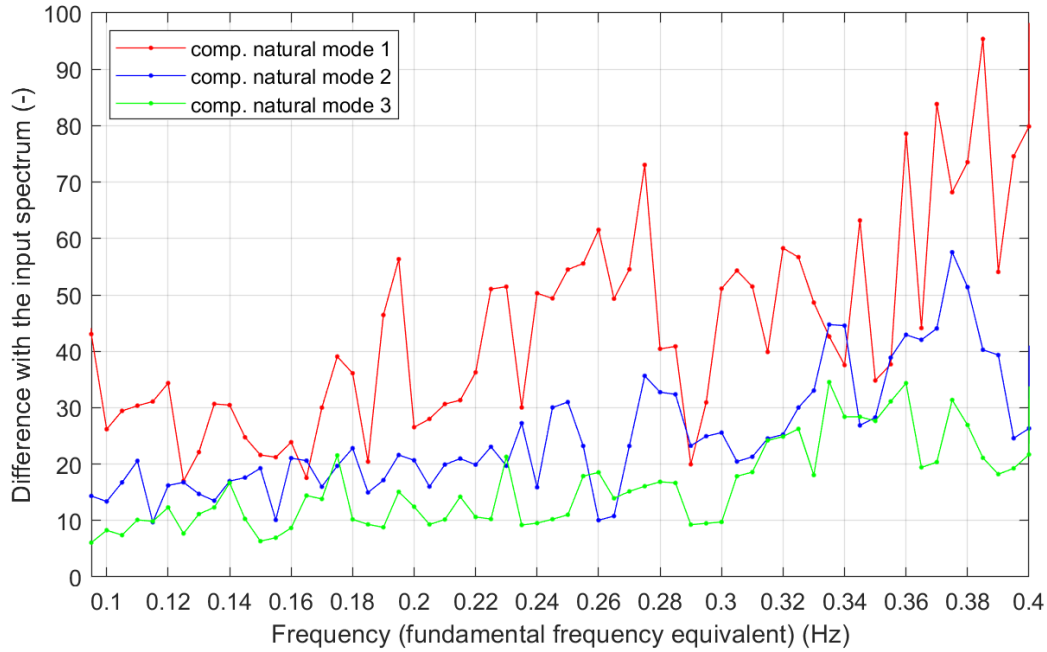

Figure 9.16: Spectrum comparison between the three first normal modes and the injected waves (zoom in input value spectrum)

Figure 9.16 is a zoom in input value spectrum limit. The pressure in the pipe could be 95 times bigger than the pressure injected. The summary of the graph is shown in the table below:

n (-)	min (-)	max (-)	mean (-)
0.5	17.01	95.38	43.97
1.0	9.70	57.57	24.94
1.5	6.07	34.53	15.99

Table 9.6: Minimum, maximum and average value in Figure 9.16 for each mode

In the current analysis, the maximum pressure in meter was analysed in function of the mode of resonance and the length of the pipe. The maximum pressure reached in pipe was equal to 1.741 meter with a pipe of 560 meters long. This maximum of pressure corresponded to a wave injected at this frequency equal to 0.0375 m. The pressure in pipe corresponded to 46 times the pressure injected at the outfall at the same frequency.

The frequencies of the three first resonance modes were analysed in function of the length of the pipe:

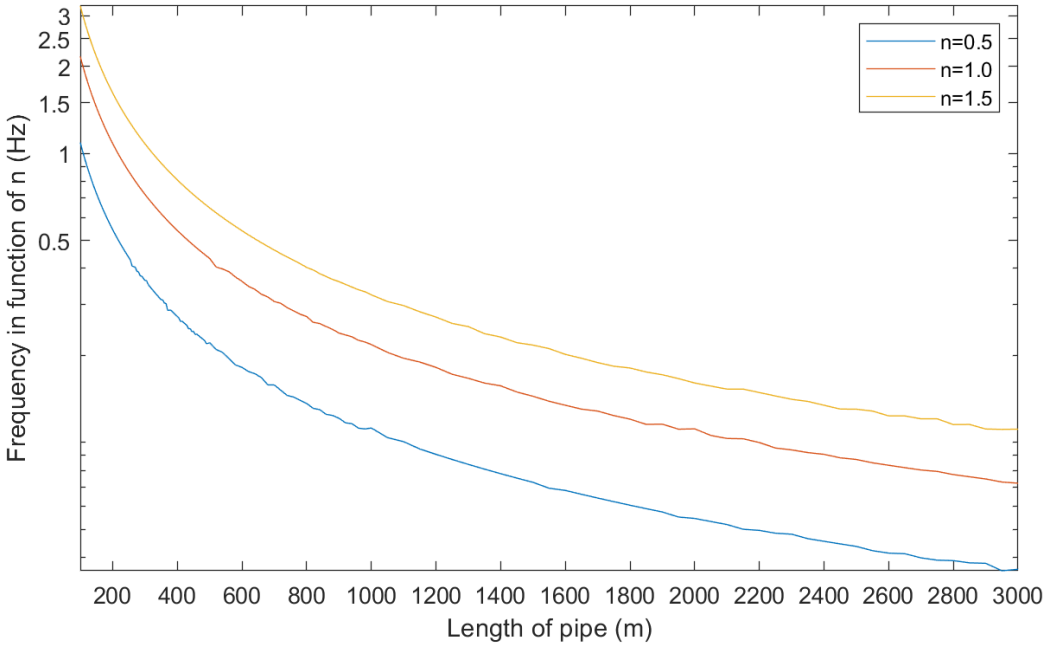

Figure 9.17: Frequency in function of the length of pipe for the three first normal modes

Figure 9.17 shows the passage in the low frequencies as the tube lengthened. These frequencies could easily be calculated with Equation 8.3: $\left(F = \frac{na}{L}\right)$.

In this section, we showed that the absolute pressure in pipe was tolerable for the installation. The example of the typical pipe in HDPE with a D/e ratio equal to 21 in ISO PE100 classification had to resist to 10 bar of nominal pressure and 80 bar of maximum stress (See Table 3.2). It is important to note that these pressure peaks were linked with the injected amplitudes and the injected pressure could reach 95 times the pressure in pipe. This way of looking at pressure

differences raised the question of what could happen if the input spectrum was changed and a periodic input pressure became more important. Indeed, this analysis looked at the pressure response as a function of pipe lengths with a "standard" wave spectrum and the injected wave was the the main measurement uncertainty.

5 Wave Celerity Analysis

The aim of this part was to analyse the impact of wave celerity on the system's response. Simulations with the typical pipe condition were run with a wave celerity starting from 100 m/s to 1500 m/s, which corresponds to a rigid pipe. The analysis steps were the same as in the previous subsection. For more information see chapter 9, section 4.

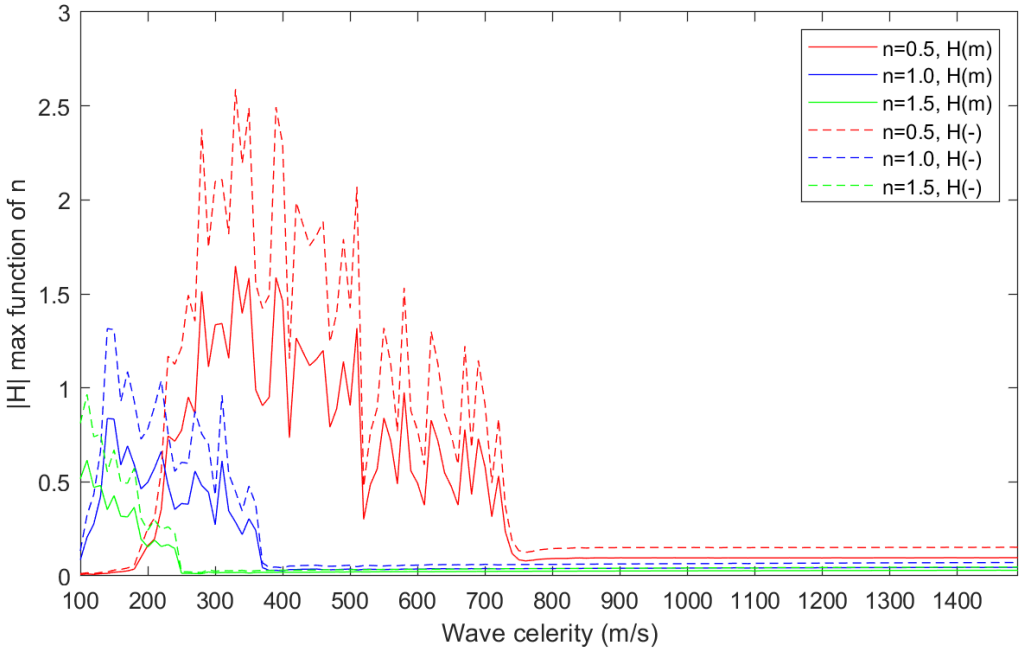

Figure 9.18: Maximum pressure in function of the wave celerity for the three first normal modes

Figure 9.18 shows the pressure response of the three first normal modes number in function of the wave celerity. The three normal mode curves had the same shape with an offset in y-axis and x-axis and a close to zero line with an increasing wave celerity.

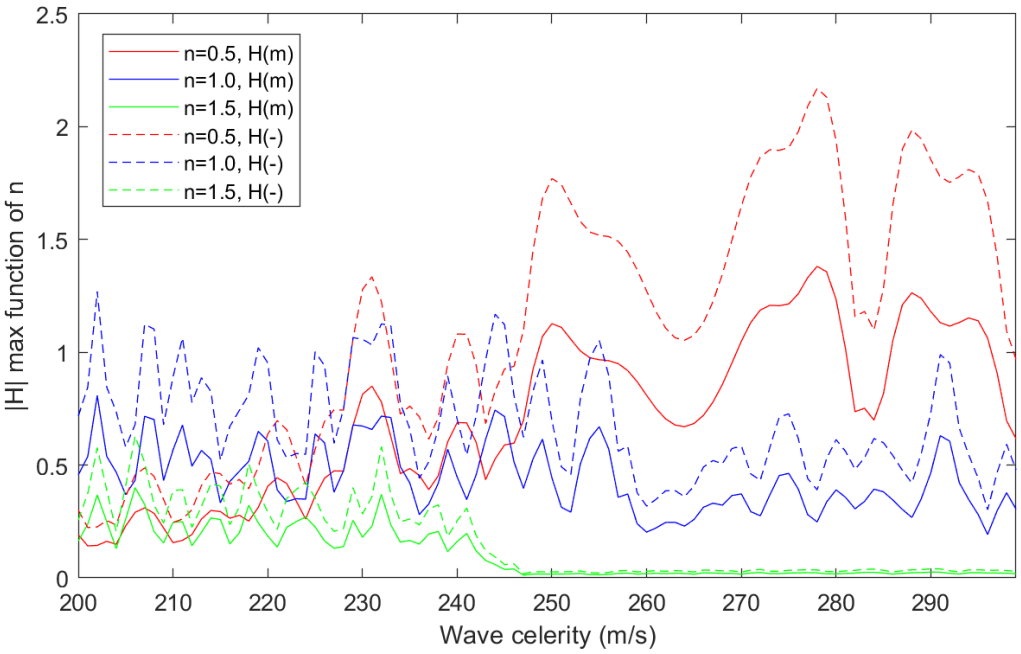

Figure 9.19: Maximum pressure in function of the wave celerity (range 200-300 m/s) for the three first normal modes

Figure 9.19 is the graph of a simulation with a range of celerity from 200 m/s to 300 m/s, incremented each m/s. In order to study the results of this graph, an analysis of the frequency equivalent to the celerity was realised. To do so, each length of pipe was linked to its own frequencies of resonance by Equation 9.5, which transforms wave celerity in corresponding frequency of resonance. In order to adjust the x-offset, Equation 9.6 was used to "fit" the different normal modes graphs. The equation adjusts the curves according to the fundamental frequency. This part was a simplification realised with more explanation in chapter 9, section 4.

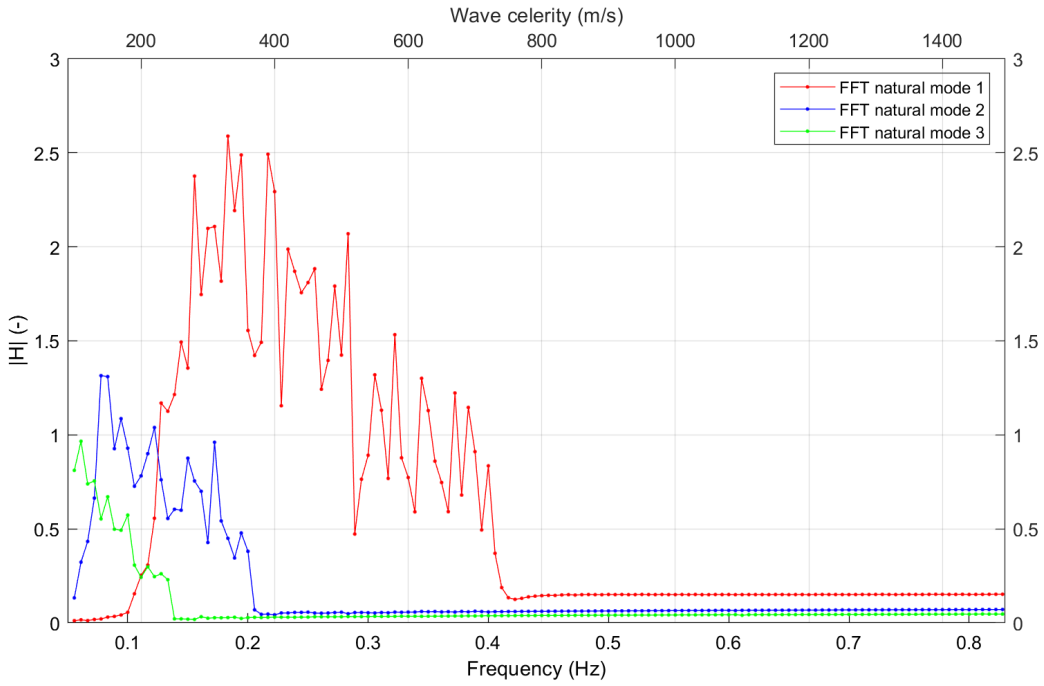

Figure 9.20

mode of resonance	a (m/s)	H (m)	H (-)	F (Hz)
1	330	1.648	2.693	0.147
2	140	0.837	1.368	0.062
3	110	0.615	1.005	0.049

Table 9.7: Summery of the maximum pressure, wave celerity and frequency for each mode

Figure 9.20 has a double x-axis scale: a frequency scale at the bottom and a scale of length at the top. In order to "fit" different normal mode, Equation 9.6 was used to adjust the curves according to the fundamental frequency. Using n in the formula brought the abscissa of the graphs back to the fundamental frequency scale[1].

[1]For more details, see previous analyse section 4 at page 59.

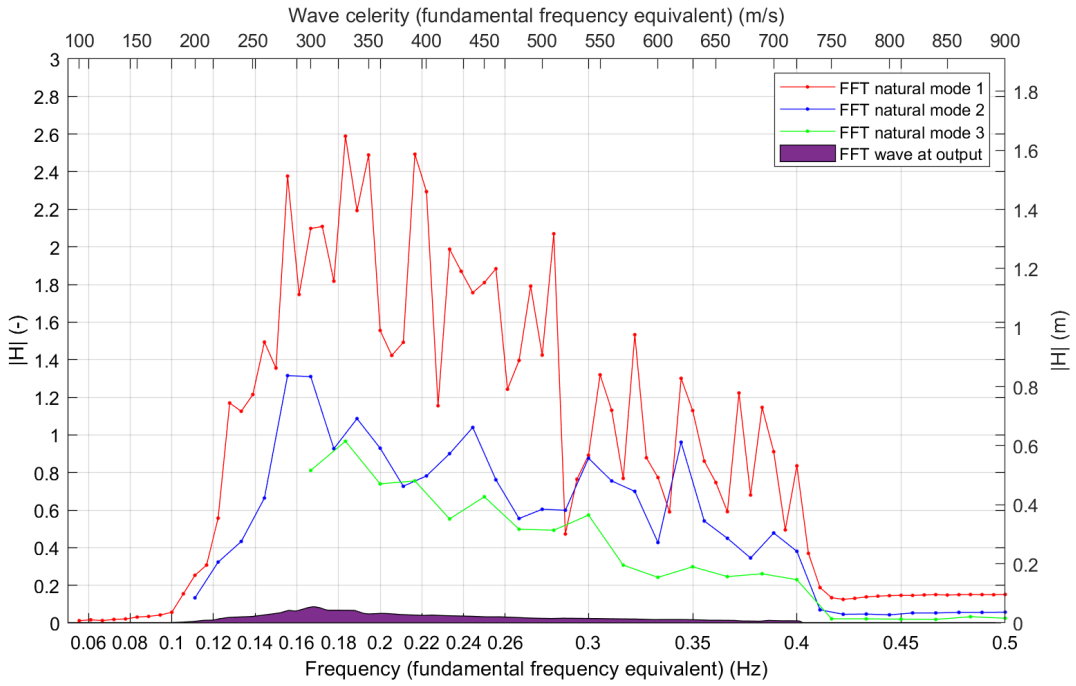

Figure 9.21: Maximum pressure in function of the equivalent wave celerity and corresponding equivalent frequency for the three first normal modes and comparison with the injected wave spectrum.

Figure 9.21 represents the pressure peaks for the three first normal modes in function of the equivalent wave celerity in relation to the frequency of the fundamental mode of vibration. The different curves of normal modes started at different values of frequency because of the original offset observed in Figure 9.18. The aim of this graph was to place the equivalent frequency and equivalent wave celerity on the same scale in order to compare it with the spectrum of the injected waves. To simplify: the terms "wave celerity equivalent to the wave celerity in the fundamental frequency" and "frequency equivalent to the fundamental frequency" were simplified by "wave celerity" and "frequency" in the next paragraph.

In the previous graphs, to obtain dimensionless measurements, the pressure of the three normal modes was divided by the significant wave of the injected waves H_s. In order to compare the normal modes with the injected waves, for each frequency, the spectrum of pressure was divided by the input spectrum.

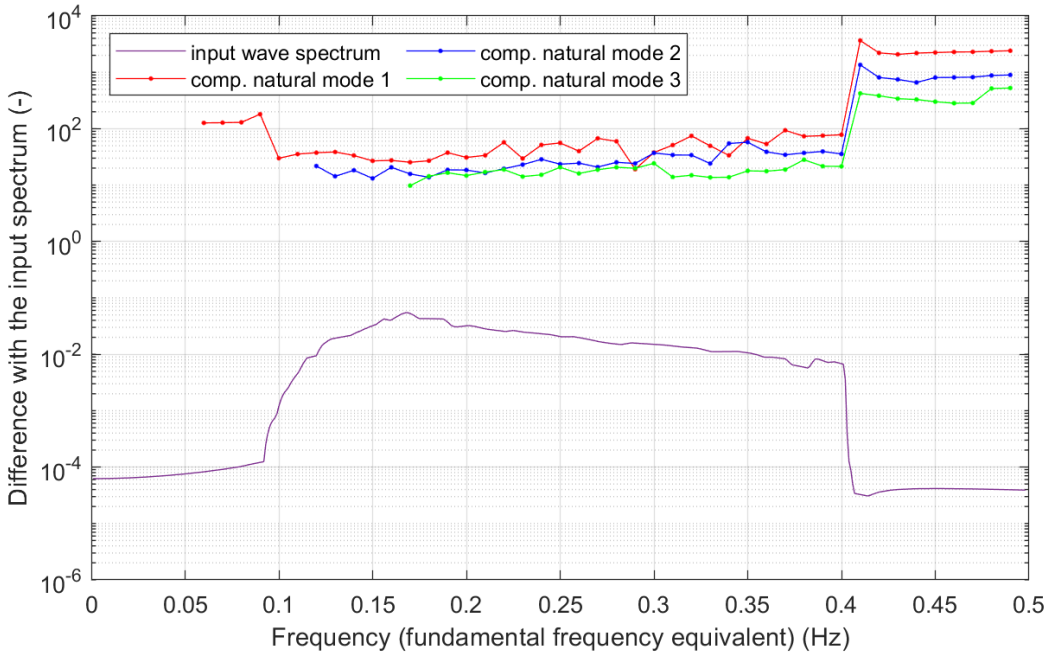

Figure 9.22: Spectrum comparison between the three first normal modes and the injected waves

Figure 9.22 shows a comparison of the difference between the original input wave spectrum and the three first normal modes. The large differences before 0.1 Hz and after 0.4 Hz were due to the input spectrum which had values close to zero. The next graph is a zoom between this value of frequency.

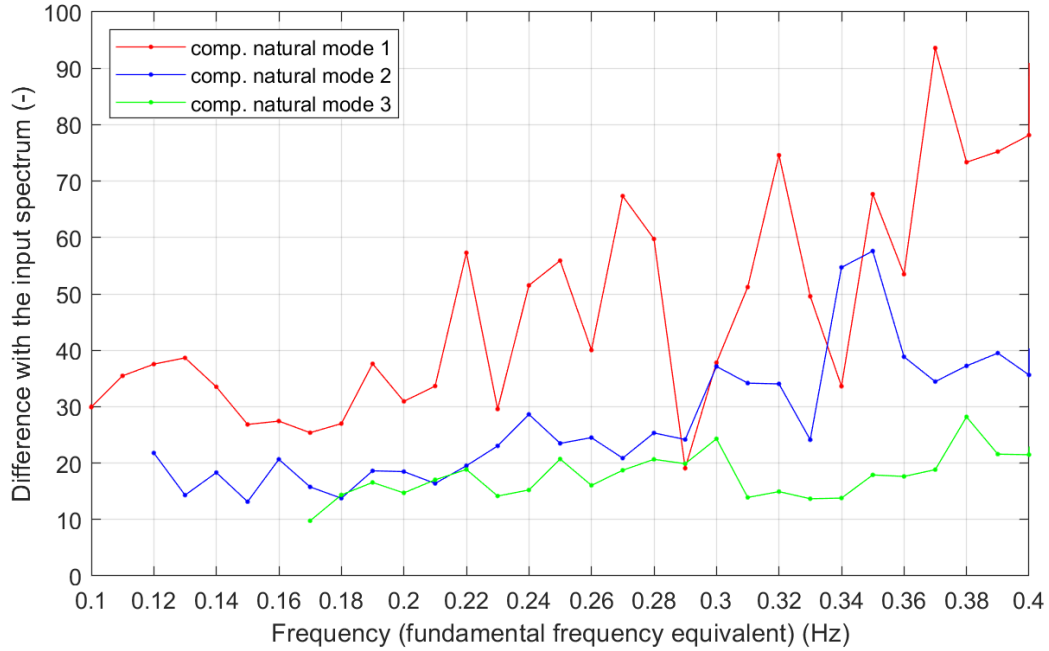

Figure 9.23: Spectrum comparison between the three first normal modes and the injected waves (zoom in input value spectrum)

Figure 9.23 is a zoom in input value spectrum limit. The pressure in the pipe could be 94 times bigger than the pressure injected. The summary of the graph is shown in Table 9.8.

n (-)	min (-)	max (-)	mean (-)
0.5	19.07	93.60	46.86
1.0	13.15	57.60	27.18
1.5	9.77	28.19	17.62

Table 9.8: Minimum, maximum and average value in Figure 9.23 for each mode

In the current analysis, the maximum pressure in meter was analysed in function of the mode of resonance and the wave celerity. The maximum pressure reached in the pipe was equal to 1.65 meter with a wave celerity equal to 330 m/s. This maximum of pressure corresponded to a wave injected at a frequency equal to 0.0431 m. The pressure in the pipe corresponded to 38 times the pressure injected at the outfall at the same frequency. This absolute value of pressures is not dangerofor the pipe because the typical pipe resists to up to 6.3 bar of nominal pressure (See Table 3.2).

The frequencies of the three first modes resonances were analysed in function of the wave celerity:

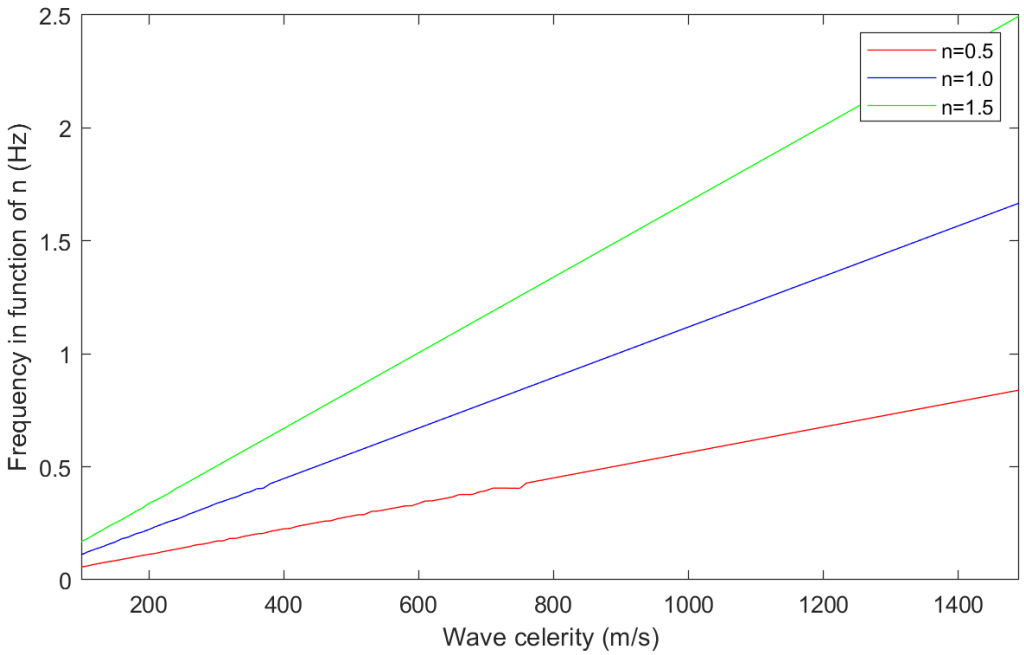

Figure 9.24: Frequency in function of the wave celerity in pipe for the three first normal modes

Figure 9.24 shows the passage in the high frequencies as the wave celerity increases. Like in the previous subsections, these frequencies could easily be calculated with Equation 8.3: $\left(F = \frac{na}{L}\right)$.

In this section, we reach the same conclusion as for the previous analysis. The maximum pressure reached until 1.6 bar while was bearable for the pipe. The pressure in pipe at the same frequency could reach 95 times the injected pressure at the same frequency. The pressure response as a function of the wave celerity with a "standard" wave spectrum and the injected wave was the

the main measurement uncertainty. To avoid the resonance zone in pipe, the wave celerity must be at least equal to 750 m/s.

6 Discussion

In this section, we analysed the frequency, magnitude and location of pressure peaks within the pipe, in function of three input parameters: depth of water, length of pipe and wave celerity. The wave celerity included several sub-parameters such as pipeline diameter or pipeline material. The aim of this study was to refine our analysis on what parameters influences the maximum of pressure within a sub-marine pipeline.

6.1 Building a Real Wave

The aim was to setup an excitation a wave in the system close to a real coastal wave. For this, we used measurements of the sea levels in Ebro Delta to build the wave to be injected in our system. In this manner, we were able to study the pipe with real conditions of wave. However, it is important to highlight that the results were here specific to the special conditions found at Ebro Delta. To improve the future simulations, the injected wave spectrum should be adapted to the specific location of the pipe of study, including the typical waves to which that pipe is subject.

6.2 Minimum Simulation Time

A first analysis determined an optimal number of oscillations to get stable results with a reasonable computing time. Indeed, a compromise had to be done between a shorter computing time, to allow running bigger ranges of input parameters, and a high simulation time, giving results closer to the reality. For this, we considered the stability of the results in function of the simulation time and the number of nodes in pipe. Following our analysis, the number of oscillations was set to 35. This number of oscillation represented 586 seconds of simulation time with typical pipe conditions. For different modes, the maximum pressure was found to lie within 5% of the mean pressure in all ranges of oscillation results. These results could now be confirmed by testing the simulations with bigger simulation time. The number of nodes was fixed to 100 because there were no difference of result between 100 nodes and 200 nodes after 25 number of oscillations.

6.3 Studying the Resonance Modes

The next step of our analysis was to study the max pressure within the pipe at different modes of resonance. As mentioned in the introduction of this chapter, we chose to include the fundamental mode (1st mode), as well as the 2nd and 3rd mode. The aim was to ensure a more complete analysis of the max of pressure within the pipe.
The frequency response of the three first normal modes were depending on the input parameters and were predicted by the equation $F = na/L$.
To find this equation, a Fourier analysis was done in order to automatically find the peaks of pressure in function of the frequency. These peaks corresponded to the different modes of resonance and the locations of the maximum of pressure in pipes were identified. The locations of resonance peaks were all fractions with the natural odd numbers (between one and the denominator value) in the denominator and a number equal to 2 times the number corresponding to the resonance mode (see Equation 9.3). The analysis revealed that the location of the peaks of pressure and the frequencies of resonance in pipe could be calculated.

6.4 Studying the Sea Depth

Following the analysis of the max of pressure at different resonance mode, a study of the impact of the sea depth on system was done. Indeed, studying the impact of the sea depth on pressures and frequencies within the pipe allowed us to understand if this parameter had an impact on the pressure level. Simulations with variable depth of sea (from 0 to 10 meters depth) in the typical installation were done. The analysis showed that the sea depth influenced the pressure in an exponential manner. The conclusion was that the a deep outfall allowed to isolate the pipeline from surface phenomena. Indeed, reported to a surface pipeline, the attenuation factor of the maximum pressure was equal to 3.8 at 2 meter depth, 10 at 3 meters depth and 1'490 at 8 meters depth.

6.5 Studying the Pipe's Length

Then, a study of the influence of the pipe's length on the pressure in pipe when a complete pressure wave spectrum is injected was done. Here we assessed the link between the injected spectrum and the frequencies of the pressure peaks. We included results for the three first modes of vibrations and our analysis revealed that the fundamental mode reached the highest pressure peaks along the different pipe's lengths. Indeed the peaks of pressure in the pipe for this mode of resonance reached until 1.74 m, which represents 2.75 times the significant injected wave (H_s = 0.637 m). The comparison between the peaks of pressure in function of the pipe's length and the corresponding injected frequencies for the critical zone (zone which the length of pipe corresponding to one of the frequency in output) showed that the frequency injected could be amplified from 17 times to 95 times at the first mode of vibration. It is important to understand the environment of a spectrum of wave. Indeed, choosing the right length of the pipeline allow to avoid resonance phenomena because it avoids that resonance of the characteristic frequencies of the waves on water surface.

6.6 Studying the wave celerity

Finally, a study of the impact of the wave celerity on pressure levels within the pipe was done. The wave celerity follows the same rules as the pipe's length because the natural resonance frequencies on the pipe depend on the pipe's length and on the wave celerity according to the formula: $F = na/L$. The resonance frequency of the pipe could be linked to a frequency in the injected pressure spectrum. In the typical pipe, the range wave celerity that implemented resonance phenomenon went from 200 m/s to 750 m/s. This range of wave celerity corresponded to the frequency of resonance in pipe of the input wave (F from 0.1 Hz to 0.4 Hz). One way to change the wave celerity is to change the material of the pipeline, Indeed, the most important factor of the wave celerity is the rigidity (Young modulus) of the pipe material. The diameter of the pipe and the way of anchoring modify the wave celerity too. In the case of typical pipe, choosing a pipe in GRP (glass reinforced plastic) or steel which have respectively a rigidity equal to 17 GPa and 200 GPa would make it possible to increase the celerity of the wave to 750 m/s and 1312 m/s. This value would allow to move the value of the resonance frequencies so that it does not interfere with the spectrum under study.

Conclusion

In this research we aimed to provide a better understanding of the transient and vibrating phenomena in sea outfalls pipes. More particularly, we wanted to study the resonance phenomena induced by a coastal wave spectrum and the influence of the depth of the sea, the length of pipe, the wave celerity in pipe and other parameters. In the end, we provided answers to the stating questions: What is the influence of the depth, of the diameter, of the material on level of pressure and vibrations in pipe? Are there any frequency of resonance in pipe and if yes, are there a location in pipe with height pressure?

The first step of this study was to define a typical pipe representing a "mean" case of the seabed pipeline. This pipe system was our case study during the project. In a second step, two software were chosen to study the typical pipe. The behaviour of the level of pressure of the water hammer and its propagation were compared with both software. However, MATLAB MOC was the only software capable to run simulations with this the outfall boundary conditions. For this reason, MATLAB MOC only was used for studying a simple pressure wave at the output and later on for studying a complete wave spectrum at output.

During this project, we rendered possible to study resonance phenomena in pipelines with a coastal wave at the outfall. Our research revealed that the location of the peaks of pressure and the frequencies of resonance in the pipe can be calculated. We found that the resonance frequency is proportional to two main parameters: the length of pipe and the wave celerity in pipe. The frequency of resonance was found with the formula: $F = na/L$, with n equal to the number of wave within the pipe according to the number of the vibration mode. With the frequency of resonance, we could located within the pipe where corresponding peaks of pressure correspond were located. The peaks of pressure followed a pattern equal to a fraction with the natural odd numbers in the denominator (between one and the denominator value) and a number equal to 2 times the number corresponding to the resonance mode.

However, while the location of the pressure peaks and the resonance frequency could be calculated, the level of pressures at this point were difficult to interpret. The pressure peaks were far from reaching the nominal pressures of the typical pipe. Indeed, the typical pipe chosen has nominal pressure equal to 10 bar and the peaks grows the maximal pressure to 2.7 bar. The interesting points of investigation were the difference between the relative pressure in pipe and the level of pressure corresponding to the same frequency in the injected wave spectrum. Indeed, there was until a difference equal to 95 times between the injected wave and the corresponding pressure within the pipe. The investigation about the level of pressure should be continued in order to predict with more accuracy the pressures reached according to those injected.

By studying the impact of sea depth on the system, we observed that it affected exponentially the level of the pressure within the pipe. Indeed, the pressure in the tube was decreased by a factor equal to the hyperbolic cosinus of the depth. A the deep outfall therefore allows to isolate the pipeline from surface phenomena. For example, reported to a surface pipeline, the attenuation factor of the maximum pressure is equal to 3.8 at 2 meter depth, 10 at 3 meters depth and 1'490 at 8 meters depth.

Our analysis also showed that the pipe's length has an impact on resonance phenomena within the pipe. Hence, as there is a link between the length of the pipe and the mode of resonance,

choosing the right length is a mean to decrease these phenomena. With the numerical model developed in this project, we are now able to determine the optimal length (or the lengths to be avoided) given a specific input wave spectrum. The research shows that the fundamental mode reach the highest pressure peaks along the different pipe's lengths.

The study of the wave celerity includes several parameters because the wave celerity is impacted by the rigidity of the material, the inner diameter, the thickness and others parameter in pipe. In this research, we simulated only a change of the wave celerity and did not look at the internal parameters. We showed for the typical pipe that the range of wave celerity that implements resonance phenomenon went from 200 m/s to 750 m/s. The typical pipe in HDPE had a wave celerity equal to 215 m/s. One way to change the wave celerity is to change the material of the pipeline, Indeed, the most important factor influencing the wave celerity is the rigidity (Young modulus) of the pipe material. For example, with a pipe in glass reinforced plastic or in steel, the celerity of the wave grows respectively to 750 m/s and 1312 m/s. Therefore, a simple change of material would allow to decrease resonance phenomena within this wave spectrum. The pipe dimension ratio (internal diameter divided by the thickness) is the second parameter where influences the wave celerity.

While we could get important results with our model, it is important to highlight some limitations. Indeed, the model was based on a "simple" test bench which is a seabed pipeline with water and a typical pressure coastal wave injected at the outfall. The coastal wave was build from measurements of the sea level at Delta Ebro. The simulations used simple steady state or quasi steady state friction in order to simplify the simulations. The pipeline consisted of one piece (no joints between sections) and no specific anchoring or ballast (only expansion joint at outfall). These parameters could be adapted to study specific installation and get more precise results. An other way to simulate a real situation with more accuracy would be to compile a fluid structure interaction (FIS) in the MATLAB code. It was an objective but it needs time to be added. This research is intended for engineers who have to understand vibrating phenomena within a pipe. However, it is important to note that we did not validate our computational results with experimental measurements. Therefore, a next step would be to check the suitability of our simulation results with a test bench.

In summary, we implemented a new computational model (derived from existing MATLAB MOC code) to simulate diverse parameters influencing the pressure and vibrations within a sea pipe. This model could be further improved to answer to different questions. However, it already allowed us to show how simple changes, such as the pipe's length or the material, could be done to decrease the vibration phenomena within the pipe and therefore improve the installation.

Bibliography

[1] Mohamed Ghidaoui, Ming Zhao, and Duncan Mclnnis. A review of water hammer theory and practice. 2005.

[2] J. Michaud. Coups de bélier dans les conduites, Etude des moyens employés pour en atteneur les effects. Bulletin de la Société Vaudoise des Ingénieurs et des Architectes, 1878.

[3] Nikolaï Legorovitch Joukovski. Memoirs of the Imperial Academy Society of St. Petersburg. 1898.

[4] L. Allievi. Teoria generale del moto perturbato dell'acquani tubi in pressione. Revue de mécanique, 1903.

[5] M. Lister. The Numerical Solution of Hyperbolic Partial Differential Equations by the Method of Characteristics. 1960.

[6] John H. Nath and Fred L. Ramsey. Probalility distributions of breaking wave heights emphasizing the utilization of the jonswap spectrum. Journal Of Phisical Oceanography, 1975.

[7] Larsen Torben. The influence of waves on the hydraulics of sea outfalls, chapter 190. University of Aalborg, Danmark, 1986.

[8] Jacques Bonnin. Ecoulement des fluides dans les tuyauteries. In Techniques de l'ingénieur, editor, Techniques de l'ingénieur. 1983.

[9] A. S. Tijsseling. Review: Fluid-structure interaction in liquid-filled pipe systems. Journal of Fluids and Structures, 10(2):109 – 146, 1996.

[10] Jul Izquierdo and P. L. Iglesias. Mathematical modelling of hydraulic transients in simple systems. Mathematical and Computer Modelling, 35(7):801 – 812, 2002.

[11] Aboudou Seck. Développement d'un outil multi-approches pour la modélisation numérique du phénomène de coup de bélier. PhD thesis, 2017.

[12] Rune Kjerrumgaard Jensen, Jesper Kær Larsen, and Kasper Lindgren Lassen. Modelling of a two phase water hammer. Master's thesis, Aalborg University, 2018.

[13] Rune Kjerrumgaard Jensen, Jesper Kær Larsen, Kasper Lindgren Lassen, Matthias Mandø, and Anders Andreasen. Implementation and validation of a free open source 1d water hammer code. Fluids, 3(3):64, sep 2018.

[14] David Ferras and Didia Covas. Frequency and time-domain analyses of pipelines achanred against longitudinal movement, 2019.

[15] Lahcen Ait Moudid. Couplage Fluide Structure pour la simulation numérique des écoulements fluides dans une conduite à parois rigides ou élastiques, en présence d'obstacles ou non. Theses, Université d'Artois, October 2007.

[16] Philip Roberts. Marine wastewater outfalls and treatment systems. IWA Publishing, London New York, 2010.

[17] Thomas M. Missimer, Burton Jones, and Robert G. Maliva. Intakes and Outfallsfor Seawater Reverse-Osmosis Desalination Facilities, volume Innovations and Environmental Impacts. Springer edition, 2015.

[18] Matweb material probriety data. http://www.matweb.com/search/datasheet.aspx?matguid=482765fad3b443169ec28fb6f9606660&ckck=1.

[19] Rich Pawlowicz. Key physical variables in the ocean: Temperature, salinity, and density. https://www.nature.com/scitable/knowledge/library/key-physical-variables-in-the-ocean-temperature-102805293/.

[20] Seawater. https://en.wikipedia.org/wiki/Seawater.

[21] R. Feistel, S. Weinreben, H. Wolf, S. Seitz, P. Spitzer, B. Adel, G. Nausch, B. Schneider, and D. G. Wright. Density and absolute salinity of the baltic sea 2006–2009. Ocean Science, 6(1):3–24, 2010.

[22] M. Hanif Chaudhry. Applied Hydraulic Transients. Springer-Verlag GmbH, 2013.

[23] Arris Tijsseling. Papers presented at 12th International Conference on Pressure Surges, Dublin, Ireland, 18-20 November 2015. BHR Group,the Fluid Engineering Centre, Cranfield, Bedfordshire, United Kingdom, 2015.

[24] M. Wesson. Analysis of spectra, wave grouping and long wave phenomena of real measured waves in coastal waters. 2010.

[25] Baharuddin Ali. Matlab-generate a signal in time domain from wave spectrum.

[26] A. Bergant and A. Tijsseling. Parameters affecting water hammer wave attenuation, shape and timing. In Proceedings of the 10th International Meeting of the IAHRWork Group on the Behaviour of Hydraulic Machinery under Steady Oscillatory Conditions, Trondheim, Norway, 2001.

[27] T. Traudt, C. Bombardieri, and C. Manfletti. Influences on water-hammer wave shape: an experimental study. CEAS Space Journal, 8(3):215–227, may 2016.

[28] Wikipedia. Wind wave.

[29] Sahil Lahane, Rachana Patil, Rashmi Mahajan, and Kavita Palve. Analysis of water hammering in pipeline and its cfd simulation. International Journal of Engineering Technologiy, Management and Apllied Sciences (IJETMAS), 2005.

[30] Ben R. Hodges, Jordan E. Furnans, and Paula S. Kulis. Thin-layer gravity current with implicationsfor desalination brine disposal. American Society of Civil Engineers, 2011.

[31] Katie Rose and Ben R. Hodges. Evaluating the effects of low impact development. Technical report, Texas A&M University West Campus, 2010.

[32] Marcel Frelin. Coups de bélier. In Techniques de l'ingénieur, editor, Technique de l'ingénieur. 2002.

[33] G. H. Jirka and P. J. Akar. Hydrodynamic classification of submerged multiport-diffuser discharges, 1991.

[34] I. R. Wood, R. G. Bell, and D. L. Wilkinson. Ocean Disposal of Wastewater, volume 8. 1993.

[35] Rashad Danoun. Desalination plants: Potential impacts of brine discharge on marine life, 2007.

[36] Louise Roberts and Michael Elliott. Good or bad vibrations? impacts of anthropogenic vibration on the marine epibenthos. Science of The Total Environment, 595:255–268, 2017.

[37] Kenji Ishihara and Susumu Yasuda. Sand liquefaction due to irregular excitation. Soils and Foundations, 12(4):65–77, 1972.

[38] Daniel Valero and Daniel B. Bung. Sensitivity of turbulent schmidt number and turbulence model to simulations of jets in crossflow. Environmental Modelling & Software, 82:218–228, 2016.

Appendix

1 List of pipe from: *Intakes And Outfalls For Seawater Reverse-Osmosis Desalination Facilities* (2015)

N	Country	Project	Year	Lenght (m)	Diameter (m)	cost (Mio$)	ENR Index	ENR factor	Cost tot (Moi$)	Cost/meter ($)	Source/material
1	Chile	Mejillones	2000	959	0.35	3.22	7959	1.07	3.45	3602	HDPE
2	Chile	Huasco	2003	850	0.36	0.86	7959	1.07	0.92	1080	HDPE
3	Israel	Soreq	1984	5200	0.40	2.70	4146	2.06	5.55	1068	HDPE
4	USA	Rockaway Beach	NaN	900	0.40	1.60	NaN	NaN	1.60	1778	Tunnel
5	DK	Kolta	1995	150	0.40	0.45	5500	1.55	0.70	4652	G&F
6	Brazil	Itaquanduba Ilhabela, SF	2008	923	0.40	5.40	7959	1.07	5.79	6269	HDPE
7	Chile	Lebu	2005	838	0.45	1.78	7959	1.07	1.91	2280	HDPE
8	Yugoslavia	Dubrovnik	1974	1500	0.45	5.50	2020	4.22	23.22	7740	G&F
9	Bermuda	Bermuda	1992	180	0.49	0.50	5000	1.71	0.85	4738	G&F
10	DK	Vallo	1985	800	0.50	0.30	4220	2.02	0.61	758	G&F
11	Turkey	Trabzon, Akç,aabat	2002	1075	0.50	1.88	6538	1.30	2.45	2280	HDPE
12	Turkey	Ordu, Fatsa	2004	1820	0.50	3.54	7115	1.20	4.24	2330	HDPE
13	Turkey	Trabzon, Sögütlü	2001	948	0.50	1.72	6343	1.34	2.32	2445	HDPE
14	Chile	Higuerillas	2002	500	0.50	3.11	7959	1.07	3.33	6667	HDPE
15	USA	Coos Bay, OR	1972	1440	0.52	1.80	1753	4.86	8.76	6081	G&F
16	USA	Toledo, OR	1965	1130	0.53	0.96	1000	8.53	8.19	7245	G&F
17	Chile	Coronel	2004	2130	0.56	2.20	7959	1.07	2.35	1104	HDPE
18	Chile	Lota	2000	1527	0.56	2.34	7959	1.07	2.51	1641	HDPE
19	Turkey	Trabzon, Havaalanı	2001	948	0.56	1.88	6343	1.34	2.52	2663	HDPE
20	USA	Los Angeles, CA	1957	11260	0.56	2.60	724	11.78	30.63	2720	G&F
21	USA	Passaic, NJ	1920	460	0.60	0.10	357	23.89	2.39	5193	G&F
22	Dom.	Sosua	2007	787	0.61	2.00	7966	1.07	2.14	2721	HDPE
23	USA	Carmel, CA	1971	272	0.61	0.41	1581	5.39	2.21	8131	G&F
24	Chile	El Tabo y El Quisco	2003	1729	0.63	1.84	7959	1.07	1.97	1142	HDPE
25	Turkey	Guzelbahce, Izmir Bay	2002	600	0.63	2.20	6538	1.30	2.87	4783	HDPE
26	DK	Ketamindc	1989	650	0.71	0.50	4800	1.78	0.89	1367	G&F
27	Chile	San Antonio	2006	1050	0.71	2.00	7959	1.07	2.14	2041	HDPE
28	Turkey	Rize, Centre	2004	1206	0.71	3.54	7115	1.20	4.25	3522	HDPE
29	USA	Salmon Creek, WA	1974	312	0.76	0.28	2100	4.06	1.14	3644	Wallis
30	USA	Seattle, WA	1962	640	0.76	0.27	872	9.78	2.64	4126	G&F
31	USA	San Elijo, CA	1965	820	0.76	0.96	1000	8.53	8.19	9984	G&F
32	Chile	Conco' n, Con Con Orien	2002	2500	0.80	1.50	7959	1.07	1.61	642	HDPE
33	DK	Guldborg	1976	700	0.80	0.20	2401	3.55	0.71	1015	G&F
34	Chile	Punta Arenas	2003	1244	0.80	1.50	7959	1.07	1.61	1292	HDPE
35	Turkey	Trabzon, Yomra	2001	957	0.80	2.90	6343	1.34	3.89	4069	HDPE
36	Turkey	Trabzon, Degirmendere	2001	1094	0.80	3.32	6343	1.34	4.46	4081	HDPE

37	Australia	Victoria, Latrobe Valley	1992	1300	0.80	5.00	7959	1.07	5.36	4121	HDPE
38	Peru	Lima, Playa Venecia	2002	900	0.80	3.57	7959	1.07	3.82	4248	HDPE
39	USA	Seattle, WA	1962	490	0.84	0.15	872	9.78	1.47	2994	G&F
40	USA	N. San Mateo CSD, CA	1962	760	0.84	0.41	945	9.02	3.70	4868	Wallis
41	USA	San Mateo, CA	1962	490	0.84	0.84	872	9.78	8.22	16765	G&F
42	Chile	San Pedro de la Paz	2006	2140	0.90	1.92	7959	1.07	2.06	963	HDPE
43	Chile	San Vicente	2000	1800	0.90	3.27	7959	1.07	3.50	2086	HDPE
44	Chile	Antofagasta	1998	985	0.90	3.49	7959	1.07	3.74	3801	HDPE
45	Turkey	Trabzon, Moloz	2001	856	0.90	2.99	6343	1.34	4.02	4701	HDPE
46	Turkey	Mersin, Mezitli	2007	1805	0.90	8.04	7966	1.07	8.60	4766	HDPE
47	Turkey	Mersin	2007	1805	0.90	8.03	7959	1.07	8.61	4770	HDPE
48	USA	Oceanside, CA	1972	2500	0.91	1.90	1753	4.86	9.24	3697	G&F
49	Sweden	Monsteras	1999	5000	1.00	3.00	6059	1.41	4.22	844	HDPE
50	USA	Watsonville, CA	1959	1170	1.00	0.47	797	10.70	5.03	4298	G&F
51	Colombia	Santa Marta	2003	500	1.00	2.00	6694	1.27	2.55	5096	HDPE
52	Australia	Coffs Harbour, NSW	2005	1550	1.00	10.00	7959	1.07	10.71	6913	HDPE
53	USA	Eureka, CA	1977	1940	1.10	9.40	3200	2.67	25.05	12913	Wallis
54	Canada	Vancouver, BC	1993	250	1.17	1.26	5300	1.61	2.03	8110	G&F
55	Spain	Albufereta	2007	4393	1.20	8.11	7959	1.07	8.69	1846	HDPE
56	Turkey	Mugla, Marmaris	2005	406	1.20	0.75	7446	1.15	0.86	2116	HDPE
57	USA	Encina, CA	1964	1370	1.20	0.35	926	9.21	3.22	2353	G&F
58	Chile	Arauco	1997	970	1.20	3.33	7959	1.07	3.57	3678	HDPE
59	USA	San Elijo, CA – extension	1975	1220	1.20	1.30	2250	3.79	4.93	4039	Wallis
60	Chile	Vina del Mar	1996	1495	1.20	5.66	7959	1.07	6.07	4059	HDPE
61	Portugal	Leirosa, Figueira de Foz	1995	1500	1.20	7.00	7959	1.07	7.50	4667	HDPE
62	USA	Aliso, CA	1976	2620	1.20	4.80	2950	2.89	13.88	5296	Wallis
63	Turkey	Istanbul	1992	450	1.20	1.50	4985	1.71	2.57	5702	Steel
64	USA	Santa Barbara, CA	1975	2660	1.20	4.60	2310	3.69	16.98	6384	Wallis
65	Portugal	Cascais	1990	1800	1.20	12.00	4732	1.80	21.63	6667	HDPE
66	Hawaii	Mokapu	1974	1547	1.20	6.20	2577	3.31	20.52	13263	G&F
67	USA	San Francisco, CA	1974	180	1.20	0.57	2020	4.22	2.41	13369	G&F
68	Turkey	Istanbul, Uskudar	1994	270	1.20	5.10	5504	1.55	7.90	14633	G&F
69	Puerto	Arecibo	1976	1070	1.20	6.80	3400	2.51	17.06	15940	Wallis
70	USA	EBMUD, Oakland, CA	1995	146	1.37	0.55	5500	1.55	0.85	5841	G&F
71	Chile	Talcahuano, Huachipato	2006	1448	1.40	2.26	7959	1.07	2.42	1672	HDPE
72	Chile	Valparaiso, Loma Larga	1999	820	1.40	5.02	7959	1.07	5.38	6556	HDPE
73	USA	Dana Point, CA	1977	3600	1.40	9.80	3200	2.67	26.12	7255	Wallis

74	USA	San Francisco, CA	1966	250	1.40	0.46	1019	8.37	3.85	15399	G&F
75	USA	Bellingham, WA	1973	850	1.50	0.44	1895	4.50	1.98	2330	G&F
76	Greece	Thessalonicki	1998	10520	1.60	16.00	7959	1.07	17.14	1630	RC
77	Romania	Constanta Nort	2006	5750	1.60	22.00	7751	1.10	24.21	4210	GRP
78	Romania	Constanta (RO)	2006	5750	1.60	22.00	7751	1.10	24.21	4210	GRP
79	France	Montpellier	2004	10800	1.60	45.00	7115	1.20	53.94	4994	HDPE
80	Turkey	Istanbul, Yenikapi	1987	1150	1.60	7.50	4406	1.94	14.52	6312	Steel
81	Turkey	Istanbul, Ahirkapi	1989	1100	1.60	13.70	4800	1.78	24.34	11064	G&F
82	USA	Hampton, VA	1981	2930	1.70	12.30	3600	2.37	29.14	9944	G&F
83	Turkey	Istanbul, Baltalimani	1994	270	1.70	9.50	5504	1.55	14.72	27258	G&F
84	Turkey	Mersin	2007	2000	1.80	3.70	7966	1.07	3.96	1981	GRP
85	USA	Contra Costa County, CA	1959	520	1.80	0.17	797	10.70	1.82	3498	G&F
86	USA	Encina, CA extension	1973	700	1.80	1.05	1980	4.31	4.52	6461	Wallis
87	USA	Encina, CA	1973	700	1.80	1.05	1895	4.50	4.73	6750	G&F
88	Philippines	Manila	1985	3600	1.80	13.00	4220	2.02	26.27	7298	G&F
89	Puerto	Ponce	1972	1550	1.80	3.30	1753	4.86	16.05	10357	G&F
90	USA	Santa Cruz, CA (2)	1976	2740	1.80	10.70	3200	2.67	28.52	10407	Wallis
91	USA	Santa Cruz, CA (1)	1976	2900	1.80	12.50	3200	2.67	33.31	11487	Wallis
92	USA	Suffolk County, NY	1981	5777	1.80	28.80	3600	2.37	68.22	11810	G&F
93	USA	Los Angeles Harbor	1995	1585	1.80	20.00	5500	1.55	31.01	19565	G&F
94	Hawaii	Barbers Point	1976	3200	1.98	12.00	2401	3.55	42.62	13319	G&F
95	Colombia	Cartagena	2009	3200	2.00	28.00	8549	1.00	27.93	8729	HDPE
96	Hawaii	Ewa Beach	1976	3210	2.00	11.84	3200	2.67	31.55	9830	Wallis
97	Hawaii	Sand Island	1976	3816	2.10	13.60	2401	3.55	48.31	12659	G&F
98	Turkey	Istanbul, Kadikoy	2004	2300	2.20	12.00	7115	1.20	14.38	6254	Steel
99	Turkey	Istanbul, Tuzla	1995	2200	2.20	18.50	5471	1.56	28.84	13108	Steel
100	USA	Los Angeles County, CA	1954	3170	2.30	2.20	628	13.58	29.88	9424	G&F
101	USA	South San Francisco Bay	1977	11600	2.40	34.50	3440	2.48	85.53	7373	Wallis
102	USA	Seattle, WA	1964	1110	2.40	1.20	986	8.65	10.38	9350	G&F
103	USA	EBMUD-original, CA	1949	1820	2.40	1.20	480	17.77	21.32	11714	Wallis
104	USA	EBMUD-extension, CA	1974	120	2.40	0.46	2220	3.84	1.77	14726	Wallis
105	Brazil	Rio de Janiero	1975	4325	2.40	22.00	2212	3.86	84.82	19611	G&F
106	India	Bombay	1985	6000	2.40	65.00	4220	2.02	131.36	21893	G&F
107	USA	Bondi, NSW	1975	3400	2.40	28.00	2600	3.28	91.84	27012	Wallis
108	UK	Aberdeen	1979	1800	2.50	13.50	3003	2.84	38.34	21299	Tunnel
109	Scotland	Aberdeen	1978	2700	2.50	17.60	2600	3.28	57.73	21381	G&F
110	Australia	Sydney, Bondi	1986	2300	2.50	55.00	4300	1.98	109.08	47426	G&F

111	USA	San Francisco, N Point		1971	1520	2.60	4.00	1850	4.61	18.44	12131	Wallis
112	USA	San Diego, CA Pt. Loma		1961	4320	2.70	7.80	940	9.07	70.76	16381	Wallis
113	USA	San Diego, CA		1962	4340	2.70	10.50	872	9.78	102.69	23661	G&F
114	USA	San Francisco, CA		1970	90	2.70	0.40	1385	6.16	2.46	27366	G&F
115	USA	San Diego, CA		1992	5330	2.70	90.00	5200	1.64	147.60	27692	G&F
116	USA	North Head, NSW		1975	3400	2.80	25.00	25	3.28	82.00	24118	Wallis
117	USA	Orange County, CA		1969	8350	3.00	9.00	1269	6.72	60.48	7243	G&F
118	USA	Los Angeles CSD (#4)		1964	3620	3.00	4.50	1020	8.36	37.62	10393	Wallis
119	USA	Los Angeles County, CA		1964	3620	3.00	4.50	986	8.65	38.92	10752	G&F
120	USA	San Diego, CA		1995	2652	3.05	50.00	5500	1.55	77.53	29234	G&F
121	USA	Malabar, NSW		1975	3100	3.10	25.00	2600	3.28	82.00	26452	Wallis
122	USA	San Diego, CA		1995	1430	3.10	36.00	5500	1.55	55.82	39035	G&F
123	USA	Redondo Beach, CA		1947	2650	3.20	2.20	413	20.65	45.43	17142	G&F
124	China	Hong Kong		1995	1200	3.25	12.50	5500	1.55	19.38	16152	G&F
125	USA	El Segundo, CA		1954	2620	3.30	2.30	629	13.56	31.18	11902	G&F
126	USA	San Diego, South Bay	NaN		8400	3.30	NaN	NaN	NaN	133.00	15833	Tunnel
127	Australia	Sydney, Malabar		1986	3500	3.30	55.00	4300	1.98	109.08	31165	G&F
128	USA	San Diego, CA		1995	5490	3.40	90.00	5500	1.55	139.55	25419	G&F
129	Australia	Sydney – North Head		1986	3400	3.50	68.00	4300	1.98	134.86	39665	G&F
130	USA	San Onofre, CA		1965	1740	3.60	3.30	1070	7.97	26.30	15116	Wallis
131	USA	San Onofre, CA		1965	1740	3.60	3.30	971	8.78	28.98	16657	G&F
132	USA	Los Angeles, CA		1950	1610	3.60	2.00	570	14.96	29.92	18586	G&F
133	USA	Huntington Beach, CA		1957	820	3.60	1.50	724	11.78	17.67	21547	G&F
134	USA	Los Angeles, CA		1957	8046	3.60	20.20	724	11.78	237.94	29572	G&F
135	Peru´	Taboada		1994	8000	3.65	264.00	5408	1.58	416.31	52038	RC
136	USA	Seattle, WA		1995	168	3.66	3.20	5500	1.55	4.96	29534	G&F
137	Argentina	Berazetagui		2008	7500	4.00	200.00	8310	1.03	205.25	27366	Tunnel
138	China	Shanghai		1984	1460	4.20	19.60	NaN	2.73	53.49	18320	G&F
139	China	Shanghai		1995	1600	4.20	23.00	5500	1.55	35.66	22289	G&F
140	USA	Ormoud Beach, CA		1969	1300	4.30	3.40	1300	6.56	22.30	17157	Wallis
141	USA	Boston, MA		1995	7650	4.30	151.10	5500	1.55	234.29	30626	G&F
142	Hong	Hong Kong		1995	1800	5.00	45.00	5500	1.55	69.77	38764	G&F
143	USA	San Onofre, CA		1976	6430	5.50	65.00	3200	2.67	173.23	26940	Wallis
144	USA	Boston		2000	16000	7.60	390.00	6221	1.37	534.63	33414	Tunnel
145	USA	Boston, MA		1995	15200	8.10	334.20	5500	1.55	518.19	34092	G&F
Mean				**1985**	**2566**	**1.82**						

2 MATLAB Source Code

```
% Choose downstream boundary condition:
% 1)     Valve_Instantaneous_Closure
% 2)     Valve_Transient_Closure
% 3)     Valve_No_Closure
% 4)     Valve_Sinusoidal
% 5)     Valve_Closure_delay
% 6)     Valve_open_and_Pressure_sin
% 7)     Valve_open_and_Pressure_Spectrum
Downstream_boundary = 'Valve_open_and_Pressure_Spectrum';
```

Listing A.1: Choose of boundary condtion in *Input* file

```
switch Downstream_boundary
        case 'Valve_Instantaneous_Closure'
                m = 0; % Valve closure coefficient  [-]
                t_c = 2;  % Closing time of valve   [s]
        case 'Valve_Transient_Closure'
                        % 1 = lineare
                m = 5;   % Valve closure coefficient  [-]
                t_c = 2; % Closing time of valve      [s]
        case 'Valve_No_Closure'
                m = inf ;
                t_c = inf ;
        case 'Valve_Sinusoidal'
                m = inf;        % keep inf [-]
                t_c = 50;       % start time sinusoidal valve [s]
                Ap_0 = 80;      % Aperture initial  [%]
                Ap = 20;        % Aperture amplitude (+/-) [%]
                P = 2;          % Periode of oscilation  [s]
        case 'Valve_Closure_delay'
                        % 1 = lineare
                m = 1;          % Valve closure coefficient  [-]
                t_c = 10;       % Closing time of valve        [s]
                t_c_0 = 10;     % Delay before cosure start time [s]
        case'Valve_open_and_Pressure_sin'
                m = abs(sind(theta)*L); % deep of sea [m]
                t_c = inf;      % no using
                Ap_0 = 0.05;    % Initial level [m]
                Ap = 0.27;      % Amplitude level (+/-) [m]
                P = 3;  % Wave periode  [s]
        case'Valve_open_and_Pressure_Spectrum'
                m = 0;          % do not remove
                t_c = 5;        % wave spectrum time start [s]
                        %         00_WaveSpectrum
                WaveVec_name = '00_WaveSpectrum';
                        % Matrix loading
                WaveFile = load(fullfile(WaveVec_name));
                WaveSpec= WaveFile.WaveSpec;
```

```
37 end
```

Listing A.2: Valve switch and parameters *Input* file

```
1  %% Downstream Boundary
2  switch Downstream_boundary
3          case 'Valve_Instantaneous_Closure'
4                  [Q(n,j), H(n,j), tau_v(j)] = Valve_Closure(a, g, A, D
                       , dx, roughness,...
5                          rho, viscosity, t(j), t_c, m, theta, Q(n,1),
                             H(n,1),...
6                          Q(n-1,j-1), H(n-1,j-1), Q, Re_0, i, j, dt,...
7                          Friction_Type, f_pre, W, dQ, n_t);
8          case 'Valve_Transient_Closure'
9                  [Q(n,j), H(n,j), tau_v(j)] = Valve_Closure(a, g, A, D
                       , dx, roughness,...
10                         rho, viscosity, t(j), t_c, m, theta, Q(n,1),
                             H(n,1),...
11                         Q(n-1,j-1), H(n-1,j-1), Q, Re_0, i, j, dt,...
12                         Friction_Type, f_pre, W, dQ, n_t);
13         case 'Valve_No_Closure' % original one
14                 [Q(n,j), H(n,j), tau_v(j)] = Valve_Closure(a, g, A, D
                       , dx, roughness,...
15                         rho, viscosity, t(j), t_c, m, theta, Q(n,1),
                             H(n,1),...
16                         Q(n-1,j-1), H(n-1,j-1), Q, Re_0, i, j, dt,...
17                         Friction_Type, f_pre, W, dQ, n_t);
18         case 'Valve_Sinusoidal'
19                 [Q(n,j), H(n,j), tau_v(j)] = Valve_Closure_Sin(a, g,
                       A, D, dx, roughness,...
20                         rho, viscosity, t(j), t_c, m, theta, Q(n,1),
                             H(n,1),...
21                         Q(n-1,j-1), H(n-1,j-1), Q, Re_0, i, j, dt,...
22                         Friction_Type, f_pre, W, dQ, n_t, Ap_0, Ap, P
                             );
23         case 'Valve_Closure_delay'
24                 [Q(n,j), H(n,j), tau_v(j)] = Valve_Closure_delay(a, g
                       , A, D, dx, roughness,...
25                         rho, viscosity, t(j), t_c, m, theta, Q(n,1),
                             H(n,1),...
26                         Q(n-1,j-1), H(n-1,j-1), Q, Re_0, i, j, dt,...
27                         Friction_Type, f_pre, W, dQ, n_t, t_c_0);
28         case 'Valve_open_and_Pressure_sin'
29                 [Q(n,j), H(n,j),tau_v(j)] = Valve_Pressure_Sin(a, L,
                       g, A, D, dx, roughness,...
30                         rho, viscosity, t(j), t_c, m, theta, H_r, Q(n
                             ,1), H(n,1),...
31                         Q(n-1,j-1), H(n-1,j-1), Q, Re_0, i, j, dt,...
32                         Friction_Type, f_pre, W, dQ, n_t, Ap_0, Ap, P
                             );
```

```
33          case 'Valve_open_and_Pressure_Spectrum'
34                  [Q(n,j), H(n,j)] = Valve_Pressure_Spectre(a, L, g, A,
                        D, dx, roughness,...
35                          rho, viscosity, t(j), t_c,m , theta, H_r, Q(n
                                ,1), H(n,1) ,...
36                          Q(n-1,j-1), H(n-1,j-1), Q, Re_0, i, j, dt,...
37                          Friction_Type, f_pre, W, dQ, n_t, WaveSpec);
38  end
```

Listing A.3: Valve switch case in *1D_Solver* file

```
1   function [Q_P, H_P, tau_v] = Valve_Closure_delay(a, g, A, D, dx,
        roughness, rho,...
2   viscosity, t, t_c, m, theta, Q_0, H_0, Q_A, H_A, Q, Re_0, i, j, dt
        ,...
3   Friction_Type, f_pre, W, dQ, n_t, t_c_0)
4   %% Calculating the dimensionless closure time for the valve
5   if t < t_c_0;
6           tau_v = 1;
7   elseif t >= (t_c_0 + t_c);
8           % Dimensionless valve closure time                  [-]
9           tau_v = 0;
10  else
11          % Dimensionless valve closure time                  [-]
12          tau_v = 1 - ((t-t_c_0)/t_c)^m;
13  end
14  %% Calculating the volumetric flow rate at the valve
15  % Pipe constant                                             [s/m^2]
16  B = PipeConst(a, g, A);
17
18  % Positive characteristics equation                         [m]
19  C_p = Characteristic_Plus(a, g, A, D, dx, roughness, rho,...
20          viscosity, theta, Q_A, H_A, Q, Re_0, i, j, dt,...
21          Friction_Type, Q_0, f_pre, W, dQ, n_t);
22
23  % Variable                                                  [m^5/s^2]
24  C_v = (Q_0*tau_v)^2/(2*H_0);
25
26  % Volumetric flow rate                                      [m^3/s]
27  Q_P = - B*C_v + sqrt((B*C_v)^2 + 2*C_v*C_p);
28
29  %% Calculation of the head
30  % Piezometric head                                          [m]
31  H_P = C_p - B*Q_P ;
32
33  end
```

Listing A.4: *Valve_Closure_delay* function

```
1   function [Q_P, H_P, tau_v] = Valve_Closure_Sin(a, g, A, D, dx,
        roughness, rho,...
```

```
        viscosity, t, t_c, m, theta, Q_0, H_0, Q_A, H_A, Q, Re_0, i,
            j, dt,...
        Friction_Type, f_pre, W, dQ, n_t, Ap_0, Ap, P)
%% Calculating the dimensionless closure time for the valve
if t >= t_c
        % Dimensionless valve closure time                    [-]
        %     tau_v = 1 - (t/t_c)^m;
                tau_v = Ap_0/100 + Ap/100*sin(2*pi*t/P+(pi/4));
else
        % Dimensionless valve closure time                    [-]
                tau_v = 1 ;
end

%% Calculating the volumetric flow rate at the valve
% Pipe constant                                              [s/m^2]
B = PipeConst(a, g, A);

% Positive characteristics equation                          [m]
C_p = Characteristic_Plus(a, g, A, D, dx, roughness, rho,...
        viscosity, theta, Q_A, H_A, Q, Re_0, i, j, dt,...
        Friction_Type, Q_0, f_pre, W, dQ, n_t);

% Variable                                                   [m^5/s^2]
C_v = (Q_0*tau_v)^2/(2*H_0);

% Volumetric flow rate                                       [m^3/s]
Q_P = - B*C_v + sqrt((B*C_v)^2 + 2*C_v*C_p);

%% Calculation of the head
% Piezometric head                                           [m]
H_P = C_p - B*Q_P ;

end
```

Listing A.5: *Valve_Closure_Sin* function

```
function [Q_P, H_P, tau_v] = Valve_Pressure_Sin(a,L, g, A, D, dx,
    roughness, rho,...
        viscosity, t, t_c, m, theta, H_r, Q_0, H_0, Q_A, H_A, Q, Re_0
            , i, j, dt,...
        Friction_Type, f_pre, W, dQ, n_t, Ap_0, Ap, P)
%% Calculating the volumetric flow rate at the valve
T = P; % T = periode of vawe
h = m; % H = depht of water
% Pipe constant                                              [s/m^2]
B = PipeConst(a, g, A);

% Positive characteristics equation                          [m]
C_p = Characteristic_Plus(a, g, A, D, dx, roughness, rho,...
        viscosity, theta, Q_A, H_A, Q, Re_0, i, j, dt,...
```

```
13          Friction_Type, Q_0, f_pre, W, dQ, n_t);
14
15 %% Piezometric head                                    [m]
16 H_P = Ap_0+Ap*sin(2*pi*t/T );
17 tau_v = H_P;
18
19 %% Volumetric flow                                    [m^3/s]
20 % Standard Q_P
21 Q_P = (C_p-H_P)/B;
22
23 end
```

Listing A.6: *Valve_Pressure_Sin* function

```
1 function [Q_P, H_P] = Valve_Pressure_Spectre(a,L, g, A, D, dx,
      roughness, rho,...
2          viscosity, t, t_c, m, theta, H_r, Q_0, H_0, Q_A, H_A, Q, Re_0
              , i, j, dt,...
3          Friction_Type, f_pre, W, dQ, n_t, WaveSpec)
4 %% Calculating the constants at valves
5 % Pipe constant                                        [s/m^2]
6 B = PipeConst(a, g, A);
7
8 % Positive characteristics equation                    [m]
9 C_p = Characteristic_Plus(a, g, A, D, dx, roughness, rho,...
10 viscosity, theta, Q_A, H_A, Q, Re_0, i, j, dt,...
11 Friction_Type, Q_0, f_pre, W, dQ, n_t);
12
13 %% indexing simulation time with wave time step
14 WaveSpecRepet = repmat(WaveSpec(:,1),[1 length(t)]); % calc int
15 [minValue, W_index] = min(abs(WaveSpecRepet-t)); % find value close
16 Wave_Value = WaveSpec(W_index,2);
17
18 %% Piezometric head                                    [m]
19 H_P = Wave_Value;
20
21 %% Volumetric flow                                    [m^3/s]
22 % Standard Q_P
23 Q_P = (C_p-H_P)/B;
24
25 end
```

Listing A.7: *Valve_Pressure_Spectre* function

```
1 %% FFT input wave
2 Nfft_W = length(WaveSpec(:,2)); % sample
3 dt_W = WaveSpec(2,1)-WaveSpec(1,1)
4 Y_W(1,:) = fft(WaveSpec(:,2)./cosh(2)); %% FFT of wave at the specify
      depth
5 P2_W(1,:) = abs(Y_W(1,:)./(Nfft_W));
6 P1_W(1,:) = P2_W(1,1:floor(Nfft_W/2));
```

```
7  P1_W(1,2:end-1) = 2*P1_W(1,2:end-1); % Amplitude in function of F
8  P1_freq_W(1,:) = (1:(Nfft_W/2))/Nfft_W*(1/(dt_W)); % Equally spaced
       frequency grid
9
10 %% Indexing F_05,_10_10,_W in function of targuet
11 % open("C:\Users\alex-\Documents\Etude\MSE\5_Delf MSc\03_Thesis\14
       _SVN Whammer Spectrum Sectrum L loop\Output\PWave_Curve2.csv") %
       extrect column vectore
12 clearvars target_F j minValue closestIndex F_05_ind F_10_ind F_15_ind
        Hfft05_comp Hfft10_comp Hfft15_comp HfftW HfftW_comp Pourc_F05
       Pourc_F10 Pourc_F15 Xq Vq
13 target_F = 0:0.005:0.6;
14 for j = 1:length(target_F);
15 [minValue(j,1), closestIndex(j,1)] = min(abs(F_05(:,1) - target_F(1,j
       )));
16 end
17 F_05_ind = closestIndex(:,1);
18 Hfft05_comp_add = AllRange.Hfftmaxn05(F_05_ind)./Hs;
19 Hfft05_comp = AllRange.Hfftmaxn05(F_05_ind);
20
21 for j = 1:length(target_F);
22 [minValue(j,1), closestIndex(j,1)] = min(abs(F_10(:,1) - target_F(1,j
       )));
23 end
24 F_10_ind = closestIndex(:,1);
25 Hfft10_comp_add = AllRange.Hfftmaxn10(F_10_ind)./Hs;
26 Hfft10_comp = AllRange.Hfftmaxn10(F_10_ind);
27
28 for j = 1:length(target_F);
29 [minValue(j,1), closestIndex(j,1)] = min(abs(F_15(:,1) - target_F(1,j
       )));
30 end
31 F_15_ind = closestIndex(:,1);
32 Hfft15_comp_add = AllRange.Hfftmaxn15(F_15_ind)./Hs;
33 Hfft15_comp = AllRange.Hfftmaxn15(F_15_ind);
34
35 Xq = 0:0.001:0.6; % x vector for interpolation of the line
36 Vq = interp1(P1_freq_W_curve,P1_W_curve./cosh(2),Xq,'linear');
37 for j = 1:length(target_F);
38 [minValue(j,1), closestIndex(j,1)] = min(abs(Xq(1,:)- target_F(1,j)))
       ; %
39 end
40 F_W_ind = closestIndex(:,1);
41 HfftW_comp = Vq(F_W_ind)';
42
43 Pourc_F05 = Hfft05_comp./HfftW_comp;
44 Pourc_F10 = Hfft10_comp./HfftW_comp;
45 Pourc_F15 = Hfft15_comp./HfftW_comp;
46
```

```
47 %% Plot L and F with offset
48 % import "\03_Thesis\14_SVN Whammer Spectrum Sectrum L loop\
       OutputAllRange.csv" in table
49 Hs =      0.6366;
50 figure(1)
51 set(gcf,'position',[100,100,875,500])
52 F_05 = 0.5*a./AllRange.Pipelength; % corresponding frequency n = 0.5
53 F_10 = a./AllRange.Pipelength; % corresponding frequency n = 1.0
54 F_15 = 1.5*a./AllRange.Pipelength; % corresponding frequency n = 1.5
55 hold on
56 plot(F_05,AllRange.Hfftmaxn05./Hs,'r.-', F_05,AllRange.Hfftmaxn10./Hs
       ,'b.-', F_05,AllRange.Hfftmaxn15./Hs,'g.-')
57 xlim1 = 0.03; xlim2 = 0.5;
58 xlim([xlim1 xlim2])
59 xticks(0:0.05:1)
60 xlabel('Frequency (Hz)')
61 ylabel('|H| (-)')
62 legend("FFT natural mode 1 ","FFT natural mode 2","FFT natural mode
       3","FFT wave output")
63 set(gca,'Xscale','log')
64 ax1 = gca; % current axes
65 ax1.XColor = 'k'; ax1.YColor = 'k';
66 ax1_pos = ax1.Position; % position of first axes
67 ax2 = axes('Position',ax1_pos,...
68 'XAxisLocation','top',...
69 'YAxisLocation','right',...
70 'Color','none','Xdir','reverse');
71 line(flip(AllRange.Pipelength),flip(AllRange.Hfftmaxn05./Hs),'Parent'
       ,ax2,'Color','r') % plot right side for adjust scale
72 %  xlim([430 2150])
73 xlim([(215/2/xlim2) (215/2/xlim1)])
74 set(gca,'Xscale','log')
75 xticks([0:100:800,1000,1500,2000,3000])
76 xlabel('Pipe length (m)')
77 grid
78
79 %% Plot L and F and outfall wave, no offset
80 figure(3)
81 set(gcf,'position',[100,100,875,500])
82 % set(gcf,'position',[50,50,1300,850])
83
84 F_05 = 0.5*a./AllRange.Pipelength;
85 F_10 = a./AllRange.Pipelength;
86 F_15 = 1.5*a./AllRange.Pipelength;
87 hold on
88 plot(F_05,AllRange.Hfftmaxn05./Hs,'r.-', F_10,AllRange.Hfftmaxn10./Hs
       ,'b.-', F_15,AllRange.Hfftmaxn15./Hs,'g.-')
89 hold on
90 area(Xq,Vq./Hs)
```

```
xlim1 = 0.08;
xlim2 = 0.5;
ylim2 = 3;
xlim([xlim1 xlim2])
ylim([0 ylim2])
xticks([0:0.02:0.26, 0.3:0.05:1])
yticks(0:0.2:10)
grid
xlabel('Frequency (fundamental frequency equivalent) (Hz)')
ylabel('|H| (-)')
legend("FFT natural mode 1 ","FFT natural mode 2","FFT natural mode 3","FFT wave at output",'Location','northeast')
set(gca,'Xscale','log')
% set(gca,'Yscale','log')

ax1 = gca; % current axes
ax1.XColor = 'k';
ax1.YColor = 'k';
ax1_pos = ax1.Position; % position of first axes
ax2 = axes('Position',ax1_pos,...
'XAxisLocation','top',...
'YAxisLocation','right',...
'Color','none','Xdir','reverse');
line(flip(AllRange.Pipelength),flip(AllRange.Hfftmaxn05),'Parent',ax2,'Color','r')
ylabel('|H| (m)')

xlim([(a/2/xlim2) (a/2/xlim1)])
ylim([0 ylim2*Hs])

% ylim([10^-4 4])
set(gca,'Xscale','log')
% set(gca,'Yscale','log')
xticks([250,300, 350:100:1000,1200,1500,2000,2500,3000])
xlabel('Pipe length (fundamental frequency equivalent) (m)')

%% comparison and ploting
figure(4)
set(gcf,'position',[100,100,700,400])
plot(Xq,Vq,'color',[0.49,0.18,0.56])
set(gca, 'YScale', 'log')
plot(target_F,Pourc_F05,'r.-', target_F,Pourc_F10,'b.-',target_F,Pourc_F15,'g.-')
hold on
grid
xlabel('Frequency (fundamental frequency equivalent) (Hz)')
ylabel('Difference with the input spectrum (-)')
xticks([0:0.02:2])
xlim([0.09 0.42])
```

```
137 legend("input wave spectrum", "comp. natural mode 1 ","comp. natural
    mode 2","comp. natural mode 3",'Location','northwest','NumColumns'
    ,2)
138
139 %% table mean max, min, average
140 target_F_zoom = target_F(1,20:81);
141 Pourc_F05_zoom = Pourc_F05(20:81,1);
142 Pourc_F10_zoom = Pourc_F10(20:81,1);
143 Pourc_F15_zoom = Pourc_F15(20:81,1);
144 Pourc_F_min = [min(Pourc_F05_zoom);min(Pourc_F10_zoom);min(
    Pourc_F15_zoom)];
145 Pourc_F_max = [max(Pourc_F05_zoom);max(Pourc_F10_zoom);max(
    Pourc_F15_zoom)];
146 Pourc_F_mean = [mean(Pourc_F05_zoom);mean(Pourc_F10_zoom);mean(
    Pourc_F15_zoom)];
147 Table_diff=table(Pourc_F_min,Pourc_F_max,Pourc_F_mean)
```

Listing A.8: *L_to_F_analyisi* function

3 Wave Steps in the Pipe with Sinusoidal Pressure Wave at the Outfall (Ap: 0.27m, T: 3s)

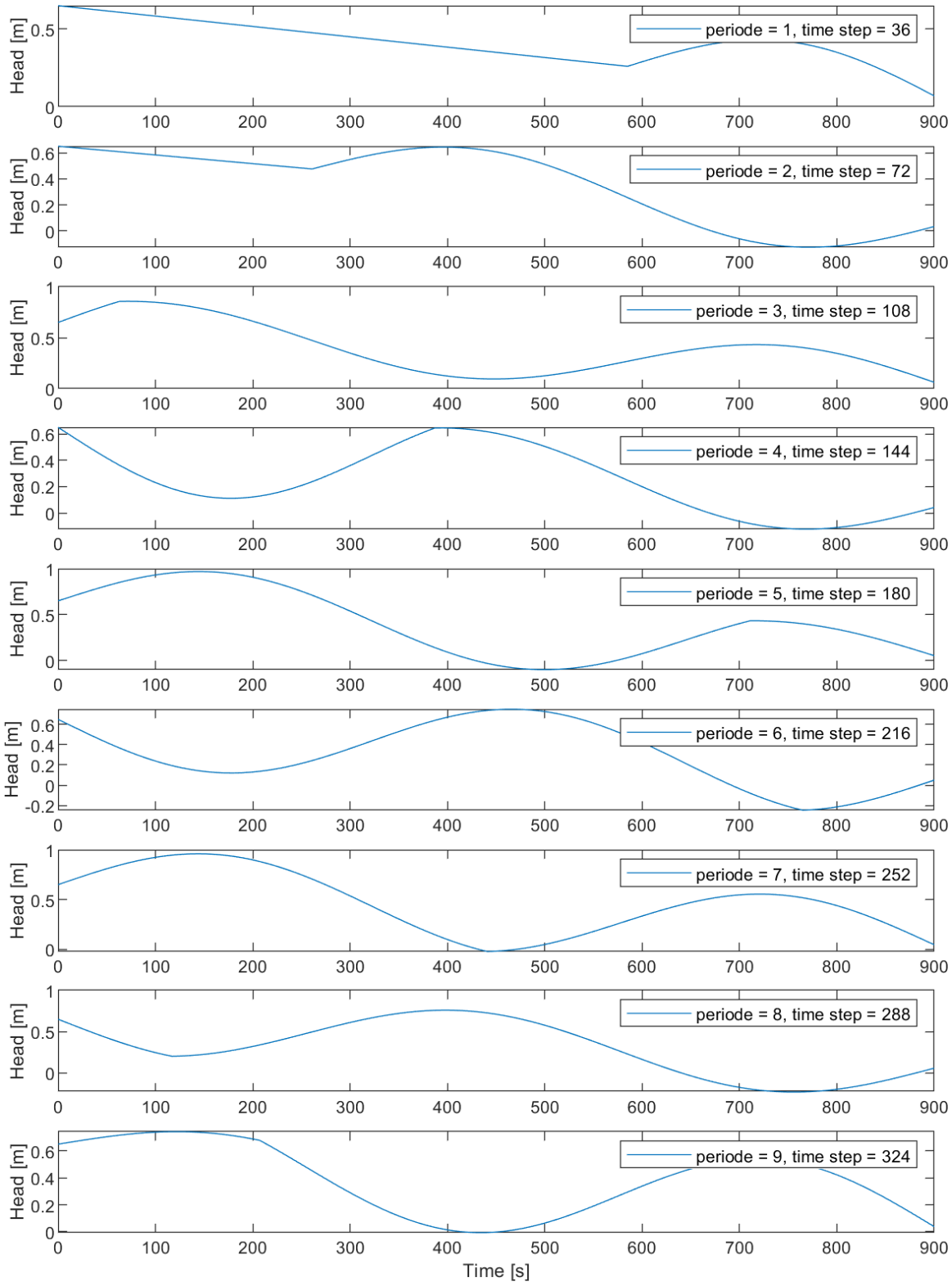

Figure A.1: Pressure head along the pipe with sinus wave at outfall for 9 first periods of injected wave for typical pipe without slope

4 Wave Steps in the Pipe with Coastal Waves at the Outfall

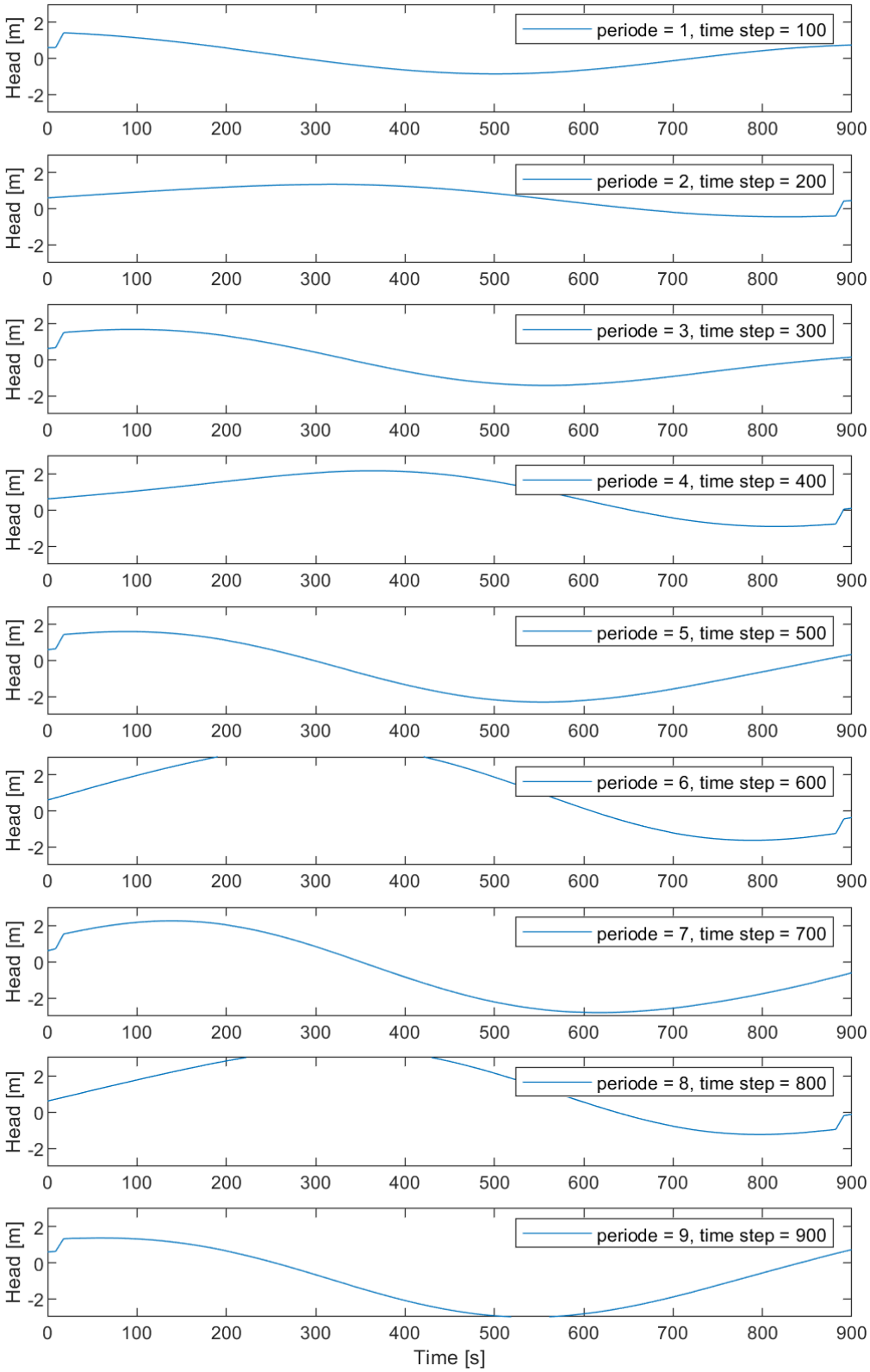

Figure A.2: Pressure head along the pipe with coastal waves at outfall for 9 first travel time periods for typical pipe without slope